

**DESIGN AND CHARACTERIZATION OF A PEO-BASED POLYMER  
COMPOSITE ELECTROLYTE EMBEDDED WITH DOPED-LLZO: ROLE  
OF DOPANT IN BULK IONIC CONDUCTIVITY**

by

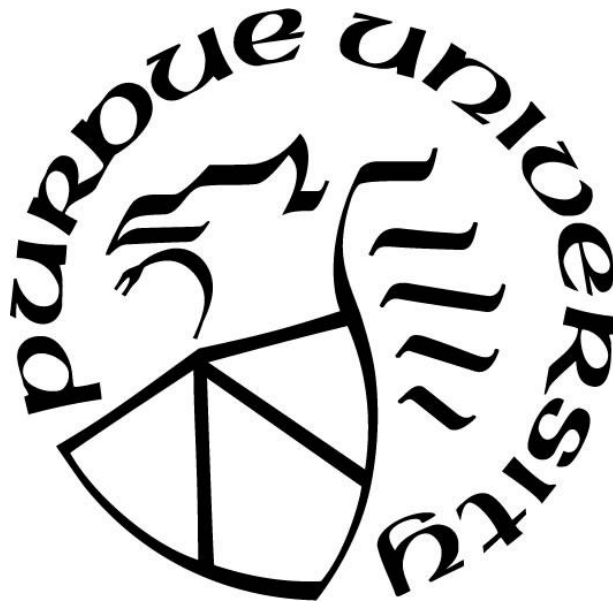
**Andrés A. Villa Pulido**

**A Dissertation**

*Submitted to the Faculty of Purdue University*

*In Partial Fulfillment of the Requirements for the degree of*

**Doctor of Philosophy**



School of Materials Engineering

West Lafayette, Indiana

December 2019

**THE PURDUE UNIVERSITY GRADUATE SCHOOL**  
**STATEMENT OF COMMITTEE APPROVAL**

**Dr. Ernesto Marinero, co-chair**

Department of Materials Engineering

**Dr. David Bahr, co-chair**

Department of Materials Engineering

**Dr. Jeffrey Youngblood**

Department of Materials Engineering

**Dr. Joseph Pekny**

Department of Chemical Engineering

**Approved by:**

Dr. David Bahr

Head of the Departmental Graduate Program

*Let everything happen to you: beauty and terror.*

*Just keep going. No feeling is final.*

**- RAINER MARIA RILKE,**

***The Book of Hours***

*For my dearest family, whose fire revived me time and time again.*

## **ACKNOWLEDGMENTS**

This work was made possible by Dr. Marinero's startup funds from Purdue University School of Materials Engineering, by the School of Materials Engineering, and by the Consejo Nacional de Ciencia y Tecnología (CONACYT). Thank you to my committee members for their advice, and to all the staff at Armstrong building that helped me on this journey.

# TABLE OF CONTENTS

LIST OF TABLES .....	7
LIST OF FIGURES .....	8
ABBREVIATIONS .....	11
ABSTRACT.....	13
1. INTRODUCTION.....	14
1.1 The role of energy storage in the next 50 years. ....	14
1.2 Li-ion technology as a main component in renewable energy generation.....	15
1.3 References .....	17
2. LITERATURE REVIEW .....	18
2.1 Lithium-ion battery: basic components and the role of the electrolyte.....	18
2.2 $\text{Li}_7\text{La}_3\text{Zr}_2\text{O}_{12}$ (LLZO) Solid-state electrolyte.....	23
2.2.1 Synthesis of LLZO .....	23
2.2.2 Li-ion transport mechanism in LLZO .....	25
2.2.3 Li, Zr, La site substitution in LLZO.....	27
2.3 Polymer composite electrolytes .....	30
2.3.1 Poly Ethylene Oxide (PEO) as a matrix for PCE.....	31
2.3.2 PEO with different Li salts .....	32
2.3.3 Effect of passive fillers on Solid Polymer Electrolytes.....	34
2.3.4 Effect of active fillers on Solid Polymer Electrolytes .....	36
2.3.5 Ionic conduction mechanism in a PCE.....	38
2.4 References .....	40
3. EFFECT OF ADDITIONAL CA, GA AND ND DOPANT ON IONIC CONDUCTIVITY OF BI-DOPED LLZO.....	46
3.1 Introduction .....	46
3.2 Materials and methods .....	48
3.3 Results and discussion.....	50
3.4 Conclusions .....	56
3.5 References .....	57
4. BI-DOPED LLZO AS A FILLER IN PEO-BASED POLYMER COMPOSITE ELECTROLYTE: EFFECT OF BI MOLAR RATIO ON BULK IONIC CONDUCTIVITY ....	61

4.1 Introduction .....	61
4.2 Materials and methods .....	62
4.3 Results and discussion.....	64
4.4 Conclusions .....	71
4.5 References .....	73
5. FURTHER ELUCIDATION OF THE PEO-BASED LLZO POLYMER COMPOSITE ELECTROLYTE: ROLE OF LI MOLAR RATIO AND POLYMER MICROSTRUCTURE...	78
5.1 Introduction .....	78
5.2 Materials and methods .....	79
5.3 Results and discussion.....	81
5.4 Conclusions .....	85
5.5 References .....	86
6. GENERAL SUMMARY AND CONCLUSIONS .....	89
6.1 Thesis summary.....	89
6.2 Research outlook.....	92
APPENDIX A. REFERENCES FOR FIGURE 2.6 AND 2.7.....	93

## LIST OF TABLES

Table 2-1. Examples of Li-ion failure in different devices.....	20
Table 2-2 Main types of solid state electrolytes. Table compiled from [6].....	23
Table 2-3 Examples of LLZO Synthesis. ....	24
Table 2-4 Examples of co-doped LLZO investigations.....	29
Table 3-1 Garnet nomenclature .....	48
Table 3-2 Relative densities, lattice constant, and ionic conductivity of co-doped LLZO garnets. .....	57
Table 5-1 Formula and sample name for LLZO garnets synthesized and used in this work. ....	80

## LIST OF FIGURES

Figure 1.1 Diagram of anode/cathode capacity vs potential of some anode and cathode materials. Image from [4].	16
Figure 2.1 Schematics of a rechargeable Li-ion battery. The anode, $\text{Li}_x\text{C}_6$ is depicted on the left side of the figure, whereas the cathode, $\text{Li}_{1-x}\text{CoO}_2$ is shown on the right section. The transport of Li ions between anode and cathode is also depicted [3].	19
Figure 2.2 Li-ion conduction in a liquid electrolyte: the organic solvent dimethyl carbonate (DMC) serves as the transport medium for Li ions between hexafluorophosphate anions.	21
Figure 2.3 Main reactions in the Pechini method. Cations like $\text{Li}^+$ , $\text{La}^{3+}$ and $\text{Zr}^{2+}$ are represented by $\text{Mn}^+$ . Diagram reproduced from ref[20].	25
Figure 2.4 Crystal structure of cubic LLZO. The green and red spheres represent Li sites. Li-ion sub-lattice in LLZO for (b) tetragonal and (c) cubic phase. Image from[21].	26
Figure 2.5 $\text{Li}^+$ ion migration bottleneck for the diffusion pathway. Red dashed lines indicate a broadening of the window, blue dashed lines indicate a tightened pathway. Figure from [23].	27
Figure 2.6 Ionic conductivity for doped LLZO in terms of molar Li.	29
Figure 2.7 Ionic conductivity for doped LLZO as a function of cubic lattice parameter.	30
Figure 2.8 Schematic of poly ethylene oxide complexation with metal cations. Reproduced from [31].	32
Figure 2.9 Arrhenius plots for PEO:Li-salt electrolytes [EO:Li=4.5] for different anions. Figure from [32].	33
Figure 2.10 The effect of weight load vs ionic conductivity for a SBA-15 mesoporous silica + PEO:LiClO <sub>4</sub> PCE. Figure reproduced from[41].	35
Figure 2.11 Weight load vs ionic conductivity at different temperatures for PEO:LiClO <sub>4</sub> system with tetragonal phase LLZO filler. Figure from ref [45].	37
Figure 2.12 Schematic representation of a spherulite. Figure from ref [51].	38
Figure 2.13 $\text{Li}^+$ transport through amorphous regions (red lines representing PEO loops) between spherulite lamellae (blue lines representing crystalline PEO). Green circles represent Li ions. Figure from[49].	39

Figure 3.1 SEM images of Bi-LLZO pellets with variation in Bi content. These samples were sintered at 900°C for 10h. Samples are: (a) $\text{Li}_7\text{La}_3\text{Zr}_2\text{O}_{12}$ , (b) $\text{Li}_{6.5}\text{La}_3\text{Zr}_{1.5}\text{Bi}_{0.5}\text{O}_{12}$ , (c) $\text{Li}_{6.25}\text{La}_3\text{Zr}_{1.25}\text{Bi}_{0.75}\text{O}_{12}$ , (d) $\text{Li}_6\text{La}_3\text{ZrBiO}_{12}$ .	47
Figure 3.2 Diagram of Bi-LLZO synthesis.	49
Figure 3.3 XRD scans for: a) BiCa-LLZO, b) BiGa-LLZO, c) BiNd-LLZO and d) reference PDF pattern corresponding to cubic LLZO (ICSD 422-259). Trace amounts of the $\text{La}_2\text{Zr}_2\text{O}_7$ identified by the (*) symbol are observed.	51
Figure 3.4 $\text{Li}^+$ ion migration bottleneck for the diffusion pathway. Figure from ref. [13]	51
Figure 3.5 SEM images of co-doped LLZO pellet microstructure for, a) BiCa-LLZO, b) BiGa-LLZO and c) BiNd-LLZO. All pellets were sintered at 900°C for 10 hours. Note that the structures are porous which is expected to impact their ionic conductivity.	53
Figure 3.6 Example of Nyquist plot measurement for a BiNd-LLZO pellet.	54
Figure 4.1 XRD patterns for: a) $\text{Li}_{6.25}\text{La}_3\text{Zr}_{1.25}\text{Bi}_{0.75}\text{O}_{12}$ and b) $\text{Li}_6\text{La}_3\text{ZrBiO}_{12}$ , c) reference PDF pattern corresponding to cubic LLZO (ICSD 422-259).	64
Figure 4.2 4.2(a) and 2(b) shows SEM images of $\text{Li}_6\text{La}_3\text{ZrBiO}_{12}$ particles dispersed in PEO:LiTFSI films, for 5% wt and 50% wt respectively.	65
Figure 4.3(a) IC dependence on temperature for PCE loaded with $\text{Li}_{7-x}\text{La}_3\text{Zr}_{2-x}\text{Bi}_x\text{O}_{12}$ , where $x=0.5, 0.75, 1$ and $1.5$ . (b) IC dependence of PCE samples with a $\text{Li}_6\text{La}_3\text{ZrBiO}_{12}$ weight load at several temperatures.	66
Figure 4.4 XRD patterns for PEO:LiTFSI with (a) 0% wt $\text{Li}_6\text{La}_3\text{ZrBiO}_{12}$ , (b) 5 % wt $\text{Al}_2\text{O}_3$ , (c) 2.5% wt $\text{Li}_6\text{La}_3\text{ZrBiO}_{12}$ , (d) 5% wt $\text{Li}_6\text{La}_3\text{ZrBiO}_{12}$ , (e) 5% wt $\text{Li}_6\text{La}_3\text{ZrBiO}_{12}$ . Bottom pattern refers to cubic LLZO (ICSD 422-259). The change in magnitude for the triple peak at $23^\circ$ indicates a slight decrease in crystalline PEO, consistent with increments in ionic conductivity. However, said changes do not fully explain the strong IC dependence on garnet particle weight load.	67
Figure 4.5 Ionic conductivity vs. $\text{Li}_{6.25}\text{La}_3\text{Zr}_{1.25}\text{Bi}_{0.75}\text{O}_{12}$ weight load in PEO:LiTFSI. The highest ionic conductivity corresponds to 10% wt $\text{Li}_{6.25}\text{La}_3\text{Zr}_{1.25}\text{Bi}_{0.75}\text{O}_{12}$ .	68
Figure 4.6 XRD scans for PEO:LiTFSI with (a) 0% wt $\text{Li}_{6.25}\text{La}_3\text{Zr}_{1.25}\text{Bi}_{0.75}\text{O}_{12}$ , (b) 5 % wt $\text{Al}_2\text{O}_3$ , (c) 5% wt $\text{Li}_{6.25}\text{La}_3\text{Zr}_{1.25}\text{Bi}_{0.75}\text{O}_{12}$ , (d) 10% wt $\text{Li}_{6.25}\text{La}_3\text{Zr}_{1.25}\text{Bi}_{0.75}\text{O}_{12}$ , (e) 30% wt $\text{Li}_{6.25}\text{La}_3\text{Zr}_{1.25}\text{Bi}_{0.75}\text{O}_{12}$ . Bottom pattern refers to cubic LLZO (ICSD 422-259). The change in magnitude for the triple peak at $23^\circ$ indicates a decrease in crystalline PEO, consistent with an increase in ionic conductivity.	69

Figure 4.7 Ionic conductivity measurements of PEO:LiTFSI with added  $\text{Li}_6\text{La}_3\text{ZrBiO}_{12}$  and  $\text{Li}_{6.25}\text{La}_3\text{Zr}_{1.25}\text{Bi}_{0.75}\text{O}_{12}$  as a function of weight load at room temperature, the inset images correspond to polarized light microscopy observations. White lines added for clarity..... 70

Figure 5.1 Ionic conductivity of PEO:LiTFSI films as a function of weight load for various garnet particle compositions: Bi-LLZO , 0.75Bi-LLZO, and BiNd-LLZO. Inset images: PLM images showing spherulite morphology changes as a function of weight load. White lines added for clarity..... 81

Figure 5.2 Schematic representation depicting how spherulite formation affects Li-ion conduction in a PCE. Yellow dots represent spherulite centers. Red line represents possible  $\text{Li}^+$  path..... 83

Figure 5.3 Arrhenius plots of ionic conductivity for thin and thick PCE samples loaded with 10% wt 0.75Bi-LLZO and 10% wt BiNd-LLZO. The image on the lower portion of the figure corresponds to a thick BiNd-LLZO sample..... 84

Figure 5.4 Arrhenius plots for the ionic conductivity of PCE films loaded with 10% wt BiNd-LLZO. The ionic conductivity vastly differs for thick and thin samples and an even lower value is measured for a thick sample obtained by fusing two thinner films. .... 85

## ABBREVIATIONS

SSE	solid state electrolyte
LIB	lithium ion battery
IC	ionic conductivity
SPE	solid polymer electrolyte
PCE	polymer composite electrolyte
LLZO	lithium lanthanum zirconium oxide
Bi-LLZO	bismuth-doped lithium lanthanum zirconium oxide
BiCa-LLZO	bismuth-calcium co-doped lithium lanthanum zirconium oxide
BiGa-LLZO	bismuth-gallium co-doped lithium lanthanum zirconium oxide
BiNd-LLZO	bismuth-neodymium co-doped lithium lanthanum zirconium oxide
PEO	poly ethylene oxide
LiTFSI	Lithium bis(trifluoromethanesulfonyl)imide
LiBF <sub>4</sub>	Lithium tetrafluoroborate
LiAsF <sub>6</sub>	Lithium hexafluoroarsenate
LiPF <sub>6</sub>	Lithium hexafluorophosphate
EC	ethyl carbonate
DMC	dimethyl carbonate
EMC	ethyl methyl carbonate
SEI	solid electrolyte interface
PVDF	polyvinylidene fluoride
PAN	polyacrylonitrile
NASICON	sodium super ionic conductor
LISICON	lithium super ionic conductor
LiPON	Lithium phosphorous oxy-nitride
MEEP	poly[bis((methoxyethoxy)ethoxy)-phosphazene]
PAN	polyacrylonitrile
PPO	poly propylene oxide

PVAc	polyvinyl acetate
MW	molecular weight
LiTf	Lithium triflate
BaTiO <sub>3</sub>	Barium titanate
Al <sub>2</sub> O <sub>3</sub>	aluminum oxide
LLTO	lithium lanthanum titanate
LiAlO <sub>2</sub>	Lithium aluminate
TiO <sub>2</sub>	Titanium dioxide
La <sub>2</sub> Zr <sub>2</sub> O <sub>7</sub>	lanthanum zirconate
La <sub>2</sub> O <sub>3</sub>	lanthanum oxide
EIS	electrochemical impedance spectroscopy

## ABSTRACT

Ionic conductivity of solid polymer electrolytes (SPEs) can be enhanced by the addition of fillers, while maintaining good chemical stability, and compatibility with popular cathode and anode materials. Additionally, polymer composite electrolytes can replace the flammable organic liquid in a lithium-ion battery design and are compatible with lithium metal. Compatibility with Li-metal is a key development towards a next-generation rechargeable Li-ion battery, as a Li-metal anode has a specific capacity an order of magnitude higher than  $\text{LiC}_6$  anodes used today in everyday devices. The addition of fillers is understood to suppress the crystalline fraction in the polymer phase, increasing the ionic conductivity, as Li-ion conduction is most mobile through the amorphous phase. A full model for a conduction mechanism has not yet constructed, as there is evidence that a semi-crystalline PEO-based electrolyte performs better than a fully amorphous electrolyte. Furthermore, it is not yet fully understood why the weight load of fillers in PCEs can range from 2.5% wt to 52.5% wt, in order to achieve high ionic conductivity ( $\sim 10^{-4} \text{ S/cm}$ ). This work seeks to investigate the conduction mechanism in the PCE through the use of doped- $\text{Li}_7\text{La}_3\text{Zr}_2\text{O}_{12}$  as a filler and analysis of the PCE microstructure. In this work, a solid-state electrolyte, doped- $\text{Li}_7\text{La}_3\text{Zr}_2\text{O}_{12}$  (LLZO) was synthesized via a sol-gel method, and characterized. The effect of doping and co-doping the Li, La and Zr sites in the LLZO garnet was investigated. A PEO-based polymer composite electrolyte (PCE) was prepared by adding bismuth doped LLZO ( $\text{Li}_{7-x}\text{La}_3\text{Zr}_2\text{O}_{12-x}\text{Bi}_x$ ) as a filler. The bismuth molar ratio was changed in value to study the dopant role on the bulk PCE ionic conductivity, polymer phase crystallinity and microstructure. Results suggest that small variations in dopant can determine the optimal weight load of filler at which the maximum ionic conductivity is reached. By understanding the relationship between filler properties and electrochemical properties, higher performance can be achieved with minimal filler content, lowering manufacturing costs a solid-state rechargeable Li-ion battery.

# 1. INTRODUCTION

## 1.1 The role of energy storage in the next 50 years.

In late 2018, the United Nations International Panel on Climate Change (IPCC) issued a special report on the effect of a global warming event of 1.5°C above pre-industrial levels. The findings were dire. The main finding was that it is with “high confidence” that we will reach a global warming of 1.5°C, between the years 2030 and 2052. Extreme temperatures on land will increase by 3°C, and the number of hot days will increase in the mid-latitude regions of the planet. As of writing, the month of June 2019 was confirmed by NASA as the hottest month in recorded history. With medium confidence, the report also concludes that droughts and floods are expected to increase in intensity and frequency, depending on the geographic location, and amount of precipitation from weather events is going to increase on average. In the next century, an increase of sea level is to be expected, an average of half a meter. If global measures aren’t taken, and the increase becomes 2°C instead of 1.5, an additional 10 million people will be affected. Moreover, if the temperature increase is reached, an irreversible ice sheet melting event in Greenland could be triggered, resulting in a multi-meter rise in sea level beyond 2100. Between 4% and 13% of global terrestrial land will undergo a change in transformation in the type of ecosystem it holds, meaning grasslands could transform to deserts, etc. Global health systems are expected to be overwhelmed by malaria and dengue fever emerging in new regions, as well as increased heat-related mortality. Several hundred million people are to be affected from increased poverty resulting from climate change by 2050.

Many measures must be taken to slow down, and eventually reverse this increase in temperature. According to the UN IPCC report, the main way to keep the temperature increase at 1.5°C is to implement an abrupt shift in energy consumption habits that today revolve around fossil fuels. The energy needs that are provided by the fossil fuel industry could be covered by renewable sources. Solar and wind are very favorable options, and depending on the location, they can provide 100% of the needs supplied by the electric grid. The main obstacle for technology implementation is energy storage. The electrical grid in any given electrical system has varied energy demand depending on the hour of day, the day of the week, and the month of the year. Solar grids and wind farms have a main drawback where the energy must be sent to the grid

immediately, as the power source is not readily available 100% of the time. For this we need storage devices, where all of the energy is stored, and sent to the electrical grid in times of high demand. Li-ion technology is positioned to take this key position as the energy storage device of choice.

## **1.2 Li-ion technology as a main component in renewable energy generation**

Currently, rechargeable Li-ion batteries are widely implemented in laptops, smartphones, drones, gaming devices, among other electronic devices. Deployment in larger scale projects, such as wind and solar farms, as well as a primary power generators is thus far limited[1]. Their wider integration into larger scale devices is hindered by their manufacturing cost, the danger of catastrophic failure caused by thermal runaway, and their limited energy and power density. These concerns are being addressed continuously. Cost is being brought to a more acceptable range by mass production and implementation in electric vehicles [2]. Solving the issues of catastrophic failure and limits on energy and power density is a challenging problem that revolves around one of the Li-ion battery's main components, the electrolyte.

Commercial rechargeable Li-ion batteries use a lithium salt dissolved in an organic solvent as an electrolyte. This liquid electrolyte soaks a polymer membrane (mostly polyolefins) that is used as a separating barrier between the anode and cathode films. Although the liquid solvent provides high ionic conductivity and facile manufacturing, it allows the formation of dendrites that can extend from the anode to the cathode electrodes causing a short-circuit. This in turn, on account of the flammability of the liquid electrolyte can result in fire and explosion of the battery device. Short-circuits caused by designing the anode, cathode or separator with the wrong thickness, has resulted in explosions[3], causing serious personal injuries and serious damage to the device the battery was incorporated in.

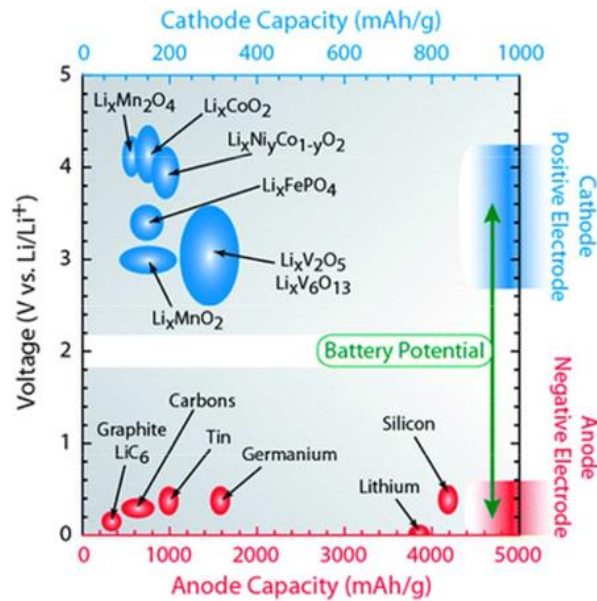


Figure 1.1 Diagram of anode/cathode capacity vs potential of some anode and cathode materials. Image from [4].

In a battery, the energy and power density is limited by the anode and cathode capacity. Graphite is currently the most commonly used material as an anode in commercial rechargeable Li-ion batteries, and it has a theoretical capacity of around 300 Ah/kg. In contrast, if Li-metal with a theoretical capacity of around 3000 Ah/kg, could be used as the anode material, it would dramatically increase the capacity of existing devices. The main roadblock hindering the use of Li-metal anodes is its reactivity with organic solvent electrolytes and the propensity to form dendrites at the interface between liquid and metal, and to break the SEI layer[5]. Figure 1.1 shows a capacity vs potential diagram for a variety of anode and cathode materials, note the difference in capacity between graphite and Li metal shown in the lower part of the figure.

Therefore, one of the key thrusts in battery materials and technology development is the search for solid state electrolytes that not only circumvent the inherent safety and performance limitations of current Li-ion batteries but enable the utilization of advanced anode and cathode materials as well as novel electrochemistries for future battery devices. This thesis describes the development of a composite solid state electrolyte comprising nanoparticles of high ionic conductivity garnet oxides embedded in a polymer matrix impregnated with Li-salts. The thesis first provides a literature review of the electrochemical properties of the solid inorganic electrolyte

nanoparticles, lithium lanthanum zirconium oxide (LLZO), as well as solid polymer electrolytes (SPEs) and composite polymer electrolytes (PCEs). The review is followed by analysis of experimental work done on doped and co-doped LLZO, as well as the PEO:LiTFSI polymer system, with added LLZO fillers. Finally, some conclusions and future work will be posited.

### 1.3 References

- [1] D. I. Stroe, V. Knap, M. Swierczynski, A. I. Stroe, and R. Teodorescu, "Operation of a grid-connected lithium-ion battery energy storage system for primary frequency regulation: A battery lifetime perspective," *IEEE Trans. Ind. Appl.*, 2017.
- [2] B. Diouf and R. Pode, "Potential of lithium-ion batteries in renewable energy," *Renewable Energy*. 2015.
- [3] J. J. Yun, J. H. Jeon, K. B. Park, and X. Zhao, "Benefits and costs of closed innovation strategy: Analysis of Samsung's Galaxy Note 7 explosion and withdrawal scandal," *J. Open Innov. Technol. Mark. Complex.*, 2018.
- [4] M. Osiak, H. Geaney, E. Armstrong, and C. O'Dwyer, "Structuring materials for lithium-ion batteries: Advancements in nanomaterial structure, composition, and defined assembly on cell performance," *J. Mater. Chem. A*, 2014.
- [5] X. B. Cheng, R. Zhang, C. Z. Zhao, and Q. Zhang, "Toward Safe Lithium Metal Anode in Rechargeable Batteries: A Review," *Chemical Reviews*. 2017.

## 2. LITERATURE REVIEW

Lithium-ion batteries are electrochemical energy storage devices. Electrochemical energy storage devices originated with the work of Alessandro Volta in the late 1700s, when he invented the first voltaic cell. Although the work of Volta dates back 300 years, the chemistry of the modern lithium-ion battery is much recent. The chemistries that we use today in most devices came from the amalgamation of three key developments.

The first, the development of lithium cobalt oxide cathode by Chemistry Nobel prize winner, John Goodenough in the early 1980's. The second came in the development of the graphite anode by Rachid Yazami in 1980. Graphite serves as an intercalation anode, wherein lithium ions are stored during charging of the device. The third came in the development of a rechargeable lithium-ion battery prototype by the SONY corporation in 1985. It wasn't until 1991 when the first rechargeable device was commercialized by SONY and started the popularity that this energy storage device enjoys today.

The success of this key technology required overcoming the most important drawback at that time regarding the tendency of the early devices to leak, explode, or catastrophically fail. This was mainly due to the use of lithium metal as an anode, as it tended to form dendrites in the electrolyte media, shorting the battery and causing cell explosion. These issues were mitigated when the graphite anode was developed as anode material, reducing the risk for dendrite formation on the interface between electrolyte and lithium metal.

### 2.1 Lithium-ion battery: basic components and the role of the electrolyte

The lithium ion battery has 4 main components: the cathode, anode, electrolyte and separator. Cathode materials for lithium ion batteries are transition metal oxides, the most popular being lithium metal oxide,  $\text{Li}_x\text{CoO}_2$  (LCO) and lithium manganese oxide  $\text{Li}_x\text{MnO}_4$  (LMO). These materials are chosen based on several key characteristics.

Cathode materials undergo oxidation reactions while maintaining charge neutrality, their crystal structure is stable across a wide range of lithium molar concentrations, and are chemically

stable against the electrolyte material. LCO has a trigonal unit cell structure consisting of a cubic close packed oxygen lattice with Li and Co ions occupying two sets of octahedral interstitial sites respectively (space group 166, O 6c sites, Li 3a sites, Co 3b sites). The  $\text{Co}^{3+}$  and  $\text{O}^{2-}$  are arranged in a sheet-like manner and the lithium ions locate between the sheets of  $\text{CoO}_2$ . This sheet-like structure is observed in Fig. 2.1. LCO also has a theoretical specific capacity of 270 Ah/kg [1] and a voltage potential vs.  $\text{Li}^+$  of around 3.9V[2]. In comparison, the cathode material LMO, has a similar voltage difference vs.  $\text{Li}^+$  at around 4V, a lower specific capacity of around 110 Ah/kg, and a stable spinel-like crystal structure under reduction and oxidation reactions.

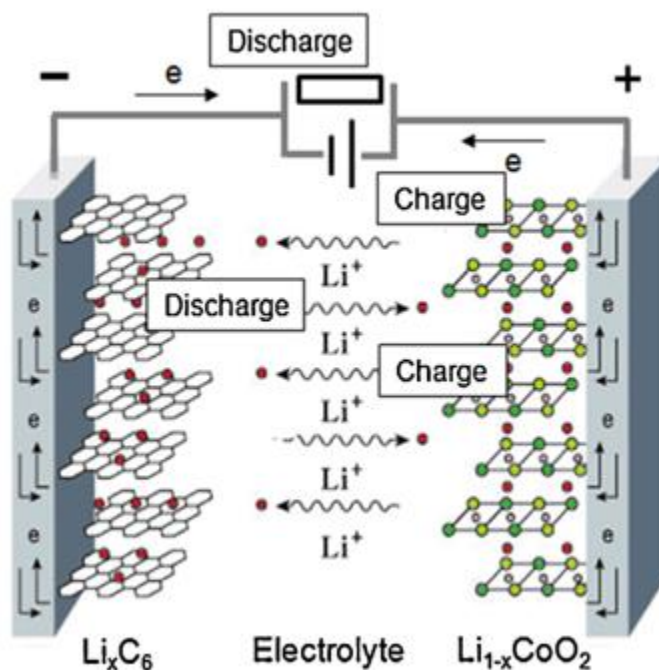


Figure 2.1 Schematics of a rechargeable Li-ion battery. The anode,  $\text{Li}_x\text{C}_6$  is depicted on the left side of the figure, whereas the cathode,  $\text{Li}_{1-x}\text{CoO}_2$  is shown on the right section. The transport of Li ions between anode and cathode is also depicted [3].

Unfortunately, these intercalation cathode materials can undergo exothermic reactions at a critical temperature, where oxygen is released and thermal runaway occurs. If not controlled, this reaction can result in an explosion of the battery. There are several examples of this happening since 2013, resulting in injury and great financial damage to the manufacturer. Some examples are shown in Table 2.1.

Table 2-1. Examples of Li-ion failure in different devices.

Company	Product	Year	Event
<b>Toshiba Panasonic</b>	Li-ion battery	2016	Overheating/melting
<b>Samsung</b>	Galaxy Note 7	2017	Fire/explosions
<b>Tesla</b>	Model 3	2019	Fire/explosions

Ideally, lithium metal should be used as an anode, however, it is chemically unstable against most electrolyte materials, and often results in dendrite formation resulting in short-circuiting of the battery and potential explosions. The most popular anode material today is graphite, as the lithium ions can be intercalated between two-dimensional carbon planes, allowing storage of 1 Li-ion per 6 atoms of carbon. Graphite has a lithiation and delithiation potential of around 0.15V, and a theoretical specific capacity of around 300 mAh/g. A major drawback of using graphite is its volumetric change upon lithiation/delithiation, which has a considerable impact on both the design phase of the battery, and the long-term life cycling of the battery. At the interphase of graphite and the electrolyte, a solid electrolyte interphase (SEI) forms, which is made up of reaction products arising from chemical interactions between the anode materials and the liquid electrolyte components during the the operation of the battery. The reaction products of the SEI are mostly lithium carbonate ( $\text{Li}_2\text{CO}_3$ ), lithium alkyl carbonate, lithium alkyoxide. The SEI microstructure and thickness can have beneficial attributes, if the interphase that forms on initial lithiation of the anode, forms a porous microstructure that allows for free lithium ions to travel through (the interphase itself is not ionically or electrically conductive[4]).

The electrolyte used in commercial lithium-ion batteries is comprised of two components, an organic solvent and a lithium salt. There are some guidelines in the selection of appropriate lithium salts. A larger anion leads to increased solvation and the generation of more free cations. The reaction products of the salt and the organic solvent also need consideration, as they can have a negative impact when interacting with anode ( $\text{LiBF}_4$ ) or with the cathode current collector ( $\text{LiTFSI}$ ) materials. Finally, safety and environmental concerns need to be addressed, as  $\text{LiAsF}_6$  is poisonous, and a popular salt,  $\text{LiClO}_4$ , is explosive. The most common salt used today is  $\text{LiPF}_6$ ,

which can decompose to form HF, a very dangerous acid, and highly reactive with the cathode and anode materials.

The organic solvent is generally an admixture of ethyl carbonate (EC), dimethyl carbonate (DMC) and ethyl methyl carbonate (EMC). The solvent is chosen based on several criteria: 1) solvent polarity, higher polarity increases the ionic conductivity through more solvation of the salt; 2) thermal stability over a wide range of temperatures, as batteries must have good ionic conductivity through the operating temperature of the device; 3) safety of the electrolyte. Figure 2.2 shows a diagram of how transport of Li ion occurs in the electrolyte. The chemo-physical properties of these solvents present constitute a major safety hazard: ethyl carbonate and the organic solvents used, are flammable. Physical damage of the battery cell (high impact, rupture), thermal runaway of the cathode, or shorting of the cell through dendrite formation, will result in an explosion.

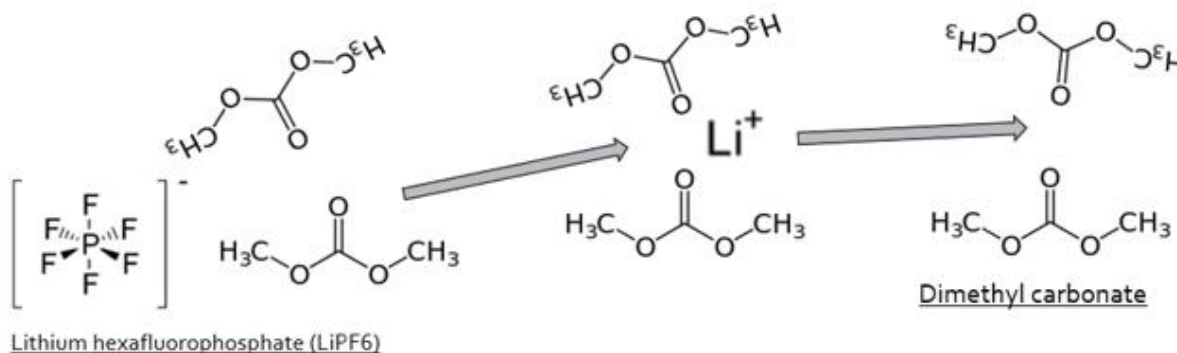


Figure 2.2 Li-ion conduction in a liquid electrolyte: the organic solvent dimethyl carbonate (DMC) serves as the transport medium for Li ions between hexafluorophosphate anions.

It is a challenge to choose a new electrolyte that can be used with current cathode and anode materials, as the combination of current organic solvent and salt is versatile and uncomplicated to implement in the manufacturing of lithium-ion batteries. A material that can adequately replace organic solvents must[5]: have ionic conductivity over  $10^{-4}$  S/cm and electronic conductivity less than  $10^{-10}$  S/cm, it must operate over a wide temperature range, and the interface between electrolyte and electrode materials must not degrade on charge and discharge of the battery. A great amount of research has been done into finding a good substitute for the electrolyte

combination we broadly use today. Ionic liquids for example, are good options for substitution, but their inherent low ionic conductivity drives researchers to add small amounts of organic solvents like EC or DMC to the electrolyte system. This has the added effect of stabilizing a SEI on the anode, which was unstable before the addition of EC or DMC. The two main solid electrolytes reviewed in this work as viable options to replace organic solvent electrolytes are solid polymer, composite polymer electrolytes, and inorganic solid state electrolytes.

Solid polymer electrolytes (SPE) are an interesting option, as they can act both as separator and electrolyte medium. They are also not flammable, are chemically stable and can form good contacts with cathode and anode materials. Unfortunately, their ionic conductivity is very low at room temperature ( $\sim 10^{-7}$  S/cm) thus, they are not viable options. Some of the polymers that have been investigated are poly ethylene oxide (PEO), polyvinylidene fluoride (PVDF), polyacrylonitrile (PAN). However, adding fillers to these SPE, has been found to increment their ionic conductivity by 2 or even 3 orders of magnitude, thereby approaching the range of accepted ionic conductivity for battery devices.

Inorganic solid-state electrolytes (SSE) is a materials class currently very actively investigated backed by large financial investments from battery manufacturers to develop viable fabrication and integration procedures for their commercial utilization. This type of electrolytes are single ion conductors, meaning, the only mobile ion in the material is  $\text{Li}^+$  and the anions and other cations are set in the crystal structure. This provides chemical stability with cathode and anode materials, as anions are not available for side reactions that result in ionic resistance increments. There are a variety of lithium SSEs, such as sulfide glasses, perovskite garnets, NASICON and LISICON-type materials. In general, their ionic conductivity is high, and are reported to reach values  $> 10^{-4}$  S/cm at room temperature. SSEs are also generally chemically stable with cathode and anode materials across a wide range of operating temperatures and voltages. The main challenge for implementing SSEs into battery devices relates to the interface between the electrolyte and electrode materials. As the battery discharges or charges, anode volume variation can degrade interface properties such as adhesion, greatly increasing the resistance for ionic conduction. A condensed summary of the main characteristics of the solid electrolytes mentioned thus far is given in Table 2.2. In this work we focus on the perovskite garnet, lithium lanthanum

zirconium oxide (LLZO). The main advantages of LLZO are chemical stability with Li metal, electrochemical stability across a wide voltage range and high ionic conductivity.

Table 2-2 Main types of solid state electrolytes. Table compiled from [6]

Solid Li electrolyte	IC (25°C)	Electrochemical stability	Elastic modulus
<b>Li<sub>2</sub>S-P<sub>2</sub>S<sub>5</sub></b>	0.3 to 3x10 <sup>-3</sup> S/cm	1.71 to 2.31V	18 to 25 GPa
<b>LLZO</b>	~0.8x10 <sup>-3</sup> S/cm	0.05 to ~3V	~150 GPa
<b>PEO:Li salt</b>	0.001 to 0.1 <sup>-3</sup> S/cm	~5V	~0.1 GPa
<b>LiPON</b>	~0.001	0.68 to 2.63	~77 GPa

## 2.2 Li<sub>7</sub>La<sub>3</sub>Zr<sub>2</sub>O<sub>12</sub> (LLZO) Solid-state electrolyte

LLZO is a single Li-ion conducting oxide, with two polymorphs, and it stabilizes into both a tetragonal and cubic crystalline structure. It has several attractive qualities for implementation in Li-ion batteries, such as electrochemical stability from 0V to 3V, chemical stability with Li metal, and in the case of the cubic phase LLZO, a high ionic conductivity of around 10<sup>-4</sup> S/cm. LLZO synthesis and characterization was first reported by Murugan *et al*[7] in 2007. Stabilizing the cubic phase however required high temperatures, typically in the range of 1000°C to 1100°C. Doping LLZO has the effect of stabilizing the cubic phase at lower temperatures, with some groups reporting stabilization of cubic LLZO with calcination temperatures of 900°C, 750°C and in our work, as low as 705°C when doping with Bi. In this chapter, a short summary of the synthesis methods employed to obtain cubic phase LLZO is provided, followed by a review of the ionic transport mechanism, and its dependence on site dopants and unit cell cubic lattice parameter changes resulting from doping.

### 2.2.1 Synthesis of LLZO

LLZO has been synthesized mainly through solid state reaction methods. Table 2.3 shows a small sample of doped versions of LLZO, and synthesis conditions. The main procedure for these methods generally include milling the precursor materials, grinding down the particle size, adding a second milling period at a higher temperature, and finally calcination at high temperatures that range from 750°C to 1100°C. The main advantages of solid state reaction synthesis are the ability to obtain a higher yield of product and the simplicity of the process. Using these dry-milling methods can take 12 to 24 hours to synthesize compounds, for example, 900°C for 12h for Nd-

doped LLZO[8], 1100°C for 12h for Ta-doped LLZO[9], or 1000°C for 4h for Ga-doped LLZO[10].

Table 2-3 Examples of LLZO Synthesis.

Doped	Author	Synthesis	Sintering	ICx10 <sup>-4</sup> S/cm	Ref.
Ca, 0.2	Hanc	SSR 700-900°C, 12h	1100°C, 12h	0.4	[8]
Nb, 0.2	Hanc	SSR 700-900°C, 12h	1100°C, 12h	0.3	[8]
Nd,0.2	Hanc	SSR 700-900°C,12h	1100°C, 12h	0.35	[8]
Ta, 0.5	Baek	900°C6h+1100°C,12h	1130°C, 36h	13.5	[9]
Ga, 0.25	Wolfenstine	Wet-mill 1000°C,4h	HP, 1000°C, 1h	3.5	[10]
NA (tetra)	Kokal, Somer	Sol-gel, carbonates	700-900°C, 5h	0.00312	[11]
Al, 0.24	Rangasamy	Milling 4h 1000°C	1000°C, 1h	4	[12]
Al, 0.3	Hu <i>et al</i>	wet milling 24h	900°C, 12h	2.11	[13]
Al, 1.2%wt	Jin, McGinn	Sol-gel, 900°C, 6h	1200°C, 6h	2	[14]
Ga, 0.25	Wu	SS reaction,900°C, 6h	1100°C, 24h	14.6	[15]
Ta, 0.3	Wang	Milling, 900°C, 10h	900°C, 36h	9.6	[16]
Ge, 0.1	Brugge	Sol-gel, nitr, 800°C, 12h	1150°C, 6h	2.8	[17]
Ce, 0.4	Rangasamy	1000C, 4h	HP, 1050°C, 1h	0.14	[18]

Beginning in 2012, sol-gel methods have been utilized to synthesize LLZO. The main advantages of using a sol-gel processing are: precise control of sample stoichiometry, lower synthesis temperatures and much shorter reaction times are needed. For example, Kokal *et al*, utilized sol-gel synthesis of tetragonal LLZO[11]. In their work, lithium and lanthanum carbonates were used as precursors and dilute nitric acid was used as solvent; citric acid and ethylene glycol were used as metal-citrate chelating complexes. For the calcination step they used a range of temperatures, from 700°C to 900°C for 5h. Jin *et al* used nitrates as precursors in a sol-gel method to prepare Al-doped LLZO[14], using a calcination temperature of 900°C, for 6h. Brugge *et al* also used a sol-gel method with nitrates as precursors to prepare a germanium-doped cubic LLZO[17]. For the calcination step they used a temperature of 800°C for 12h.

Seen in figure 2.3, are the main reactions involved in the Pechini method, a sol-gel oxide synthesis method that uses nitrate salts as precursors. This method is the one employed in this work to synthesize doped and co-doped LLZO. Two main reactions occur. The first one is chelation by mixing citric acid with the dissolved nitrate salts of lithium, lanthanum and zirconium. The second reaction is a polyesterification reaction, this happens when ethylene glycol is added, and the chelates cross-link and create a white, sticky gel. This sticky gel can be semi-pyrolized to obtain precursor powders, and a mortar and pestle can be used to create a more homogeneous particle size. Finally, the precursor powder is calcinated at high temperatures (above 500°C), burning off all the organic matter and leaving particles of the mixed cation oxide, LLZO.

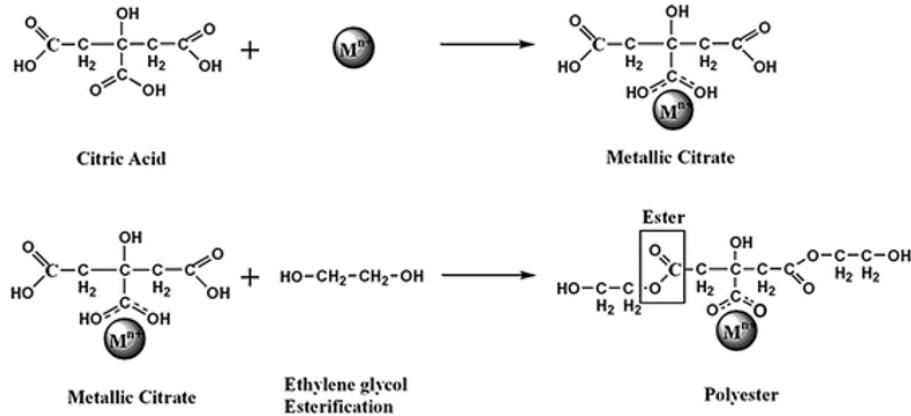


Figure 2.3 Main reactions in the Pechini method. Cations like  $Li^+$ ,  $La^{3+}$  and  $Zr^{2+}$  are represented by  $M^{n+}$ . Diagram reproduced from ref[20].

### 2.2.2 Li-ion transport mechanism in LLZO

Cubic phase LLZO belongs to the garnet family type  $A_3B_2C_3O_{12}$ , with 8-coordinated  $La^{3+}$ , 6-coordinated  $Zr^{4+}$ , and  $Li^+$  occupying tetrahedral and octahedral sites in the unit cell. Octahedral and tetragonal  $Li^+$  sites arise from the formation of edge-shared dodecahedron ( $LiO_8$ ) and octahedron ( $LaO_6$ ) structures in the unit cell. The high ionic conductivity of LLZO derives from the fact that all lithium sites (tetrahedral and octahedral) are partially occupied. In the tetragonal form of LLZO, both site types are fully occupied, and a third site that exists in the tetragonal phase LLZO (another octahedral site) is fully empty. Figure 2.4 shows the cubic phase unit cell, and the pathway Li-ion takes on charge and discharge.

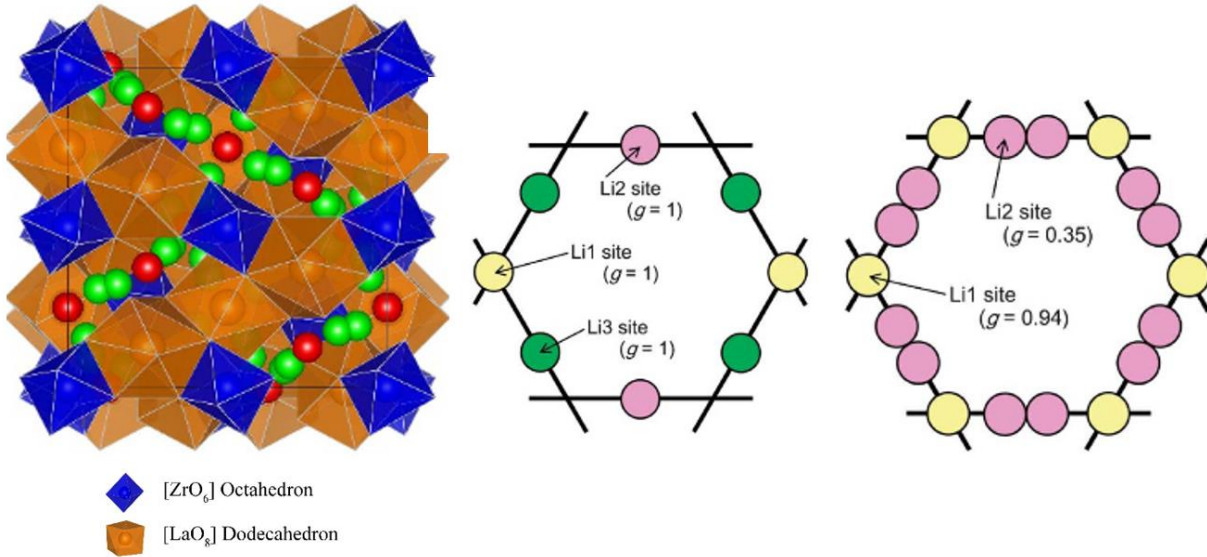


Figure 2.4 Crystal structure of cubic LLZO. The green and red spheres represent Li sites. Li-ion sub-lattice in LLZO for (b) tetragonal and (c) cubic phase. Image from[21].

Li-ion diffusion is driven by the low energetic cost of hopping from tetragonal to octahedral, and octahedral to octahedral sites. Meier *et al* determined from first-principle calculations that Li<sup>+</sup> ion diffusion happens through single-jump events[22]. From the same work, it was determined that increasing the Li<sup>+</sup> ion vacancies in the unit cell can increase ionic conductivity, by increasing the number of available sites for single Li<sup>+</sup> ion jumps. In fact, Li<sup>+</sup> ion migration happens mainly through a specific path, from a tetrahedral site to an octahedral site continuing to another tetrahedral site. Figure 2b and 2c shows the lithium ion sub-lattice for tetragonal and cubic phase LLZO. Notice that for the cubic phase, the distance between jumps is shorter and the lower occupancy for each Li site is lower.

Stabilizing the cubic phase has been the main objective of doping LLZO with various elements, this is due to the fact that the ionic conductivity of the cubic phase increases by two orders of magnitude when compared with that of the tetragonal phase. Dopants modify the LLZO unit cell, the degree of change is dopant-dependent, so it becomes of high interest to understand their role in terms of: their ionic radius, the site they occupy and how the addition of this cation maintains charge neutrality and changes the Li molar ratio.

Literature review indicates that there exists a relationship between the cubic phase lattice parameter of LLZO and its ionic conductivity. In general, a larger cubic lattice parameter is associated with an increase in ionic conductivity. When a doping cation is inserted into the unit cell, lattice constant is modified, altering also the bottleneck for diffusion of the  $\text{Li}^+$  ion pathway through the LLZO crystal structure. The bottleneck size is determined by three coplanar oxygen atoms made up of  $\text{Li}_2\text{O}_6$  and  $\text{LiO}_4$ . When a cation substitutes on Zr or La site, the bottleneck area is increased or decreased, because the O atoms are shared with the  $\text{Li}_2\text{O}_6$  and  $\text{Li}_2\text{O}_4$  polyhedrons. The bottleneck area change is dependent on the dopant ionic radius. Figure 2.5 shows the arrangement of  $\text{Li}_2\text{O}_6$  and  $\text{LiO}_4$  and how the bottleneck window for  $\text{Li}^+$  is altered by changing the ionic radius of cations sharing the  $\text{Li}_2\text{O}_6$  and  $\text{LiO}_4$  substructure.

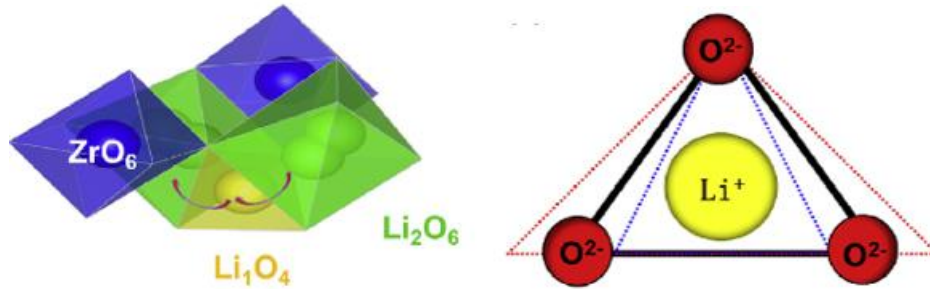


Figure 2.5  $\text{Li}^+$  ion migration bottleneck for the diffusion pathway. Red dashed lines indicate a broadening of the window, blue dashed lines indicate a tightened pathway. Figure from [23].

### 2.2.3 Li, Zr, La site substitution in LLZO

Most research on aliovalent substitution in LLZO has centered around the Zr site. Doping on the Zr site has the effect of stabilizing the cubic phase, as well as having a role in decreasing the sintering temperature and time. A propensity to sinter results in higher relative densification which in turn, determines the maximum value of ionic conductivity measurable in garnet pellet samples. To measure ionic conductivity, pellet samples of LLZO powder need to be prepared: powders are pressed at room-temperature, and then sintered at high temperatures ranging from  $900^\circ\text{C}$  to  $1200^\circ\text{C}$  for time periods ranging from 6h to 24h. Rangasamy *et al* used hot-pressing at 40MPa, at  $1000^\circ\text{C}$  for 1h, to obtain samples with 98% relative density. Thus, any materials

processing that can decrease the energy needs to obtain fully densified samples is important to reduce their fabrication costs.

Doping on the Li-site has also been extensively explored. The first doped-LLZO was reported by Murugan *et al*, for the case of Al cations[24]. The mechanism behind the increase of ionic conductivity is that by maintaining charge neutrality created by  $\text{Al}^{3+}$ ,  $\text{Li}^+$  ion vacancies are created, creating disorder in the Li sub-lattice. A relationship between molar lithium concentration and ionic conductivity has been established. Rangsamy *et al* varied the Al dopant in cubic LLZO, and found an optimal amount of Al before the ionic conductivity started to decrease[12]. Their work reveals that, for a certain concentration, a minimal amount of Al is necessary to stabilize the cubic phase. Above a certain concentration, Al solubility in cubic LLZO is exceeded and a second phase is formed, decreasing the bulk ionic conductivity. A similar trend was observed in the work of Wu *et al*, where the molar concentration of Ga was varied from 0.1 to 0.4[15]. The ionic conductivity exhibits a maximum for a Ga molar concentration of 0.25 which decreases for higher concentrations.

La-site substitutions are less explored compared to work with Zr and Li site substitution, and it has been shown to have a greater effect on the crystal structure of LLZO. Most of the work done with La site substitution has been done in co-doping studies, investigating the effect of Ga and Rb[25] (Ga substituting on Li and Rb substituting on La), and the effect of doping with Ca and Ta[26] (Ca substituting on La and Li, and Ta substituting on Zr and Li). As of this writing, and to the best of the author's knowledge, only one single dopant site substitution has been published, done by Hanc *et al*[8]. In the work of Hanc *et al*, Nd was chosen to substitute on the La site, having a negative effect on the ionic conductivity. The reduction in ionic conductivity was observed together with a decrease in cubic lattice parameter, due to a lower ionic radius for Nd when compared to La.

Co-doping cubic-phase LLZO is a subject less explored, but an important avenue of research that lead to potential improvements of its ionic conductivity. For example, doping LLZO on the  $\text{Zr}^{4+}$  site with  $\text{Ta}^{5+}$  is understood to increase ionic conductivity by creating lithium vacancies and promoting sintering. Co-doping the same LLZO with  $\text{Ca}^{2+}$ , adds lithium back to the sublattice, thus providing a way of modifying the crystal structure to increase ionic conductivity. Chen *et al*

achieved a bulk ionic conductivity of  $7.43 \times 10^{-4}$  S/cm for a  $\text{Li}_{6.45}\text{Ca}_{0.05}\text{La}_{2.95}\text{Ta}_{0.6}\text{Zr}_{1.4}\text{O}_{12}$  pellets compared to  $1.19 \times 10^{-5}$  S/cm for an undoped-LLZO. A small sample of these investigations are summarized in Table 2.4.

Table 2-4 Examples of co-doped LLZO investigations.

Co-doped	Author	Synthesis	Sintering	IC $\times 10^{-4}$ S/cm	Ref.
Nb,0.5, Y,0.5	Gai <i>et al</i>	SSR, 900°C, 8h	1230°C,15h	8.29	[27]
Al,0.05, Sb,0.075	Yang	SSR, 900°C, 6h	1170°C, 6h	4.1	[28]
Ta,0.6, Ca, 0.05	Chen	750°C, 8h	1125°C, 6h	4.03	[26]
Ga,0.3, Rb,0.05	Wu	SSR, 900°C, 6h	1100°C, 24h	16.2	[25]

There is consensus from numerous reports that there is an optimal value of lithium molar ratio in LLZO. The cubic lattice has a maximum value of Li molar ratio of 7.5. Comparison of ionic conductivity measurements in doped-LLZO indicate that the highest values are obtained for a lithium molar ratio 6.25 to 6.75. This is shown in figure 2.6. This figure as well as figure 2.7 was obtained from published results compiled from references listed at the end of this chapter. It is also apparent that broadening the pathway for Li diffusion by altering the cubic lattice parameter also increases ionic conductivity. This is consistent with figure 2.7, where a slight relationship between lattice constant and ionic conductivity can be observed.

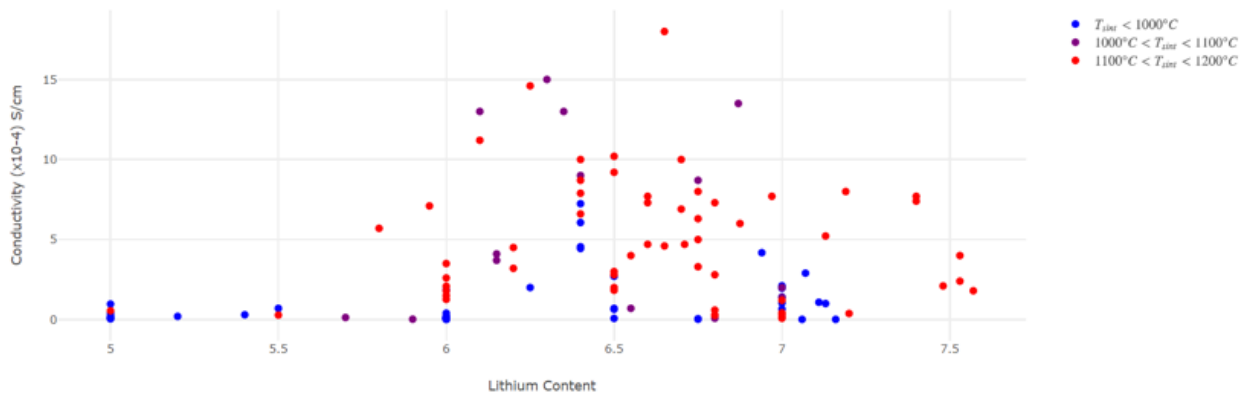


Figure 2.6 Ionic conductivity for doped LLZO in terms of molar Li.

The effect of dopants on LLZO ionic conductivity has been widely investigated. However, comparison of results is complicated by the differences in their relative densities resulting from process sintering temperatures and protocols. Relative density plays a large role in determining ionic conductivity in LLZO pellets. This will be addressed in in chapter 2.

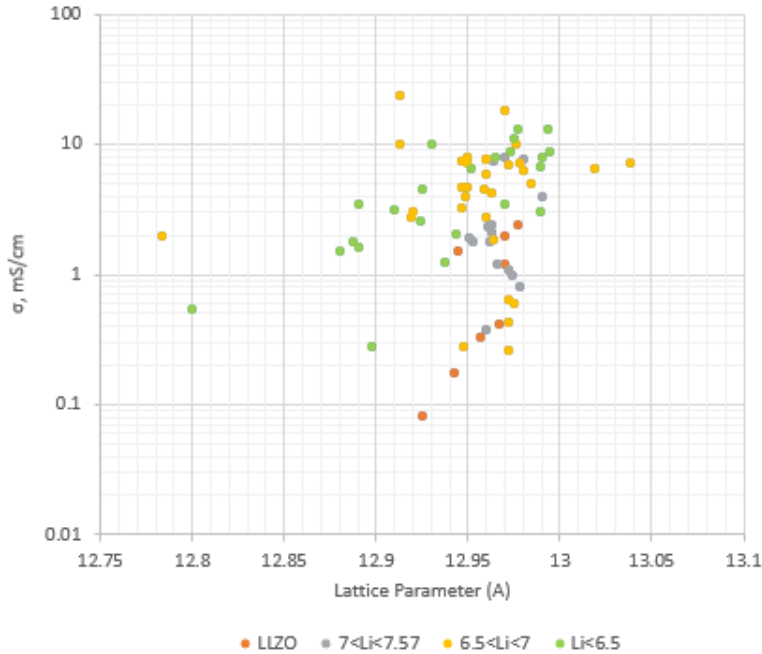


Figure 2.7 Ionic conductivity for doped LLZO as a function of cubic lattice parameter.

### 2.3 Polymer composite electrolytes

Polymer electrolytes could potentially replace organic solvent electrolytes. They are electrochemically stable across a wide voltage range, they are cheap to produce, chemically stable against Li metal and non-flammable. Furthermore, a polymer electrolyte doubles as a separator. There are a variety of polymer electrolyte types, based on the component added to a polymer:salt system. Agrawal divided them into five categories[29]: dry polymer electrolytes, plasticized polymer electrolyte and polymer gel electrolyte, rubbery electrolytes and composite polymer electrolytes or polymer composite electrolytes (PCEs). A brief review of dry polymer electrolytes is provided, followed by a discussion of polymer composite electrolytes, in particular, on the effect composite ingredients on ionic conductivity.

### 2.3.1 Poly Ethylene Oxide (PEO) as a matrix for PCE

Poly-ethylene oxide (PEO) is a polymer electrolyte with a -C-C-O- structure. PEO's usage as an electrolyte dates back to 1973, when Fenton reported a PEO-based electrolytes with sodium and potassium salts[30]. Although no ionic conductivity was reported, some basic characterization was performed. Spherulite growth was observed, X-ray characterization and infrared spectra were obtained. Additionally, it was reported that the ether oxygen on the polymer chain interacts with the metal cation, and that ionic conductivity increases as the amorphous fraction increases.

Since then, a variety of polymer complexes have been investigated as possible lithium ion electrolytes. Some examples of these polymers are poly[bis((methoxyethoxy)ethoxy)-phosphazene] (MEEP), polyacrylonitrile (PAN), poly(propylene oxide) (PPO), polyvinyl acetate (PVAc). The highest ionic conductivity has been recorded for PEO-based electrolytes. The higher value for ionic conductivity in PEO and PPO is believed to be due to the ether oxygen's ability to break the bonding energies of the added metal salts yielding cations and anions. PEO can form complexes with cations such as  $\text{Li}^+$ . Cation transport happens when these bonds are broken and the cation forms new complexes with ether oxygens of the polymer chain or with adjacent polymer structures. Figure 2.8 shows the PEO complexation with a cation.

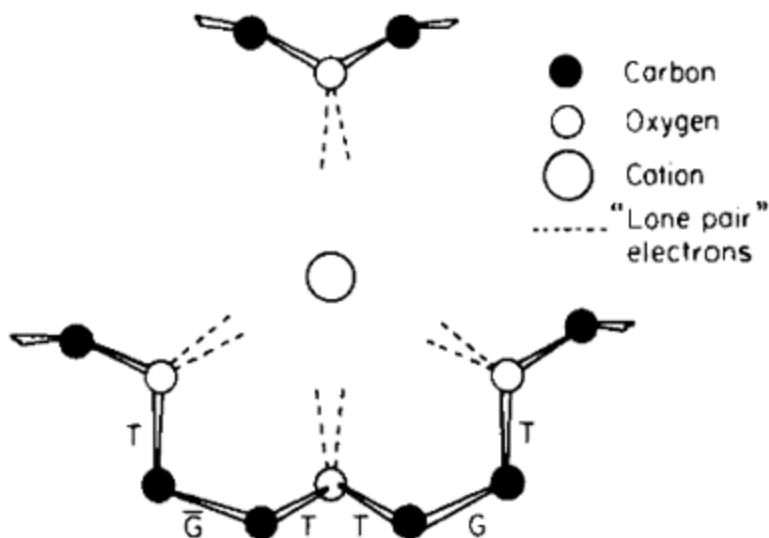


Figure 2.8 Schematic of poly ethylene oxide complexation with metal cations. Reproduced from [31].

Integration of polymer electrolytes in Li-ion batteries requires the correct choice of Li salt to increment ionic conductivity. The next sub-section addresses considerations on selecting Li salts.

### 2.3.2 PEO with different Li salts

A variety of lithium salts have been tested with PEO to identify the best cation-anion pair in terms of ionic conductivity. In a paper by Rietman *et al*[32], different lithium salts were prepared with PEO ( $5 \times 10^6$  g/mol). The EO to Li ratio was kept at 4.5. In their work the salts that better performed in the temperature range  $54^\circ\text{C}$  to  $83^\circ\text{C}$  were  $\text{LiBF}_4$ ,  $\text{LiNO}_3$ ,  $\text{LiClO}_4$  and  $\text{LiPF}_6$ . The PEO:Li-salt systems exhibit Arrhenius behavior at temperature below and above the melting point of the admixtures [33]. The differences in ionic conductivity for the salts studied were ascribed to changes in anion size, which reduces the energy required to break cation-anion pairs[34]. Figure 2.9 shows Arrhenius plots for different PEO:salt complexes. Note the two temperature ranges, for example, for the PEO complexes with  $\text{LiH}_2\text{PO}_4$ ,  $\text{LiCF}_3\text{SO}_3$  and  $\text{LiClO}_4$ .

Next the optimal EO:Li ratio for ionic conductivity is addressed. The PEO: $\text{LiPF}_6$  system was investigated by Magistris *et al*, in their work the  $\text{LiPF}_6$  molar content was varied in PEO

(MW $4 \times 10^6$ )[35]. The ionic conductivity increased with salt content, and it reached a maximum value for a EO:Li ratio of 30, at around  $10^{-8}$  S/cm. At a lower EO:Li ratio, the ionic conductivity of the system decreased.

In another study, LiClO<sub>4</sub> was added to PEO (MW=5 $\times 10^6$ )[36]. The same increase and subsequent decrease in ionic conductivity was observed compared with the PEO:LiPF<sub>6</sub> system. In this case, an ionic conductivity maximum was observed for a EO:Li ratio of 6, and started to decrease with a lower EO:Li ratio. A similar study[37] was performed with another with PEO (4 $\times 10^6$ ) and LiBF<sub>4</sub>, where the EO:Li ratio was varied between 98 to 2. Similar to the PEO:LiClO<sub>4</sub> and PEO:LiPF<sub>6</sub> systems, adding LiBF<sub>4</sub> to PEO results in an initial increase in ionic conductivity, reaching a maximum room temperature value at  $\sim 10^{-6}$  S/cm for a EO:Li ratio between 4 and 6, and decreasing substantially with a lower EO:Li ratio.

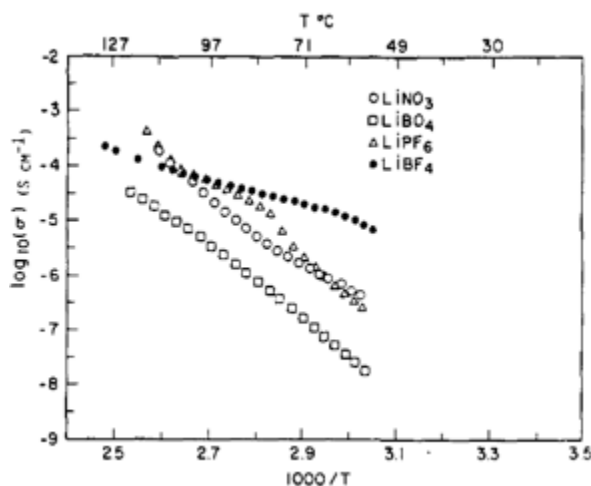


Figure 2.9 Arrhenius plots for PEO:Li-salt electrolytes [EO:Li=4.5] for different anions. Figure from [32].

Based on these results, the ideal cation-anion bond must be readily broken meaning, having the largest anion possible. Furthermore, the optimal ratio must be experimentally determined. LiTFSI is an ideal candidate to use as a Li salt, as it fulfills this requirement and disassociates easily in moderate polymeric solvents[38]. However, the room temperature ionic conductivity of  $10^{-6}$  S/cm for the best PEO:salt system reported is not competitive for battery applications. The addition of fillers is known to enhance the performance of solid polymer electrolytes. The

following sub-section will review what type of fillers have been used, how they improve ionic conductivity, and the main mechanisms responsible for these improvements.

### 2.3.3 Effect of passive fillers on Solid Polymer Electrolytes

Around the mid-90's, research began on the addition of fillers to polymer electrolytes. The first fillers employed were passive fillers, implying that the filler material does not conduct lithium ions. Depending on the concentration and type, the filler had the effect of increasing the ionic conductivity by an order of magnitude while improving the mechanical stability of the PCE sample film. For example, in Wieczorek's work[36], Al<sub>2</sub>O<sub>3</sub> particles were added to a PEO (MW=5x10<sup>6</sup>):LiClO<sub>4</sub> system. An increase of an order of magnitude of the specific ionic conductivity at room temperature, was obtained with an added Al<sub>2</sub>O<sub>3</sub> specific concentration of 1.73 mol/kg.

In the work of Sun *et al*, BaTiO<sub>3</sub> was added to PEO(MW=6x10<sup>5</sup>):LiClO<sub>4</sub>, and its electrochemical properties characterized[39]. The EO:Li ratio tested was 8 and 16. With an added 5% wt of 1.8um BaTiO<sub>3</sub>, the room temperature ionic conductivity increased by more than order of magnitude to ~10<sup>-5</sup> S/cm. An important observation made in this work is that at room temperature the increase in ionic conductivity performance is substantial, but at temperatures above the PEO:LiClO<sub>4</sub> melting temperature, the ionic conductivity improvement is lessened. The authors explain that above the melting temperature, the polymer amorphous fraction drives ionic conduction. Furthermore, electrostatic interaction between particles and lithium salt could further salt disassociation, increasing the number of free Li<sup>+</sup> ions. Reducing the BaTiO<sub>3</sub> particle size to a range of 0.6 to 1.2 um, the same effect was observed, but with only a filler amount of 1.4% wt instead of 5% wt. The authors speculate that the shift in optimal weight load could be related to the polarization of the ferroelectric particles, however, they conclude that the dielectric constant of the particle does not determine the shift in optimal weight load[39].

Similarly, in work done by Pitawala *et al* [40], a PCE was prepared by adding Al<sub>2</sub>O<sub>3</sub> to PEO:LiTf (MW=4x10<sup>6</sup>), with a EO:Li ratio of 9. The ionic conductivity at 25°C increased by 2 orders of magnitude, from 2x10<sup>-7</sup> S/cm to 2x10<sup>-5</sup> S/cm with an added 15% wt of Al<sub>2</sub>O<sub>3</sub>. The ionic conductivity increases with a low weight load of filler particles, reaches a high point at 15% wt, and starts to decrease reaching a level on par with a 0% wt load.

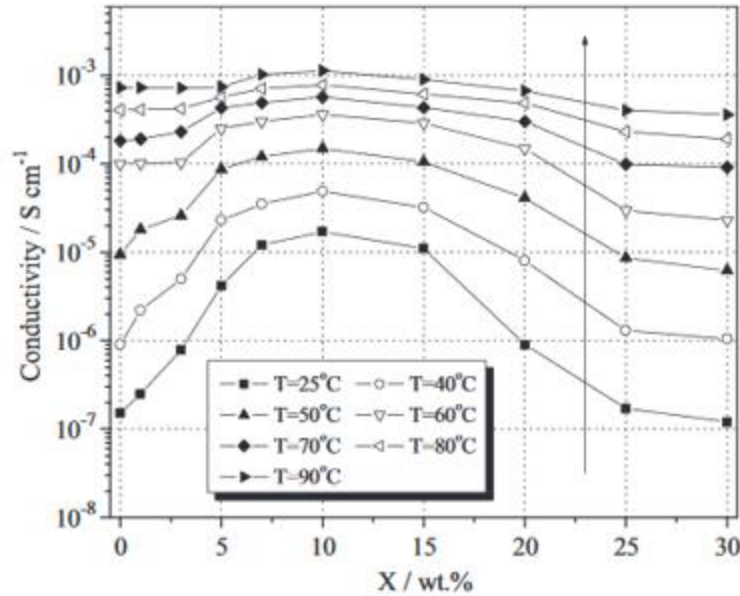


Figure 2.10 The effect of weight load vs ionic conductivity for a SBA-15 mesoporous silica + PEO:LiClO<sub>4</sub> PCE. Figure reproduced from [41].

In Xi *et al*'s work, SBA-15 mesoporous silica was added to a PEO(MW=1×10<sup>6</sup>):LiClO<sub>4</sub> with a EO:Li ratio of 12 and analyzed [41]. Similar to the PCE with PEO:LiTf + Al<sub>2</sub>O<sub>3</sub>, the ionic conductivity increased from ~1×10<sup>-7</sup> S/cm to 2×10<sup>-5</sup> S/cm at 25°C with an addition 10% wt of the mesoporous silica. An increase of ionic conductivity of one order of magnitude with just 5% wt, it reaches a high point at 10% wt, and then decreases at 30% wt to the value with no added filler. The effect of weight load vs ionic conductivity at different temperatures is shown in figure 2.10.

In none of the reports on the effect of passive fillers, an explanation is offered to explain the optimal weight load dependence on the nature of the filler. Croce *et al* offers an explanation in their 2001 paper [42]. The authors cast PEO:LiCF<sub>3</sub>SO<sub>3</sub> films, with a EO:Li ratio of 20, with an added filler of 10% wt of Al<sub>2</sub>O<sub>3</sub>. Acidic, neutral and basic versions of Al<sub>2</sub>O<sub>3</sub> were used in this study. The authors propose that a filler prevents reorganization of PEO chains, and that Lewis acid-base interactions on the surface of the filler particle further promotes disassociation of the lithium salt, increasing the concentration of free ions in the polymer matrix. Thus, the interactions at the particle surface are specific to each filler, and the manipulation of the surface, by either changing the chemistry or surface area, directly impacts ionic conductivity. To further elucidate this point, in

the next sub-section a review of PCE with active fillers and their differences from passive ones is provided.

### 2.3.4 Effect of active fillers on Solid Polymer Electrolytes

PCE research in the 2000s has focused around adding different fillers to increase the average amorphous fraction of the PCE. During this decade, research groups started to add active fillers to the polymer:salt system; an active filler being a filler capable of conducting lithium ions. Additionally, XRD characterization has been used to provide information on crystallinity changes in the PCEs to correlate them to ionic conductivity.

Zhu *et al* experimented adding the active filler  $\text{Li}_{0.33}\text{La}_{0.55}\text{TiO}_3$  (LLTO) to a PEO:LiTFSI solid polymer electrolyte[43] via a casting method. The fabricated films with a load of 15%wt of LLTO nanowires register more than an order of magnitude increase in ionic conductivity compared to the PEO:LiTFSI polymer electrolyte. The samples with the highest amorphous fraction in the polymer matrix, shown through the depression of characteristic peaks for crystalline PEO in an XRD scan, corresponds to this weight load. The authors note that the better performance is due to both the slowing down of the recrystallization kinetics, and the formation of ionic pathways for the lithium ions, promoted by the aspect ratio of the LLTO nanowires. It is hypothesized that the filler weight load that leads to a higher amorphous fraction, results in higher ionic conductivity. However, this is not always the case, indicating that there are other factors leading to optimal ionic conductivity.

For example, Hu *et al* added lithium titanate ( $\text{LiAlO}_2$ ) to a PEO (MW=300,000): $\text{LiClO}_4$  complex [44], keeping the EO:Li ratio at 16. By adding 15%wt of  $\text{LiAlO}_2$ , the ionic conductivity increased more than two orders of magnitude, from  $1 \times 10^{-7} \text{S/cm}$  to  $\sim 2 \times 10^{-5} \text{S/cm}$  at room temperature. It is noted by the authors that the addition of the filler decreased the  $T_g$  and crystallinity fraction, but made no comment why the sample with the lowest fraction does not correspond to the sample with the highest ionic conductivity. The increased performance is ascribed to the high surface area of the filler particle.

Tetragonal LLZO has been also used as an active filler in PEO-based PCEs[45]. Adding tetragonal LLZO increased the room temperature ionic conductivity more than 2 orders of

magnitude to  $10^{-5}$  S/cm compared to the sample without filler (PEO:LiClO<sub>4</sub>, at a EO:Li ratio of 15). In contrast to other works presented beforehand, Choi *et al* needed a 52%wt filler load to obtain this ionic conductivity. The authors do not comment on how the ionic conductivity is increased, or why a bigger weight load is needed compared with other active fillers available in the literature (the weight load vs ionic conductivity curve from Choi's work is shown in figure 2.11).

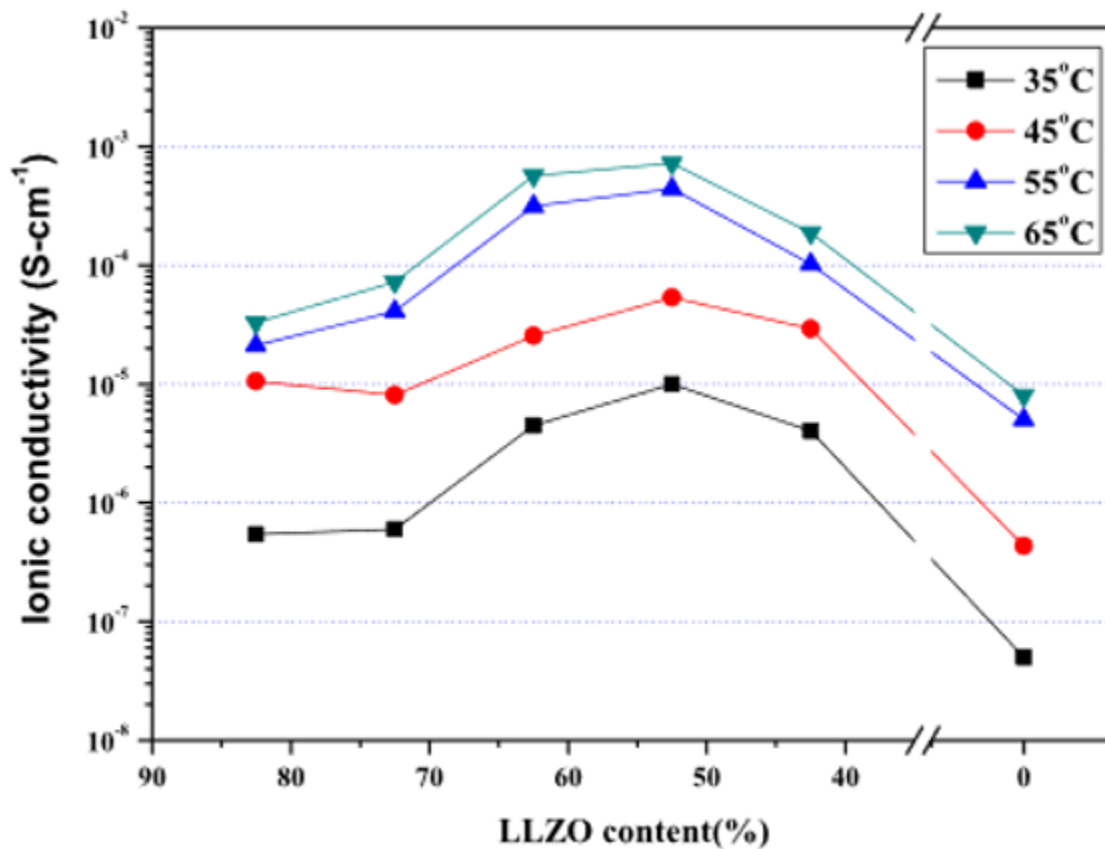


Figure 2.11 Weight load vs ionic conductivity at different temperatures for PEO:LiClO<sub>4</sub> system with tetragonal phase LLZO filler. Figure from ref [45].

In another study, Yang *et al*[46] fabricated nanowires of Al-doped LLZO, un-doped LLZO, and nanowires of Al<sub>2</sub>O<sub>3</sub>, and embedded them in a PAN:LiClO<sub>4</sub> matrix. They found that the LLZO-based PCEs outperformed the Al<sub>2</sub>O<sub>3</sub>-based samples, and that nanoparticles of LLZO performed worse than nanowires LLZO. The authors admit that it is unclear on why a weight load of 5%wt

is necessary for this high performance of  $10^{-4}\text{S/cm}$ , and why this optimal weight load changes according to the filler. This thesis work will address this unanswered question.

### 2.3.5 Ionic conduction mechanism in a PCE

Ionic conduction in a PCE system occurs by the dissolution of cation-anion pairs, and subsequent cation complexation with ether oxygens on the polymer chain.  $\text{Li}^+$  ions are transported along and between polymer chains. As the polymer phase starts to crystallize from the melt, polymer chains start to fold into lamellar structures of specific thicknesses. These lamellae are nucleated from a single site, forming a spherulite. The regions between lamellae are amorphous regions through which fast ionic transport occurs. Figure 2.13 shows a schematic representation of a lamellar structure, as well as how ions are transported between crystalline lamellar structures, through the amorphous phase. It is understood from the literature that an increase in amorphous fraction of the polymer electrolyte or polymer composite electrolyte, leads an increase in ionic conductivity. Hence, PCE materials research has centered around lowering the average crystalline fraction and on improvements of each component of the system: the polymer molecular structure, identifying superior lithium salts, and assessing passive and active fillers to improve ionic conductivity.

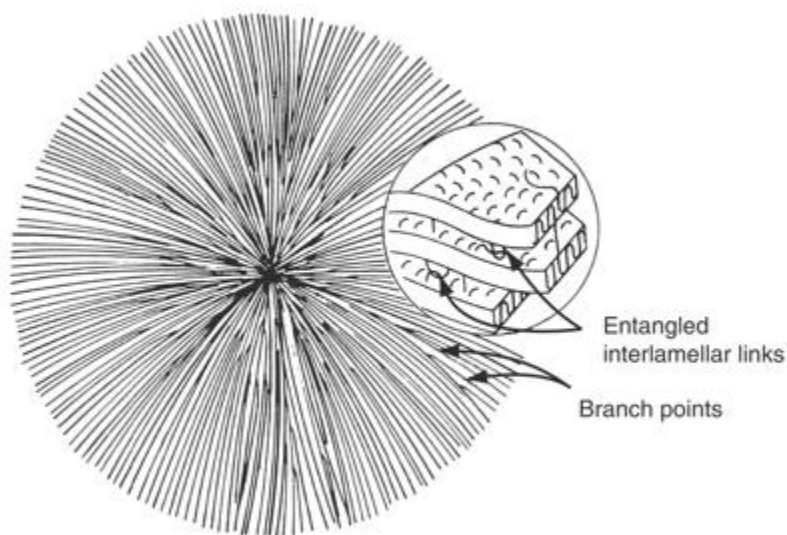


Figure 2.12 Schematic representation of a spherulite. Figure from ref [51].

There is evidence to suggest that there are other material properties that must be taken into account, besides the amorphous fraction. In Best's paper[47], the authors address a discrepancy in ionic conductivity results for their prepared samples, compared to other similar systems in the literature[48]. They measured ionic conductivities at elevated temperatures where the samples are fully amorphous, and they observe that a difference exists between unloaded samples and samples with filler particles. The difference in ionic conductivity cannot then be ascribed only to a larger amorphous fraction. The authors also analyzed Raman spectra for a poly-triol sample with  $\text{LiClO}_4$  with and without 10% wt  $\text{TiO}_2$ . They observed active modes at  $200\text{-}300\text{cm}^{-1}$ , and around  $530\text{cm}^{-1}$ , that could be attributed to longitudinal backbone motions and to salt- $\text{TiO}_2$  interactions. The authors conclude that the fillers not only depress the formation of the crystalline fraction, but also interact with the lithium salt, providing more free  $\text{Li}^+$  ions to the PCE system.

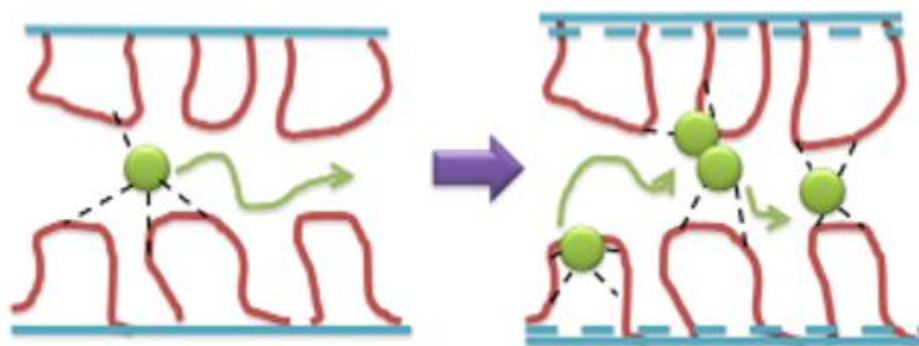


Figure 2.13  $\text{Li}^+$  transport through amorphous regions (red lines representing PEO loops) between spherulite lamellae (blue lines representing crystalline PEO). Green circles represent  $\text{Li}^+$  ions. Figure from[49].

The role of the polymer microstructure and spherulite formation on ionic conduction has recently been investigated by Li *et al*, they determined a strong correlation between ionic conductivity and  $\text{Li}^+$  ion path tortuosity[49]. The  $\text{Li}^+$  ion pathway is confined to the amorphous region between crystalline lamellae, this region consisting of loops anchored to the lamellae. Figure 13 shows a schematic representation of  $\text{Li}^+$  ion transport through amorphous regions between lamellae, figure 2.12 shows a formed spherulite. The authors conclude that at low salt concentrations, conductivity is determined by polymer crystal orientation and the interaction between  $\text{Li}^+$  and free EO sites.

Further evidence pointing towards a relationship between tortuosity arising from spherulitic formation, and ionic conductivity is observed in a paper by Fullerton-Shirey and Maranas[50]. A PEO:LiClO<sub>4</sub> polymer electrolyte was analyzed, the EO:Li ratio varied from 100 to 4, characterizing the crystalline fraction, and determining the lamellar spacing. Results show that the sample with the highest ionic conductivity does not correspond to the one with lowest crystalline fraction. It does correspond however, to the sample with the largest bilayer thickness (the amorphous region between lamellae). The authors speculate that the bilayer drives ionic conductivity, creating directed transport pathways for the Li<sup>+</sup> ions.

## 2.4 References

- [1] N. Nitta, F. Wu, J. T. Lee, and G. Yushin, “Li-ion battery materials: Present and future,” *Materials Today*. 2015.
- [2] G. E. Blomgren, “The Development and Future of Lithium Ion Batteries,” *J. Electrochem. Soc.*, 2017.
- [3] R. Hausbrand *et al.*, “Fundamental degradation mechanisms of layered oxide Li-ion battery cathode materials: Methodology, insights and novel approaches,” *Materials Science and Engineering B: Solid-State Materials for Advanced Technology*. 2015.
- [4] S. S. Zhang, “A review on electrolyte additives for lithium-ion batteries,” *Journal of Power Sources*. 2006.
- [5] J. B. Goodenough and Y. Kim, “Challenges for rechargeable batteries,” *J. Power Sources*, 2011.
- [6] D. Lin, Y. Liu, and Y. Cui, “Reviving the lithium metal anode for high-energy batteries,” *Nature Nanotechnology*. 2017.
- [7] R. Murugan, V. Thangadurai, and W. Weppner, “Fast lithium ion conduction in garnet-type Li(7)La(3)Zr(2)O(12).,” *Angew. Chem. Int. Ed. Engl.*, 2007.

- [8] E. Hanc, W. Zajac, and J. Molenda, "Synthesis procedure and effect of Nd, Ca and Nb doping on structure and electrical conductivity of  $\text{Li}_7\text{La}_3\text{Zr}_2\text{O}_{12}$  garnets," *Solid State Ionics*, 2014.
- [9] S. W. Baek, J. M. Lee, T. Y. Kim, M. S. Song, and Y. Park, "Garnet related lithium ion conductor processed by spark plasma sintering for all solid state batteries," *J. Power Sources*, 2014.
- [10] J. Wolfenstine, J. Ratchford, E. Rangasamy, J. Sakamoto, and J. L. Allen, "Synthesis and high Li-ion conductivity of Ga-stabilized cubic  $\text{Li}_7\text{La}_3\text{Zr}_2\text{O}_{12}$ ," *Mater. Chem. Phys.*, 2012.
- [11] I. Kokal, M. Somer, P. H. L. Notten, and H. T. Hintzen, "Sol-gel synthesis and lithium ion conductivity of  $\text{Li}_7\text{La}_3\text{Zr}_2\text{O}_{12}$  with garnet-related type structure," *Solid State Ionics*, 2011.
- [12] E. Rangasamy, J. Wolfenstine, and J. Sakamoto, "The role of Al and Li concentration on the formation of cubic garnet solid electrolyte of nominal composition  $\text{Li}_7\text{La}_3\text{Zr}_2\text{O}_{12}$ ," *Solid State Ionics*, 2012.
- [13] Z. Hu, H. Liu, H. Ruan, R. Hu, Y. Su, and L. Zhang, "High Li-ion conductivity of Al-doped  $\text{Li}_7\text{La}_3\text{Zr}_2\text{O}_{12}$  synthesized by solid-state reaction," *Ceram. Int.*, 2016.
- [14] Y. Jin and P. J. McGinn, "Al-doped  $\text{Li}_7\text{La}_3\text{Zr}_2\text{O}_{12}$  synthesized by a polymerized complex method," *J. Power Sources*, 2011.
- [15] J. F. Wu *et al.*, "Gallium-doped  $\text{Li}_7\text{La}_3\text{Zr}_2\text{O}_{12}$  garnet-type electrolytes with high lithium-ion conductivity," *ACS Appl. Mater. Interfaces*, 2017.
- [16] Y. Wang and W. Lai, "High ionic conductivity lithium garnet oxides of  $\text{Li}_{7-x}\text{La}_3\text{Zr}_{2-x}\text{Ta}_x\text{O}_{12}$  compositions," *Electrochem. Solid-State Lett.*, 2012.
- [17] R. H. Brugge, J. A. Kilner, and A. Aguadero, "Germanium as a donor dopant in garnet electrolytes," *Solid State Ionics*, 2019.

- [18] E. Rangasamy, J. Wolfenstine, J. Allen, and J. Sakamoto, "The effect of 24c-site (A) cation substitution on the tetragonal-cubic phase transition in  $\text{Li}_{7-x}\text{La}_3\text{AxZr}_2\text{O}_{12}$  garnet-based ceramic electrolyte," *J. Power Sources*, 2013.
- [19] L. J. Miara *et al.*, "Effect of Rb and Ta doping on the ionic conductivity and stability of the garnet  $\text{Li}_{7+2x-y}(\text{La}_{3-x}\text{Rbx})(\text{Zr}_{2-y}\text{Tay})\text{O}_{12}$  Superionic conductor: A first principles investigation," *Chem. Mater.*, 2013.
- [20] L. Dimesso, "Pechini processes: An alternate approach of the sol-gel method, preparation, properties, and applications," in *Handbook of Sol-Gel Science and Technology: Processing, Characterization and Applications*, 2018.
- [21] S. Cao *et al.*, "Modeling, preparation, and elemental doping of  $\text{Li}_7\text{La}_3\text{Zr}_2\text{O}_{12}$  garnet-type solid electrolytes: A review," *J. Korean Ceram. Soc.*, 2019.
- [22] K. Meier, T. Laino, and A. Curioni, "Solid-state electrolytes: Revealing the mechanisms of Li-Ion conduction in tetragonal and cubic LLZO by first-principles calculations," *J. Phys. Chem. C*, 2014.
- [23] Y. Zhang *et al.*, "Regulation mechanism of bottleneck size on  $\text{Li}^+$  migration activation energy in garnet-type  $\text{Li}_7\text{La}_3\text{Zr}_2\text{O}_{12}$ ," *Electrochim. Acta*, 2018.
- [24] C. A. Geiger *et al.*, "Crystal Chemistry and Stability of ' $\text{Li}_7\text{La}_3\text{Zr}_2\text{O}_{12}$ ' Garnet: A Fast Lithium-Ion Conductor," *Inorg. Chem.*, 2011.
- [25] J. F. Wu, W. K. Pang, V. K. Peterson, L. Wei, and X. Guo, "Garnet-Type Fast Li-Ion Conductors with High Ionic Conductivities for All-Solid-State Batteries," *ACS Appl. Mater. Interfaces*, 2017.
- [26] X. Chen *et al.*, "Synthesis of Ta and Ca doped  $\text{Li}_7\text{La}_3\text{Zr}_2\text{O}_{12}$  solid-state electrolyte via simple solution method and its application in suppressing shuttle effect of Li-S battery," *J. Alloys Compd.*, 2018.

- [27] J. Gai *et al.*, “Improving the Li-ion conductivity and air stability of cubic Li<sub>7</sub>La<sub>3</sub>Zr<sub>2</sub>O<sub>12</sub> by the co-doping of Nb, Y on the Zr site,” *J. Eur. Ceram. Soc.*, 2018.
- [28] T. Yang *et al.*, “The synergistic effect of dual substitution of Al and Sb on structure and ionic conductivity of Li<sub>7</sub>La<sub>3</sub>Zr<sub>2</sub>O<sub>12</sub> ceramic,” *Ceram. Int.*, 2018.
- [29] R. C. Agrawal and G. P. Pandey, “Solid polymer electrolytes: Materials designing and all-solid-state battery applications: An overview,” *J. Phys. D. Appl. Phys.*, 2008.
- [30] D. E. Fenton, J. M. Parker, and P. V. Wright, “Complexes of alkali metal ions with poly(ethylene oxide),” *Polymer (Guildf.)*, 1973.
- [31] P. V. Wright, “Electrical conductivity in ionic complexes of poly(ethylene oxide),” *Br. Polym. J.*, 1975.
- [32] E. A. Rietman, M. L. Kaplan, and R. J. Cava, “Lithium ion-poly (ethylene oxide) complexes. I. Effect of anion on conductivity,” *Solid State Ionics*, 1985.
- [33] C. Berthier, W. Gorecki, M. Minier, M. B. Armand, J. M. Chabagno, and P. Rigaud, “Microscopic investigation of ionic conductivity in alkali metal salts-poly(ethylene oxide) adducts,” *Solid State Ionics*, 1983.
- [34] M. Z. A. Munshi, B. B. Owens, and S. Nguyen, “Measurement of li<sup>+</sup> ion transport numbers in poly(ethylene oxide)-lix complexes,” *Polym. J.*, 1988.
- [35] A. Magistris, P. Mustarelli, E. Quartarone, and C. Tomasi, “Transport and thermal properties of (PEO)<sub>n</sub>-LiPF<sub>6</sub> electrolytes for super-ambient applications,” *Solid State Ionics*, 2000.
- [36] W. Wiczorek, D. Raducha, A. Zalewska, and J. R. Stevens, “Effect of Salt Concentration on the Conductivity of PEO-Based Composite Polymeric Electrolytes,” *J. Phys. Chem. B*, 1998.

- [37] G. Chiodelli, P. Ferloni, A. Magistris, and M. Sanesi, "Ionic conduction and thermal properties of poly (ethylene oxide)-lithium tetrafluoroborate films," *Solid State Ionics*, 1988.
- [38] W. Gorecki, M. Jeannin, E. Belorizky, C. Roux, and M. Armand, "Physical properties of solid polymer electrolyte PEO(LiTFSI) complexes," *J. Phys. Condens. Matter*, 1995.
- [39] H. Y. Sun, H. J. Sohn, O. Yamamoto, Y. Takeda, and N. Imanishi, "Enhanced lithium-ion transport in PEO-based composite polymer electrolytes with ferroelectric BaTiO<sub>3</sub>," *J. Electrochem. Soc.*, 1999.
- [40] H. M. J. C. Pitawala, M. A. K. L. Dissanayake, and V. A. Seneviratne, "Combined effect of Al<sub>2</sub>O<sub>3</sub> nano-fillers and EC plasticizer on ionic conductivity enhancement in the solid polymer electrolyte (PEO)<sub>9</sub>LiTf," *Solid State Ionics*, 2007.
- [41] J. Xi *et al.*, "Composite polymer electrolyte doped with mesoporous silica SBA-15 for lithium polymer battery," *Solid State Ionics*, 2005.
- [42] F. Croce, L. L. Persi, B. Scrosati, F. Serraino-Fiory, E. Plichta, and M. A. Hendrickson, "Role of the ceramic fillers in enhancing the transport properties of composite polymer electrolytes," *Electrochim. Acta*, 2001.
- [43] P. Zhu *et al.*, "Li<sub>0.33</sub>La<sub>0.557</sub>TiO<sub>3</sub> ceramic nanofiber-enhanced polyethylene oxide-based composite polymer electrolytes for all-solid-state lithium batteries," *J. Mater. Chem. A*, 2018.
- [44] L. Hu, Z. Tang, and Z. Zhang, "New composite polymer electrolyte comprising mesoporous lithium aluminate nanosheets and PEO/LiClO<sub>4</sub>," *J. Power Sources*, 2007.
- [45] J. H. Choi, C. H. Lee, J. H. Yu, C. H. Doh, and S. M. Lee, "Enhancement of ionic conductivity of composite membranes for all-solid-state lithium rechargeable batteries incorporating tetragonal Li<sub>7</sub>La<sub>3</sub>Zr<sub>2</sub>O<sub>12</sub> into a polyethylene oxide matrix," *J. Power Sources*, 2015.

- [46] T. Yang, J. Zheng, Q. Cheng, Y. Y. Hu, and C. K. Chan, "Composite Polymer Electrolytes with  $\text{Li}_7\text{La}_3\text{Zr}_2\text{O}_{12}$  Garnet-Type Nanowires as Ceramic Fillers: Mechanism of Conductivity Enhancement and Role of Doping and Morphology," *ACS Appl. Mater. Interfaces*, 2017.
- [47] A. S. Best, A. Ferry, D. R. MacFarlane, and M. Forsyth, "Conductivity in amorphous polyether nanocomposite materials," *Solid State Ionics*, 1999.
- [48] W. Wieczorek, P. Lipka, G. Zukowska, and H. Wyciřlik, "Ionic interactions in polymeric electrolytes based on low molecular weight poly(ethylene glycol)s," *J. Phys. Chem. B*, 1998.
- [49] S. Cheng, D. M. Smith, and C. Y. Li, "How does nanoscale crystalline structure affect ion transport in solid polymer electrolytes?," *Macromolecules*, 2014.
- [50] S. K. Fullerton-Shirey and J. K. Maranas, "Effect of  $\text{LiClO}_4$  on the structure and mobility of PEO-based solid polymer electrolytes," *Macromolecules*, 2009.
- [51] A. S. Argon, "Structure of solid polymers," in *The Physics of Deformation and Fracture of Polymers*, Cambridge: Cambridge University Press, 2013, pp. 40–76

### 3. EFFECT OF ADDITIONAL CA, GA AND ND DOPANT ON IONIC CONDUCTIVITY OF BI-DOPED LLZO

#### 3.1 Introduction

As discussed in the previous chapter, LLZO is a promising solid-state lithium electrolyte, compatible with Li metal (that would allow for design for next-generation Li-ion batteries), compatible with anode and cathode materials, and with a wide electrochemical window (up to 6V). LLZO stabilizes in cubic and tetragonal phases[1] the former being characterized by ionic conductivity up to 2 orders of magnitude than the latter[2]. Cubic phase LLZO can be stabilized at a variety of temperatures, 1000°C[3], 900°C[4], and by doping LLZO with a variety of elements, the cubic phase can be stabilized at low temperatures, as low as 700°C[5]. For example, by doping LLZO with bismuth, the cubic phase is stabilized at a lower temperature, to a temperatures between 650°C to 701°C[6].

Most authors use a solid-state reaction to obtain LLZO, a process that requires long reaction times and high temperatures. The sintering of LLZO pellets also has required long times and high temperatures (1000°C - 1200°C) to increase the relative density, and obtain high ionic conductivity. In this work, a sol-gel method is used to fabricate doped and co-doped LLZO garnets, allowing for lower reaction temperatures and times, reduced calcination temperatures, a more homogeneous mixture of reactants and higher reaction yield.

A wide variety of elements have been chosen to dope LLZO, and ionic conductivity and electrochemical performance has been characterized. For example, doping with elements that substitute on the Zr site, can decrease sintering temperatures and times, thus decreasing energetic needs necessary to obtain higher ionic conductivity. Other work has focused on doping on the La site, focusing on enlarging or decreasing the cubic lattice parameter of the LLZO unit cell. Work on La is less abundant, compared with Zr site substitution and Li site substitution. Li-site doping allows more direct manipulation of Li in the unit cell. Increasing or decreasing Li content has a significant effect on bulk ionic conductivity, showing that the highest ionic conductivity, independent of dopant, happens for a Li molar ratio between 6.25 and 6.75, where the cubic garnet lattice has a maximum of 7.5 Li<sup>+</sup> (octahedral and tetrahedral) sites.

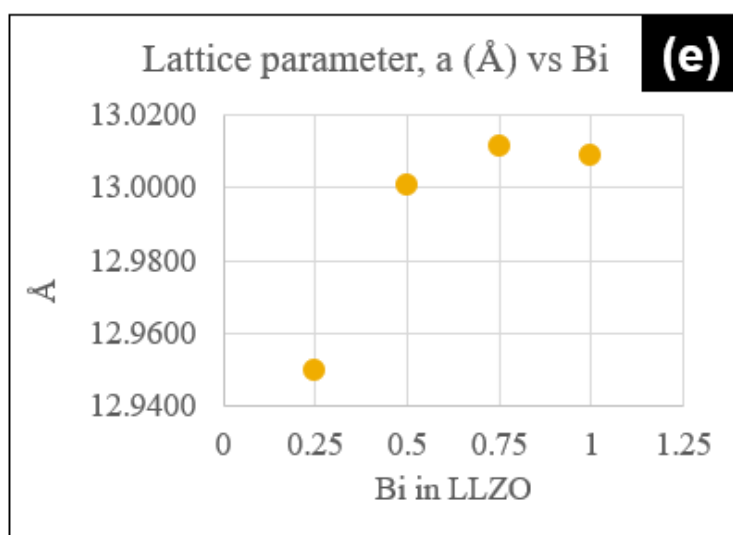
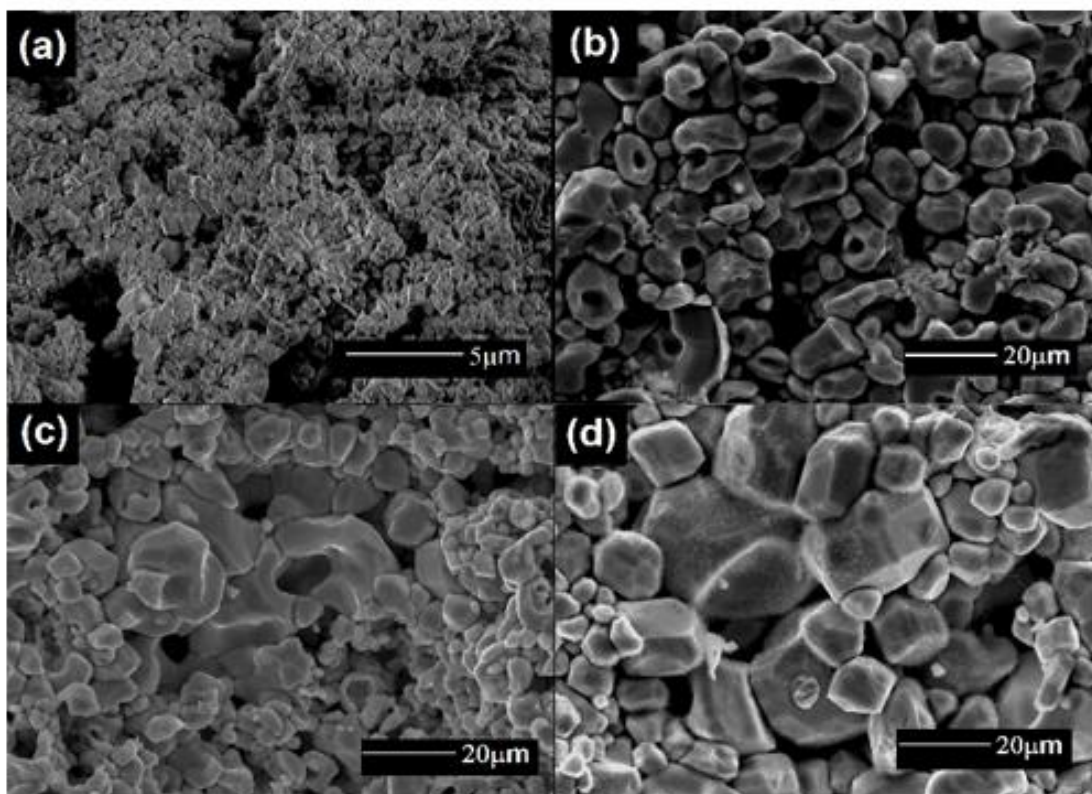


Figure 3.1 SEM images of Bi-LLZO pellets with variation in Bi content. These samples were sintered at 900°C for 10h. Samples are: (a)  $\text{Li}_7\text{La}_3\text{Zr}_2\text{O}_{12}$ , (b)  $\text{Li}_{6.5}\text{La}_3\text{Zr}_{1.5}\text{Bi}_{0.5}\text{O}_{12}$ , (c)  $\text{Li}_{6.25}\text{La}_3\text{Zr}_{1.25}\text{Bi}_{0.75}\text{O}_{12}$ , (d)  $\text{Li}_6\text{La}_3\text{ZrBiO}_{12}$ .

Doping  $\text{Li}_{7-x}\text{La}_3\text{Zr}_{2-x}\text{Bi}_x\text{O}_{12}$  with Bi has several beneficial effects, as reported in previous studies[6]. When  $x=0.75$  an ionic conductivity of  $\sim 2 \times 10^{-4}$  S/cm, was observed. The effect of Bi-

addition on grain growth is also remarkable as illustrated in Fig.3.1. XRD measurements indicate that the highest value of the cubic lattice parameter is observed for the  $x=0.75$  LLZBO. A summary of cubic lattice parameter changes as a function of Bi-doping is shown also in Fig. 3.1(e). The addition of Bi increases the cubic lattice parameter due to its larger ionic radius compared to Zr. Most importantly, the calcination temperature needed to obtain cubic Bi-LLZO is  $700^{\circ}\text{C}$ , and the sintering conditions employed were  $900^{\circ}\text{C}$  for 10 hours, these parameters are significantly lower than the values reported in the literature and partially compiled in Table 3.2.

Co-doping the LLZO garnet can provide insight on how modifications of the crystal structure impact the bulk ionic conductivity and the grain size after sintering [7] [8]. Doping LLZO with  $\text{Bi}^{5+}$  substitute on the  $\text{Zr}^{4+}$  site, and creates  $\text{Li}^{+}$  vacancies to maintain charge neutrality. By adding a second dopant that substitutes on the La-site, or Li-site, the structural and electronic properties of LLZO can be further engineered. In this work, we have synthesized and characterized dual-doped LLZO garnets as indicated in Table 3.1.

Table 3-1 Garnet nomenclature

<b>General formula</b>	<b>Sample Formula</b>	<b>Sample name</b>
$\text{Li}_{7-x}\text{La}_3\text{Zr}_{2-x}\text{Bi}_x\text{O}_{12}$	$\text{Li}_{6.25}\text{La}_3\text{Bi}_{0.75}\text{Zr}_{1.25}\text{O}_{12}$	Bi-LLZO
$\text{Li}_{7-x+y}\text{Ca}_y\text{La}_{3-y}\text{Bi}_x\text{Zr}_{2-x}\text{O}_{12}$	$\text{Li}_{6.45}\text{Ca}_{0.2}\text{La}_{2.8}\text{Bi}_{0.75}\text{Zr}_{1.25}\text{O}_{12}$	BiCa-LLZO
$\text{Li}_{7-x-3y}\text{Ga}_y\text{La}_{3-y}\text{Bi}_x\text{Zr}_{2-x}\text{O}_{12}$	$\text{Li}_{5.5}\text{Ga}_{0.25}\text{La}_3\text{Bi}_{0.75}\text{Zr}_{1.25}\text{O}_{12}$	BiGa-LLZO
$\text{Li}_{7-x}\text{Nd}_y\text{La}_{3-y}\text{Bi}_x\text{Zr}_{2-x}\text{O}_{12}$	$\text{Li}_{6.25}\text{Nd}_{0.2}\text{La}_{2.8}\text{Bi}_{0.75}\text{Zr}_{1.25}\text{O}_{12}$	BiNd-LLZO

Aliovalent substitution in LLZO with Ca [9], Ga [10], Nd [9] has been investigated in the literature, but to the best of the author's knowledge, no co-doped work involving Bi-LLZO with Ca or Nd has been reported. Very recently work on BiGa-LLZO garnet has been reported [11]).

### 3.2 Materials and methods

Reagent grade chemicals of  $\text{LiNO}_3$  (99.0% Sigma Aldrich),  $\text{La}(\text{NO}_3)_3 \cdot 6\text{H}_2\text{O}$  (99.9% Alfa Aesar),  $\text{ZrO}(\text{NO}_3)_2 \cdot x\text{H}_2\text{O}$  (99% Sigma Aldrich),  $\text{Bi}(\text{NO}_3)_3 \cdot 5\text{H}_2\text{O}$  (98% Alfa Aesar), and when

synthesizing co-doped LLZO,  $\text{Ca}(\text{NO}_3)_2 \cdot 4\text{H}_2\text{O}$  ( $\geq 99.0\%$  Sigma Aldrich),  $\text{Ga}(\text{NO}_3)_3 \cdot x\text{H}_2\text{O}$  (99.9998% Fisher scientific) and  $\text{Nd}(\text{NO}_3)_3 \cdot 6\text{H}_2\text{O}$  (99.0% Sigma Aldrich) were used. Stoichiometric amounts of the previous chemicals were dissolved with citric acid and ethylene glycol in 10%  $\text{HNO}_3$ . Citric acid is used as chelating agent and ethylene glycol is used as a complexing agent. To avoid auto-ignition of the solution, an ethylene glycol to citric acid ratio of 60:40 was used. The solution is mixed for 24h between  $70^\circ\text{C}$  -  $75^\circ\text{C}$  in a round-bottom flask with a water reflux setup. Afterwards, the solution is poured into a teflon beaker to allow the polyesterification reaction and evaporation of the nitric acid to take place.

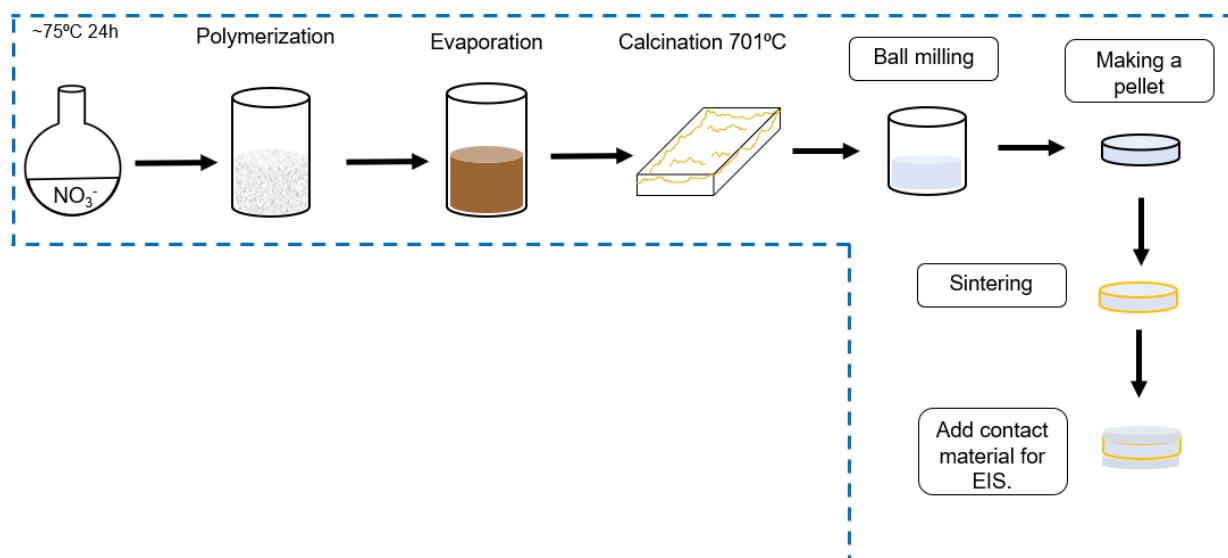


Figure 3.2 Diagram of Bi-LLZO synthesis.

Subsequently, the teflon beaker with the polymerized compound inside, was put in a small box furnace and heated to  $\sim 150^\circ\text{C}$  to completely evaporate the solvent. A brownish, polymerized material remains after this step. Next, this brown material is pulverized with mortar and pestle, and filtered through a number 100 sieve. The brown powder is then calcinated for 10 hours at temperatures between  $700^\circ\text{C}$  to  $710^\circ\text{C}$ , the heating ramp rate employed in the tube furnace was  $5^\circ/\text{min}$ . After cooling down to room temperature, the brown precursor powder turns into a whitish powder. XRD measurements confirm that this whitish powder corresponds to the cubic phase of Bi-LLZO. Traces of  $\text{La}_2\text{Zr}_2\text{O}_7$  impurities are also present. Figure 3.2 provides a flow diagram of the synthesis of Bi-LLZO and co-doped LLZO garnets.

The cubic nature of the LLZO garnet was verified by XRD employing a Bruker D-8 Focus apparatus, Cu source (1.54Å), with a scan rate of 5°/min. EDS was used to confirm the presence of the dopants. Relative densities were calculated using the Archimedes method. Electrochemical Impedance Spectroscopy (EIS) was used to determine ionic conductivity. A frequency range of 0.1 Hz to 300 kHz was used, employing a Solartron 1260 impedance analyzer. In order to determine ionic conductivity, approximately 1g of each batch of Bi-LLZO powder was pressed into pellets with a diameter of 13.7mm and a thickness of ~1mm. Each pellet was enclosed in its powder to prevent Li volatilization and sintered for 10 hours at 900°C. SEM was employed to study the microstructure after sintering. In order to collect EIS data, colloidal gold paint (PELCO) was used to coat both sides of the pellet as well as the surface of the stainless steel electrodes of the EIS apparatus that contacts the pellet.

### **3.3 Results and discussion**

Figure 3 shows XRD patterns for BiCa-LLZO, BiGa-LLZO and BiNd-LLZO garnet powders. All samples exhibit cubic phase garnet formation with some evidence of impurities of  $\text{La}_2\text{Zr}_2\text{O}_7$  and  $\text{La}_2\text{O}_3$ . The peaks for these impurities are identified at 28.5° and at around 30° respectively. The presence of these phases has been previously documented and can be attributed to Li evaporation during calcination [12].

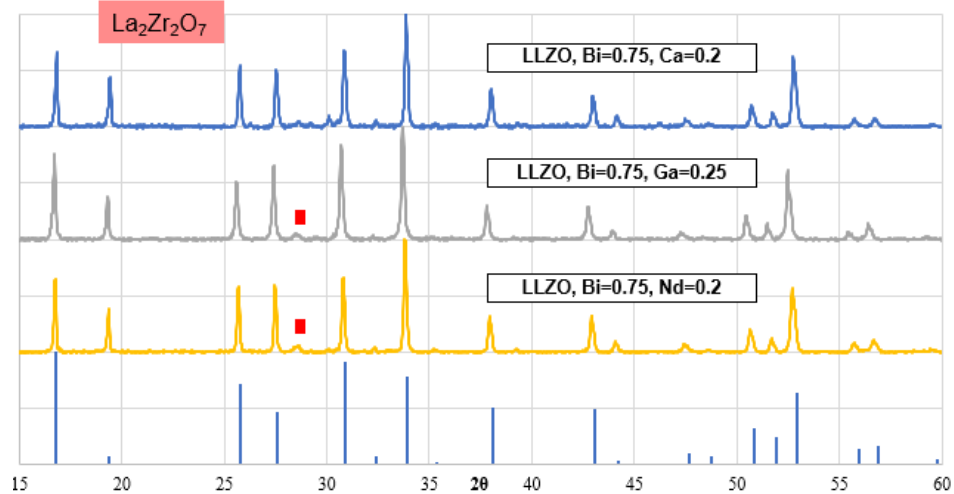


Figure 3.3 XRD scans for: a) BiCa-LLZO, b) BiGa-LLZO, c) BiNd-LLZO and d) reference PDF pattern corresponding to cubic LLZO (ICSD 422-259). Trace amounts of the  $\text{La}_2\text{Zr}_2\text{O}_7$  identified by the (\*) symbol are observed.

Changes in cubic lattice parameter are also observed from shifts in peak positions in the XRD patterns. The lattice constant value for Bi-LLZO, at Bi=0.75, is  $13.00897\text{\AA}$  and adding Ca to the Bi-LLZO decreases the lattice constant, to  $12.9899\text{\AA}$ . This decrease can be attributed to the smaller ionic radius for  $\text{Ca}^{2+}$ , which substitutes on the  $\text{La}^{3+}$  sites. Both  $\text{La}^{3+}$  and  $\text{Zr}^{4+}$  share oxygen atoms with the  $\text{Li}_2\text{O}_6$  and  $\text{Li}_2\text{O}_4$  polyhedrons in the LLZO unit cell, forming a  $\text{Li}^+$  ion pathway, and atom substitutions on either site can increase or decrease the structural bottleneck for the  $\text{Li}^+$  transport. This is illustrated in this chapter in figure 3.4, and previously seen in figure 2.5.

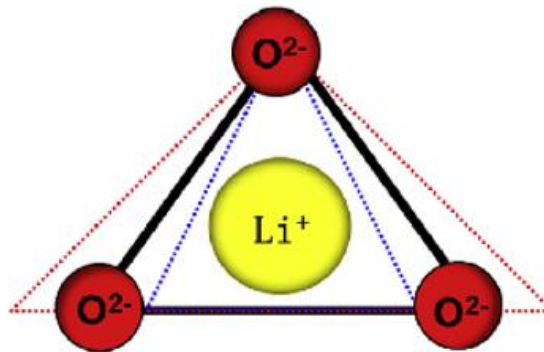


Figure 3.4  $\text{Li}^+$  ion migration bottleneck for the diffusion pathway. Figure from ref. [13]

In the case of BiGa-LLZO, the cubic lattice parameter is increased to 13.02189Å. The ionic radius of Ga<sup>3+</sup> is 0.47Å compared to that of Li<sup>+</sup> = 0.59Å, and a decrease in lattice constant is expected, as Ga<sup>3+</sup> substitute on Li<sup>+</sup> sites. This unexpected result has been reported by others. For example, in a very recent paper on Li<sub>6.5-3x</sub>Ga<sub>x</sub>La<sub>3</sub>Bi<sub>0.5</sub>Zr<sub>1.5</sub>O<sub>12</sub>, (x=0, 0.1, 0.2, and 0.3) was synthesized and characterized. A trend in increased lattice constant for dopant amounts x=0.2 and higher was observed. The authors attribute the increment to stress effects [11]. The effect of Ga doping initially decreasing the lattice constant up to a certain molar ratio in LLZO, and the subsequent increase at higher ratios, has been observed also for the case when Ga is used as a single dopant. Rettenwander *et al*[14]'s studied Ga-doped LLZO and observed that as molar ratio of Ga increased from 0 to 0.24, the cubic lattice parameter decreased, but as the ration was increased to x=0.84, the lattice constant increased. There is evidence that suggests that Ga<sup>3+</sup> substitutes on 24d sites (tetrahedral)[15], but recent papers have singled out 96h (octahedral) site as the location of Ga<sup>3+</sup> dopant. Although doping with Ga<sup>3+</sup> increases the ionic conductivity of the LLZO garnet, the mechanism through which an increase in cubic lattice parameter is observed is not clear. Adding Nd as dopant to Bi-doped LLZO decreases the lattice constant to 12.99067Å from a value of 13.00897Å. This is attributed to the lower ionic radius of Nd<sup>3+</sup> (1.109Å) compared to the La<sup>3+</sup> (1.16Å).

SEM images of sintered pellets for the 3 co-doped garnets are shown in figure 3.5. Grain size is larger for the BiCa-LLZO pellet, whereas for the case of BiGa-LLZO and BiNd-LLZO there appears to be little difference in grain size. The measured pellets relative densities are: BiCa-LLZO = 0.823, BiGa-LLZO 0.797 and BiNd-LLZO = 0.814. Indicating that these samples are far from fully densified, which as discussed is expected to significantly impact measurements of their ionic conductivity. EDS was used to confirm the presence of the Bi, Ca, Ga and Nd and rule out contaminants from the crucible.

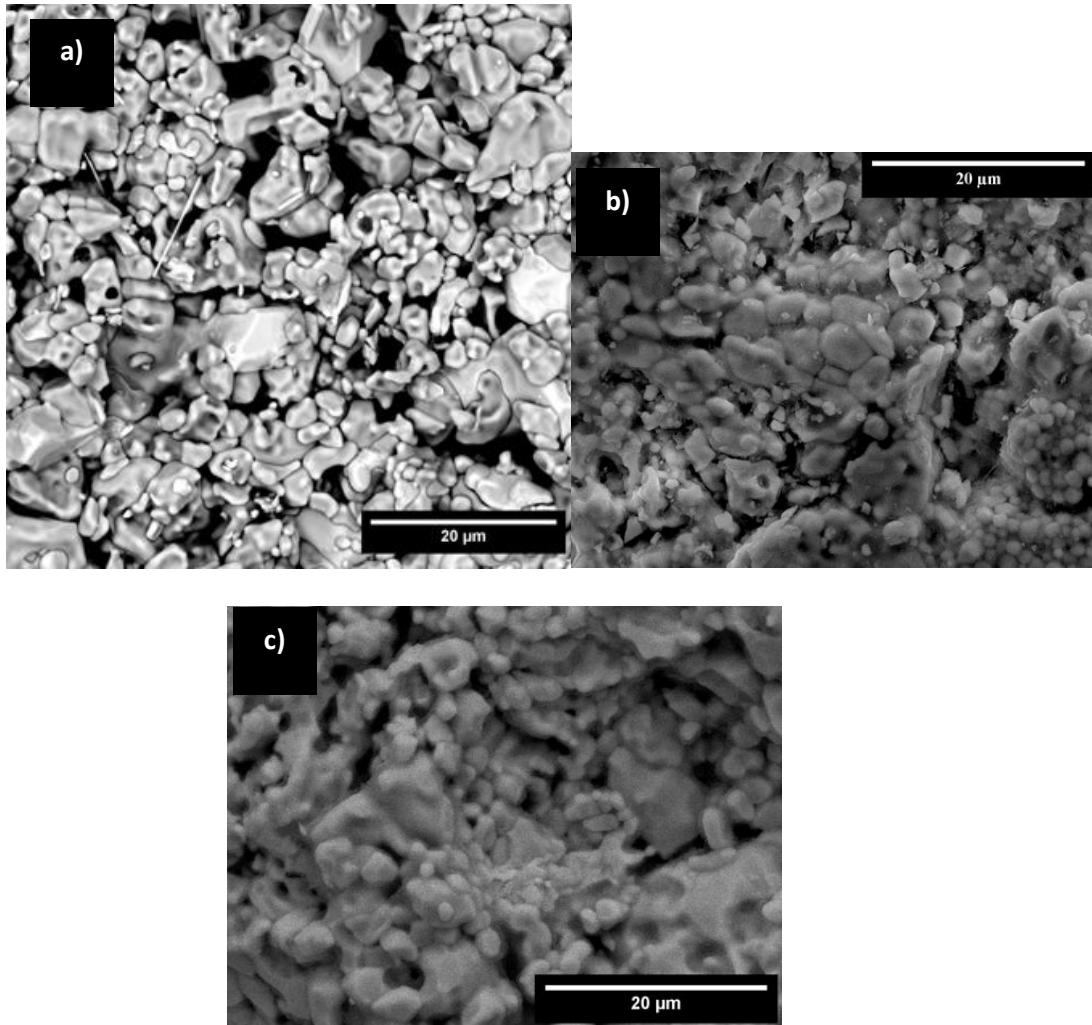


Figure 3.5 SEM images of co-doped LLZO pellet microstructure for, a) BiCa-LLZO, b) BiGa-LLZO and c) BiNd-LLZO. All pellets were sintered at 900°C for 10 hours. Note that the structures are porous which is expected to impact their ionic conductivity.

An example of Nyquist plots obtained using EIS is given in figure 3.6. The plots show a double semi-circle, where the first, semi-circle is the resistance attributed to bulk of the grain. The full first semi-circle is not able to be displayed in the figure as it requires frequencies higher than those available in the EIS apparatus employed. This is consistent with previous papers investigating LLZO pellet resistance at a variety of sintering conditions [8][16][17][18][19]. For analysis of impedance plots an equivalent circuit comprising bulk resistance and grain boundary resistance for each of the synthesized pellets is considered. It is important to note that the lower the relative density of the pellet, the more difficult it is to achieve good results for ionic conductivity. Au paint is used on both sides of the pellet and on the stainless steel electrode to

obtain good contact between electrode and the pellet sample. Data collection becomes more difficult with increasing roughness, as it becomes more difficult to obtain uniform contact between the LLZO garnet and electrode.

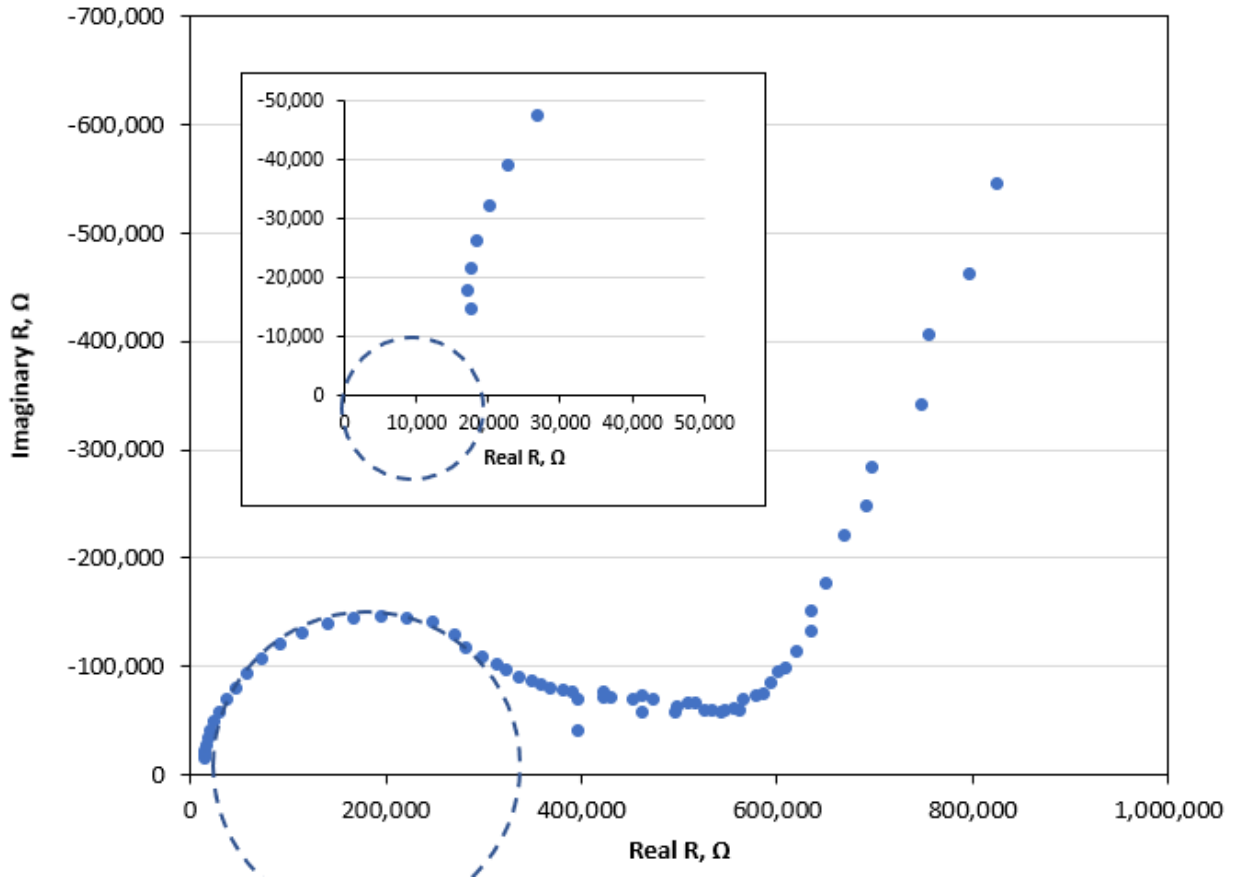


Figure 3.6 Example of Nyquist plot measurement for a BiNd-LLZO pellet.

In the following paragraphs a comparison in terms of ionic conductivity between Bi-LLZO and the prepared co-doped garnets will be made. As previously discussed,  $\text{Li}_{7-x}\text{La}_3\text{Zr}_{2-x}\text{Bi}_x\text{O}_{12}$  with  $x=0.75$  exhibited an ionic conductivity of  $\sim 2 \times 10^{-4}$  S/cm at room temperature[6]. This IC is undoubtedly limited by the low relative density for this sample (0.83). The IC value measured for BiCa-LLZO was  $0.68 \times 10^{-4}$  S/cm and this sample exhibited a comparable relative density (0.82) to  $\text{Li}_{6.25}\text{La}_3\text{Zr}_{0.25}\text{Bi}_{0.75}\text{O}_{12}$ . Thus, one would be inclined to conclude that additions of Ca has a detrimental effect on the ionic conductivity, however the IC measurement is most likely impacted by the low relative density and limited grain connectivity evident in Fig 3.5a. Previous reports of a Ca-doped LLZO reported an ionic conductivity of  $4 \times 10^{-5}$  S/cm with a molar ratio of 0.2[9]. Ca

substitution has previously been reported to have little effect improving ionic conductivity[20]. Although there is a previous report of Ca substituting Zr[21], it has been more consistently confirmed that Ca substitutes on La sites [9][8]. The magnitude of this decrease can be explained by a lower relative density and a higher lithium stoichiometric amount compared to the Bi-LLZO garnet. For cubic LLZO, the literature shows a relationship between lithium molar ratio and ionic conductivity. When sintering conditions remain the same, ionic conductivity reaches a maximum value at a molar ratio between 6.25 and 6.75, and decreases as the molar ratio is increased. This is prevalent with dopants that effect Li molar ratio like Ta[22][20], Ce[23], Ga[24] and Al[3].

The BiGa-LLZO pellet exhibited the highest ionic conductivity with a value of  $1.07 \times 10^{-4}$  S/cm at room temperature, a decrease in value compared to the Bi-LLZO pellet at the same temperature and sintering conditions. However the relative density measure is only 0.79 compared to 0.83 for  $\text{Li}_{6.25}\text{La}_3\text{Zr}_{0.25}\text{Bi}_{0.75}\text{O}_{12}$ . Other authors have investigated Ga-doped LLZO with the same molar ratio of 0.25, reporting a value of  $1.46 \times 10^{-3}$  S/cm, in samples sintered at 1100°C for 24h in air[10]. Similarly, Wolfenstine *et al*, reported an ionic conductivity for a Ga-doped LLZO of  $3.5 \times 10^{-4}$  S/cm at room temperature, they employed hot pressing sintering at 1000°C for 1 hour at 40MPa and a molar ratio of 0.25[25]. Once again the important effect of densification is highlighted by these comparisons.

The lower value for ionic conductivity reported in this work can be ascribed to low densification and to the low concentration of molar  $\text{Li}^+$ . It is understood that  $\text{Li}^+$  occupies two sites in the Li sub-lattice, the octahedral (96h) and tetrahedral (24d) sites, and that occupation of octahedral sites favors a higher ionic conductivity and at lower Li concentrations, tetrahedral sites are more occupied compared to octahedral, limiting Li-ion conductivity [26]. Although BiGa-LLZO has a larger cubic lattice parameter compared with Bi-LLZO, the ionic conductivity is lower than the value reported for Bi-LLZO, suggesting that Li concentration outweighs mobility as a driving force for ionic conduction in cubic LLZO. However, samples with higher densification need to be obtained to fully understand the effects of the aliovalent substitution on the conduction bottleneck vs. ion transport limitations in current samples due to inadequate grain connectivity.

The ionic conductivity for the BiNd-LLZO garnet was  $0.77 \times 10^{-4}$  S/cm. This value is higher compared with reported with works for single dopant Nd, and with lower and shorter sintering

conditions[9]. The drop in ionic conductivity when compared with Bi-LLZO could be attributed to a reduction in lattice constant. The Li molar ratio is kept constant at 6.25, as Nd substitutes on La sites[9], so there is no change in Li ion concentration to affect the ion conduction. Nevertheless in the absence of full densification and improved grain inter-connectivity in the BiND-LLZO samples, these conclusions are tentative.

### 3.4 Conclusions

Single doped and co-doped LLZO garnets, Bi-LLZO, BiCa-LLZO, BiGa-LLZO and BiNd-LLZO, were synthesized via a sol-gel Pechini method. The effect of doping and co-doping on IC, relative densification, grain morphology and cubic lattice parameter changes were examined. At room temperature, the highest ionic conductivity value of  $2 \times 10^{-4}$  S/cm was obtained in the single-doped Bi-LLZO garnet the IC in the co-doped BiGa-LLZO sample was determined to be  $1.07 \times 10^{-4}$  S/cm.

Table 3.2 summarizes the experimental results done in these materials. The following observations are offered in reference to the obtained results and on strategies for further enhancements on IC in these garnet oxides: ionic conductivity enhancements can be achieved by selecting a first dopant that only alters the molar concentration of Li, and a second dopant that increments the lattice constant to reduce the transport bottleneck in the garnet structure. Substitutions on either the La or Zr sites can be pursued in this respect. Future work will focus on Sr and Ga as co-dopants in LLZO. The importance of sample densification and grain interconnectivity is highlighted in this study in evaluating the maximum ionic conductivity measurable in these samples. This has not been the focus of our work thus far, but we believe the values reported throughout this work are gated by the low relative density values displayed by our samples. Future work will employ high pressure densification to circumvent this issue.

Table 3-2 Relative densities, lattice constant, and ionic conductivity of co-doped LLZO garnets.

LLZO garnet	Relative density	Lattice parameter, Å	Molar Li ratio	Ionic conductivity $\times 10^{-4}$ (s/cm)
$\text{Li}_{6.25}\text{La}_3\text{Bi}_{0.75}\text{Zr}_{1.25}\text{O}_{12}$	0.83	13.00897	6.25	2.00
$\text{Li}_{6.45}\text{La}_{2.8}\text{Ca}_{0.2}\text{Bi}_{0.75}\text{Zr}_{1.25}\text{O}_{12}$	0.82	12.9899	6.45	0.68
$\text{Li}_{5.5}\text{Ga}_{0.25}\text{La}_3\text{Bi}_{0.75}\text{Zr}_{1.25}\text{O}_{12}$	0.797	13.02189	5.5	1.07
$\text{Li}_{6.25}\text{La}_{2.8}\text{Nd}_{0.2}\text{Bi}_{0.75}\text{Zr}_{1.25}\text{O}_{12}$	0.814	12.99067	6.25	0.77

### 3.5 References

- [1] K. Meier, T. Laino, and A. Curioni, "Solid-state electrolytes: Revealing the mechanisms of Li-Ion conduction in tetragonal and cubic LLZO by first-principles calculations," *J. Phys. Chem. C*, 2014.
- [2] S. Ramakumar, L. Satyanarayana, S. V. Manorama, and R. Murugan, "Structure and Li+ dynamics of Sb-doped  $\text{Li}_7\text{La}_3\text{Zr}_2\text{O}_{12}$  fast lithium ion conductors," *Phys. Chem. Chem. Phys.*, 2013.
- [3] E. Rangasamy, J. Wolfenstine, and J. Sakamoto, "The role of Al and Li concentration on the formation of cubic garnet solid electrolyte of nominal composition  $\text{Li}_7\text{La}_3\text{Zr}_2\text{O}_{12}$ ," *Solid State Ionics*, 2012.
- [4] Z. Hu, H. Liu, H. Ruan, R. Hu, Y. Su, and L. Zhang, "High Li-ion conductivity of Al-doped  $\text{Li}_7\text{La}_3\text{Zr}_2\text{O}_{12}$  synthesized by solid-state reaction," *Ceram. Int.*, 2016.
- [5] I. Kokal, M. Somer, P. H. L. Notten, and H. T. Hintzen, "Sol-gel synthesis and lithium ion conductivity of  $\text{Li}_7\text{La}_3\text{Zr}_2\text{O}_{12}$  with garnet-related type structure," *Solid State Ionics*, 2011.
- [6] D. K. W. Schwanz, "Solution based processing of garnet type oxides for optimized lithium-ion transport," 2016.

- [7] T. Yang *et al.*, “The synergistic effect of dual substitution of Al and Sb on structure and ionic conductivity of Li<sub>7</sub>La<sub>3</sub>Zr<sub>2</sub>O<sub>12</sub> ceramic,” *Ceram. Int.*, 2018.
- [8] X. Chen *et al.*, “Synthesis of Ta and Ca doped Li<sub>7</sub>La<sub>3</sub>Zr<sub>2</sub>O<sub>12</sub> solid-state electrolyte via simple solution method and its application in suppressing shuttle effect of Li-S battery,” *J. Alloys Compd.*, 2018.
- [9] E. Hanc, W. Zając, and J. Molenda, “Synthesis procedure and effect of Nd, Ca and Nb doping on structure and electrical conductivity of Li<sub>7</sub>La<sub>3</sub>Zr<sub>2</sub>O<sub>12</sub> garnets,” *Solid State Ionics*, 2014.
- [10] J. F. Wu *et al.*, “Gallium-doped Li<sub>7</sub>La<sub>3</sub>Zr<sub>2</sub>O<sub>12</sub> garnet-type electrolytes with high lithium-ion conductivity,” *ACS Appl. Mater. Interfaces*, 2017.
- [11] J. Li *et al.*, “Effect of Ga-Bi Co-doped on Structural and Ionic Conductivity of Li<sub>7</sub>La<sub>3</sub>Zr<sub>2</sub>O<sub>12</sub> Solid Electrolytes Derived from Sol–Gel Method,” *J. Electron. Mater.*, 2019.
- [12] C. Bernuy-Lopez, W. Manalastas, J. M. Lopez Del Amo, A. Aguadero, F. Aguesse, and J. A. Kilner, “Atmosphere controlled processing of ga-substituted garnets for high li-ion conductivity ceramics,” *Chem. Mater.*, 2014.
- [13] Y. Zhang *et al.*, “Regulation mechanism of bottleneck size on Li<sup>+</sup> migration activation energy in garnet-type Li<sub>7</sub>La<sub>3</sub>Zr<sub>2</sub>O<sub>12</sub>,” *Electrochim. Acta*, 2018.
- [14] D. Rettenwander, C. A. Geiger, M. Tribus, P. Tropper, and G. Amthauer, “A synthesis and crystal chemical study of the fast ion conductor Li<sub>7-3x</sub>Ga<sub>x</sub>La<sub>3</sub>Zr<sub>2</sub>O<sub>12</sub> with x = 0.08 to 0.84,” *Inorg. Chem.*, 2014.
- [15] M. A. Howard *et al.*, “Effect of Ga incorporation on the structure and Li ion conductivity of La<sub>3</sub>Zr<sub>2</sub>Li<sub>7</sub>O<sub>12</sub>,” *Dalt. Trans.*, 2012.
- [16] Y. Suzuki *et al.*, “Transparent cubic garnet-type solid electrolyte of Al<sub>2</sub>O<sub>3</sub>-doped Li<sub>7</sub>La<sub>3</sub>Zr<sub>2</sub>O<sub>12</sub>,” *Solid State Ionics*, 2015.

- [17] Y. Yamada, Y. Iriyama, T. Abe, and Z. Ogumi, "Kinetics of lithium ion transfer at the interface between graphite and liquid electrolytes: effects of solvent and surface film," *Langmuir*, 2009.
- [18] R. Murugan, V. Thangadurai, and W. Weppner, "Fast lithium ion conduction in garnet-type  $\text{Li}_7\text{La}_3\text{Zr}_2\text{O}_{12}$ ," *Angew. Chem. Int. Ed. Engl.*, 2007.
- [19] D. Rettenwander *et al.*, "Synthesis, Crystal Chemistry, and Electrochemical Properties of  $\text{Li}_{7-2x}\text{La}_3\text{Zr}_2\text{O}_{12-x}\text{Mox}$  ( $x = 0.1-0.4$ ): Stabilization of the Cubic Garnet Polymorph via Substitution of  $\text{Zr}^{4+}$  by  $\text{Mo}^{6+}$ ," *Inorg. Chem.*, 2015.
- [20] X. Chen, T. Cao, M. Xue, H. Lv, B. Li, and C. Zhang, "Improved room temperature ionic conductivity of Ta and Ca doped  $\text{Li}_7\text{La}_3\text{Zr}_2\text{O}_{12}$  via a modified solution method," *Solid State Ionics*, 2018.
- [21] S. Song, D. Sheptyakov, A. M. Korsunsky, H. M. Duong, and L. Lu, "High Li ion conductivity in a garnet-type solid electrolyte via unusual site occupation of the doping Ca ions," *Mater. Des.*, 2016.
- [22] Y. Wang and W. Lai, "High ionic conductivity lithium garnet oxides of  $\text{Li}_{7-x}\text{La}_3\text{Zr}_{2-x}\text{Ta}_x\text{O}_{12}$  compositions," *Electrochem. Solid-State Lett.*, 2012.
- [23] E. Rangasamy, J. Wolfenstine, J. Allen, and J. Sakamoto, "The effect of 24c-site (A) cation substitution on the tetragonal-cubic phase transition in  $\text{Li}_{7-x}\text{La}_3\text{AxZr}_2\text{O}_{12}$  garnet-based ceramic electrolyte," *J. Power Sources*, 2013.
- [24] S. Aktaş *et al.*, "Study of the local structure and electrical properties of gallium substituted LLZO electrolyte materials," *J. Alloys Compd.*, 2019.
- [25] J. Wolfenstine, J. Ratchford, E. Rangasamy, J. Sakamoto, and J. L. Allen, "Synthesis and high Li-ion conductivity of Ga-stabilized cubic  $\text{Li}_7\text{La}_3\text{Zr}_2\text{O}_{12}$ ," *Mater. Chem. Phys.*, 2012.

- [26] Y. Zhang, F. Chen, R. Tu, Q. Shen, X. Zhang, and L. Zhang, "Effect of lithium ion concentration on the microstructure evolution and its association with the ionic conductivity of cubic garnet-type nominal  $\text{Li}_7\text{Al}_{0.25}\text{La}_3\text{Zr}_2\text{O}_{12}$  solid electrolytes," *Solid State Ionics*, 2016.
- [27] J. L. Allen, J. Wolfenstine, E. Rangasamy, and J. Sakamoto, "Effect of substitution (Ta, Al, Ga) on the conductivity of  $\text{Li}_7\text{La}_3\text{Zr}_2\text{O}_{12}$ ," *J. Power Sources*, 2012.

## 4. BI-DOPED LLZO AS A FILLER IN PEO-BASED POLYMER COMPOSITE ELECTROLYTE: EFFECT OF BI MOLAR RATIO ON BULK IONIC CONDUCTIVITY

### 4.1 Introduction

Lithium-ion batteries are energy storage systems used for a wide variety of electric devices and vehicles. For high-power devices, high ionic conductivity of the electrolyte is imperative[1]. The electrolytes currently employed in lithium ion batteries are flammable organic electrolytes, their safety concerns hinder their wider implementation in transportation[2]. Several electrolyte alternatives have been investigated to replace liquid electrolytes: ionic liquids[3], solid polymer electrolytes[4], solid state electrolytes[5], [6], [7] and gel polymer electrolytes[8]. Solid state electrolytes (SSE) with high ionic conductivity at room temperature are of particular interest in current battery research[9]. Additional SSE advantages are wider electrochemical stability voltage window, higher thermal stability[10] and transference numbers approaching 1.0[11][12] vs  $< 0.5$  for other electrolytes[13],[14].

Solid polymer electrolytes offer several advantages, such as flexibility and high mechanical strength, however, they exhibit low ionic conductivity at room temperature[15]. The fillers in polymer composite electrolytes (PCEs) can be passive or active, and they can improve the ionic conductivity by orders of magnitude. The difference between passive and active fillers is that the passive fillers do not directly participate in the Li ion transport process[16]. Examples of passive fillers used are  $\text{Al}_2\text{O}_3$ [17],  $\text{MgO}$ [18]; active fillers, include lithium titanium aluminum phosphate ( $\text{Li}_{1.3}\text{Ti}_{1.7}\text{Al}_{0.3}(\text{PO}_4)_3$  or LTAP)[19], and LLZO[20][21]. Adding fillers to a polymer[22] has the effect of decreasing the extent of crystalline regions in the polymer matrix, by impeding the reorganization of polymer chains, thereby allowing for higher ionic conductivity[23].

A particular SSE of interest is lithium lanthanum zirconium oxide (LLZO). This garnet material was first reported by Murugan to exhibit good ionic conductivity and chemical stability for use in lithium ion batteries[7]. The authors reported IC values as high as  $3 \times 10^{-4}$  S/cm at  $25^\circ\text{C}$ . However, high synthesis and annealing temperatures were needed to attain these values. The range of synthesis temperatures employed ranged from  $1100^\circ\text{C}$ [24] to  $900^\circ\text{C}$ [25] and  $750^\circ\text{C}$ [26].

It is understood that the surface of the fillers can act as Lewis base or acid centers[27], influencing total lithium salt disassociation[28] and polymer reorganization and crystallization[29], resulting in an increased ionic conductivity. In the case of a PEO:Li-salt system with added LLZO, the particle surface can act as Lewis-base centers[30], and these surface sites are formed from lithium vacancies that arise from doping LLZO with various elements such as Al, Ta [30].

To better understand the role of the LLZO dopant on the bulk ionic conductivity of PCE,  $\text{Li}_{7-x}\text{La}_3\text{Zr}_{2-x}\text{Bi}_x\text{O}_{12}$  is synthesized, where  $x=1$  and  $0.75$ , and added to a PEO:LiTFSI polymer electrolyte. The weight load of LLZBO is also varied in the polymer electrolyte to measure the effect of each Bi-LLZO powder composition on IC. PCE films are prepared and XRD is used to characterize changes in crystallinity. Electrochemical Impedance Spectroscopy (EIS) is used to determine the ionic conductivity. Polarized light microscopy was used to study the polymer composite microstructure, and to establish a relationship with ionic conductivity.

## 4.2 Materials and methods

$\text{Li}_{7-x}\text{La}_3\text{Zr}_{2-x}\text{Bi}_x\text{O}_{12}$  (LLZO) garnet powders were synthesized using a sol-gel Pechini method described in the previous chapter. LLZO powders were doped with Bi, where  $x=0.25$ ,  $0.5$ ,  $0.75$ , and  $1.5$  and the desired garnet cubic phase obtained after calcination at  $700^\circ\text{C}$  for 10 hours. The powders were mixed with polyethylene oxide (PEO, Sigma Aldrich, molecular weight 100,000), lithium bis(trifluoromethanesulfonyl)imide (LiTFSI, Sigma Aldrich, 99.8%) and acetonitrile (ACN, Sigma Aldrich, 99.9%) was used as solvent to mix all the materials. ACN was mixed at a 2.5:1 liquid to solids ratio to form the electrolyte slurry. All the materials were mixed and wet ball milled for 12 hours at 400 rpm with a Fritsch Pulverisette 6 apparatus. The ball milling time and rpm were chosen based on the work of Oduncu[31], to obtain sub-micron average particle size. Milling for 12 hours at 400 rpm yielded  $d_{50}$  particle size of  $\sim 437$  nm. The films were cast-dried for 72 hours at room temperature at atmospheric pressure to allow evaporation of acetonitrile. After the 72 hours of slow drying, the films were held in vacuum overnight to completely remove the solvent.

The load amounts of  $\text{Li}_{7-x}\text{La}_3\text{Zr}_{2-x}\text{Bi}_x\text{O}_{12}$  investigated in this work were 2.5%, 5%, 10%, 30% and 50% by weight. The resulting slurry for every composition was cast on a 1" x 1" square-shaped mold, 1 mm deep mold using a syringe to pour the slurry. Employing the same experimental procedure, PCE films loaded with a passive filler, 5% wt  $\text{Al}_2\text{O}_3$  (Almatis, 16-SG,  $d_{50}=500\text{nm}$ ), were prepared, to compare their IC vs.  $\text{Li}_{7-x}\text{La}_3\text{Zr}_{2-x}\text{Bi}_x\text{O}_{12}$ -loaded PCE films.

The cubic nature of the LLZO garnet was verified by XRD employing a Bruker D-8 Focus apparatus, Cu source ( $1.54\text{\AA}$ ), with a scan rate of  $5^\circ/\text{min}$ . The PCE films were also characterized with XRD, with a scan rate of  $2.5^\circ/\text{min}$ . The composite microstructure was studied by SEM. Polarized microscopy was employed to investigate spherulite formation. Samples for this study were prepared by pressing a film sample on the casting mold with a glass slide at  $99^\circ\text{C}$  on a hot stage for 10 minutes to decrease the sample thickness, then removing the glass slide at room temperature. Finally, the pressed film was put again on the casting mold to observe the sample on the same mold material. Then the mold was put on the hot stage, and held at  $35^\circ\text{C}$  from the melt. The tested samples were for 5%wt and 10%w as higher weight percentages the films were too opaque to obtain higher-quality images.

The ionic conductivity of the  $\sim 15$  to  $25\ \mu\text{m}$  thick membranes was characterized employing Electrochemical Impedance Spectroscopy (EIS). Temperature dependent measurements were performed at  $\sim$  room temperature ( $22^\circ\text{C}$ - $23^\circ\text{C}$ ),  $35^\circ\text{C}$ ,  $45^\circ\text{C}$ ,  $55^\circ\text{C}$ , using two stainless steel electrodes with an AC potential of 50 mV employing a custom-built Swagelok-type cell, where the electrodes were tightened to maximize contact between the electrode and the PCE film. A Solartron SI 1260 impedance/gain-phase analyzer and SI 1287 electrochemical interface operating in the frequency range 100 mHz to 1 MHz was employed. EIS measurements at all temperatures were performed after waiting for 2 hours to allow for thermal equilibrium of the materials and electrode components. EIS measurements were performed on each composite film having different weight loads over the same temperature range.

### 4.3 Results and discussion

Figure 1(a) shows the XRD scan for  $\text{Li}_{6.25}\text{La}_3\text{Zr}_{1.25}\text{Bi}_{0.75}\text{O}_{12}$ , whereas Fig. 4.1(b) presents the scan for  $\text{Li}_6\text{La}_3\text{ZrBiO}_{12}$ . Figure 1(c) corresponds to the reference pattern for cubic LLZO (ICSD 422-259). The cubic phase formation is verified at a calcination temperature of  $700^\circ\text{C}$ . Note that the peak at  $28.45^\circ$  is identified to correspond to  $\text{La}_2\text{Zr}_2\text{O}_7$ , a common byproduct in LLZO synthesis. The ionic conductivity was determined[32] to be  $2 \times 10^{-4}$  S/cm for a sample of  $\text{Li}_{6.25}\text{La}_3\text{Zr}_{1.25}\text{Bi}_{0.75}\text{O}_{12}$  having a relative density of 0.83 and  $1.2 \times 10^{-5}$  S/cm for  $\text{Li}_6\text{La}_3\text{ZrBiO}_{12}$  (relative density of 0.84). The presence of trace amounts of  $\text{La}_2\text{Zr}_2\text{O}_7$  is suggestive of probable Li loss[33].

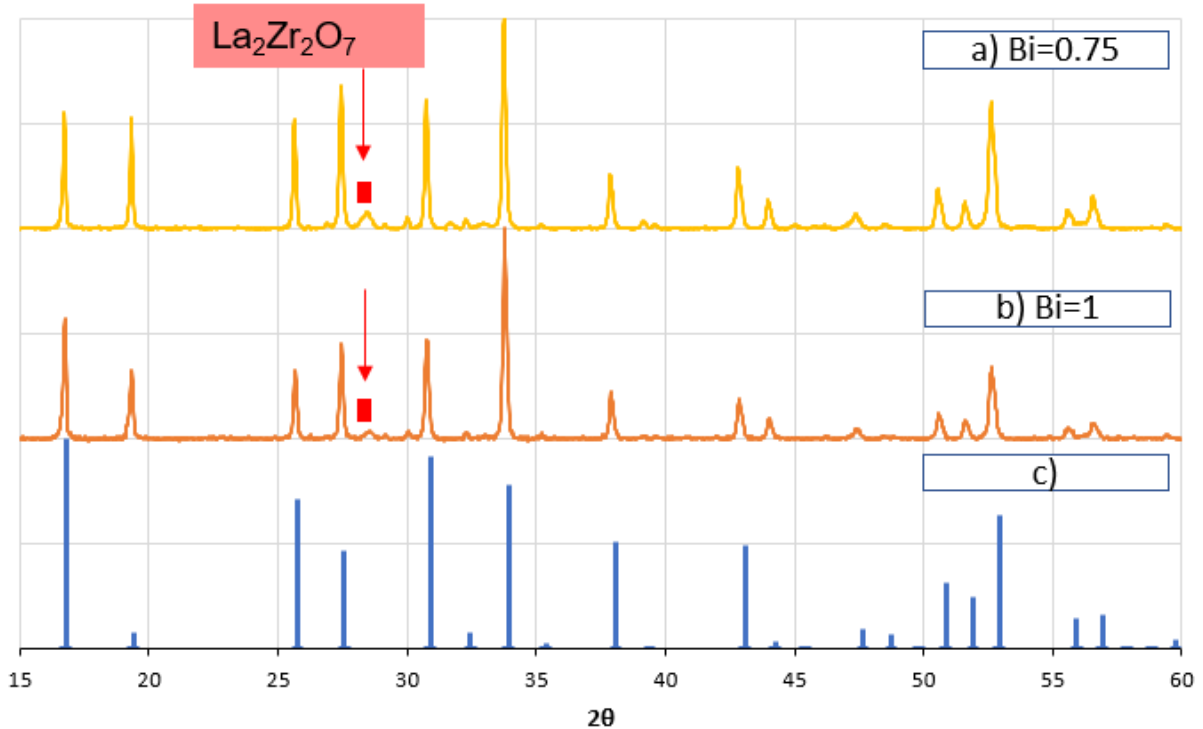


Figure 4.1 XRD patterns for: a)  $\text{Li}_{6.25}\text{La}_3\text{Zr}_{1.25}\text{Bi}_{0.75}\text{O}_{12}$  and b)  $\text{Li}_6\text{La}_3\text{ZrBiO}_{12}$ , c) reference PDF pattern corresponding to cubic LLZO (ICSD 422-259).

Figure 4.2 shows the distribution of LLZO particles in the polymer matrix. At 5% wt, a rather uniform distribution of  $\text{Li}_6\text{La}_3\text{ZrBiO}_{12}$  particles within a contiguous, smooth polymer surface is observed. For the case of the  $\text{Li}_6\text{La}_3\text{ZrBiO}_{12}$  50% wt, a rougher surface is observed, cracks in the middle of the image are visible in this case. Note that the particles observed are those near the surface of the films.

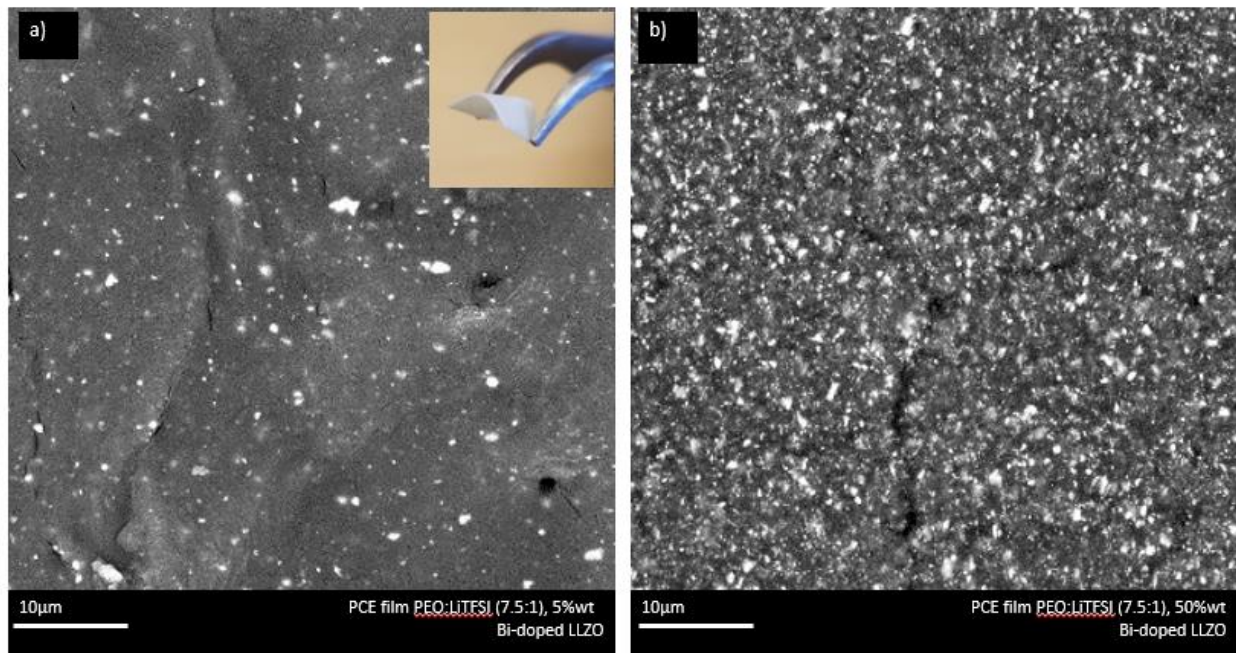


Figure 4.2 4.2(a) and 2(b) shows SEM images of  $\text{Li}_6\text{La}_3\text{ZrBiO}_{12}$  particles dispersed in PEO:LiTFSI films, for 5% wt and 50% wt respectively.

Figure 4.3 (a) shows ionic conductivity measurements of PCE films loaded with 5% wt of  $\text{Li}_{7-x}\text{La}_3\text{Zr}_{2-x}\text{Bi}_x\text{O}_{12}$  particles as a function of temperature. As observed in Fig. 4.3(a), minor additions of  $\text{Li}_6\text{La}_3\text{ZrBiO}_{12}$  increases the ionic conductivity of the PEO:LiTFSI matrix more than an order of magnitude. IC values for this 5% wt. load are  $2 \times 10^{-5} \text{ S/cm}$  and  $5.45 \times 10^{-3} \text{ S/cm}$  at room temperature and  $55^\circ\text{C}$  respectively. It is noted that the IC of the 5% wt  $\text{Li}_6\text{La}_3\text{ZrBiO}_{12}$  PCE film at room temperature is higher than that of the pellet sample of the same composition at  $27^\circ\text{C}$ .

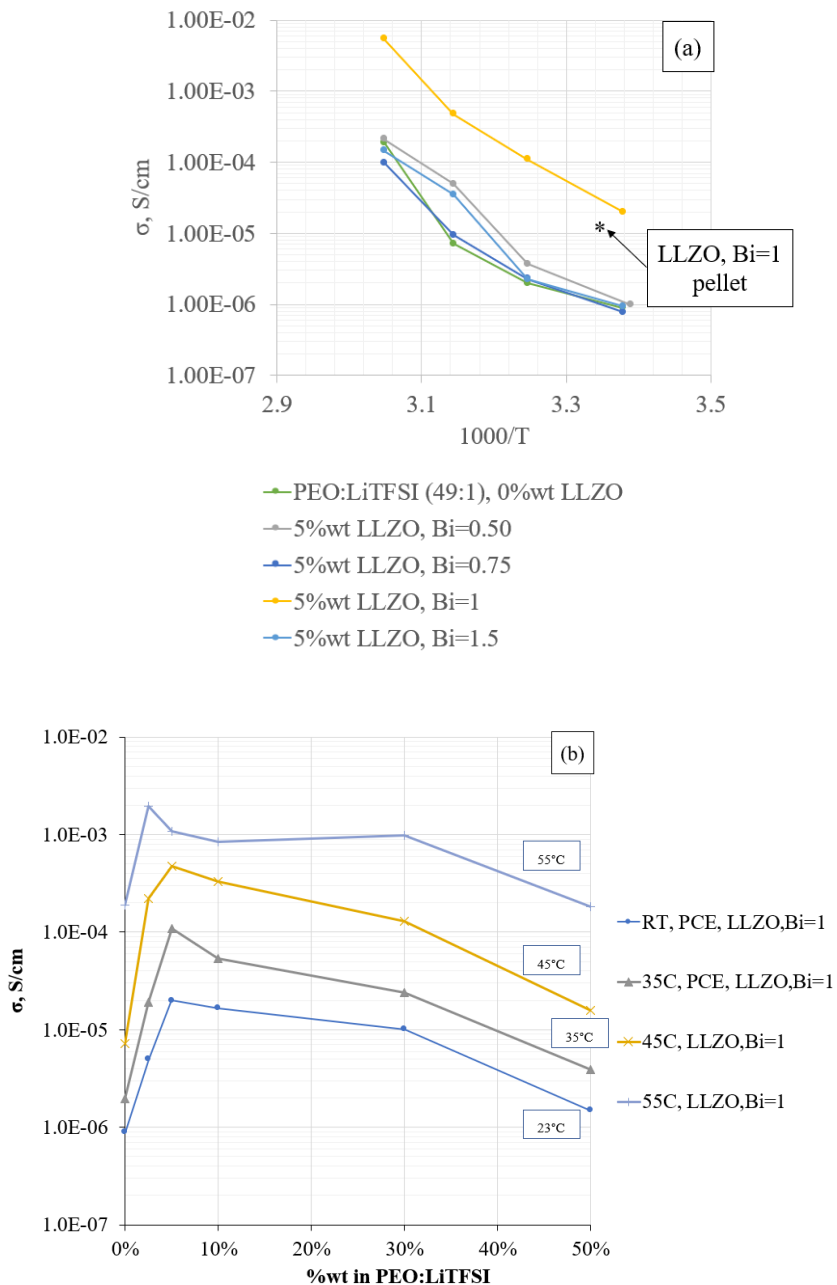


Figure 4.3(a) IC dependence on temperature for PCE loaded with  $\text{Li}_{7-x}\text{La}_3\text{Zr}_{2-x}\text{Bi}_x\text{O}_{12}$ , where  $x=0.5, 0.75, 1$  and  $1.5$ . (b) IC dependence of PCE samples with a  $\text{Li}_6\text{La}_3\text{ZrBiO}_{12}$  weight load at several temperatures.

Figure 4.4 shows XRD patterns of PCE films with 0% to 30% wt  $\text{Li}_6\text{La}_3\text{ZrBiO}_{12}$  load, as well as for a sample with 5% wt  $\text{Al}_2\text{O}_3$  particle load. With added particles, the characteristic triple peak for crystalline PEO at  $23^\circ$  decreases in magnitude compared to the sample without particles. However, peak intensity changes between the 2.5% and 5% wt load samples is small and does not

appear to indicate a drastic change in crystallinity related to the large IC change observed for the 5% wt load sample. This indicates that there are likely other contributing factors to the significant increase in ionic conductivity at 5% wt load.

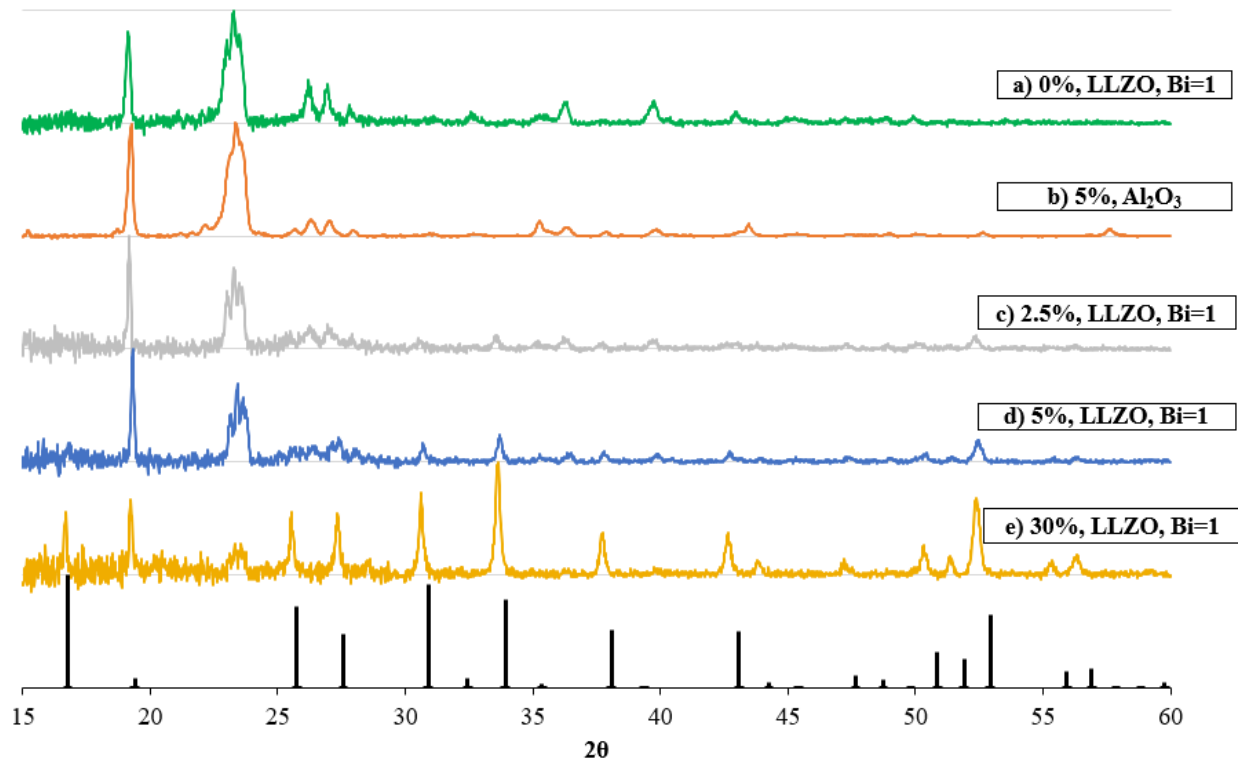


Figure 4.4 XRD patterns for PEO:LiTFSI with (a) 0% wt  $\text{Li}_6\text{La}_3\text{ZrBiO}_{12}$ , (b) 5% wt  $\text{Al}_2\text{O}_3$ , (c) 2.5% wt  $\text{Li}_6\text{La}_3\text{ZrBiO}_{12}$ , (d) 5% wt  $\text{Li}_6\text{La}_3\text{ZrBiO}_{12}$ , (e) 5% wt  $\text{Li}_6\text{La}_3\text{ZrBiO}_{12}$ . Bottom pattern refers to cubic LLZO (ICSD 422-259). The change in magnitude for the triple peak at  $23^\circ$  indicates a slight decrease in crystalline PEO, consistent with increments in ionic conductivity. However, said changes do not fully explain the strong IC dependence on garnet particle weight load.

Figure 4.5 shows the effect of  $\text{Li}_{6.25}\text{La}_3\text{Zr}_{1.25}\text{Bi}_{0.75}\text{O}_{12}$  additions to the PEO:LiTFSI system. In this case, the ionic conductivity at 5% wt does not change significantly compared to the PCE with no filler, but as weight load increases to 10% wt, the ionic conductivity reaches a high value of  $8.05 \times 10^{-6}$  S/cm at room temperature and  $3.36 \times 10^{-4}$  S/cm at  $55^\circ\text{C}$ . Figure 4.6 shows XRD patterns for PCE films with  $\text{Li}_{6.25}\text{La}_3\text{Zr}_{1.25}\text{Bi}_{0.75}\text{O}_{12}$ . It shows a slight decrease in the magnitude of the characteristic crystalline triple peak of PEO, when comparing 5% wt to 10% wt. The depression of crystallinity may be difficult to assess with this technique, as the XRD scan detects more of the Bi-LLZO phase as weight load is increased.

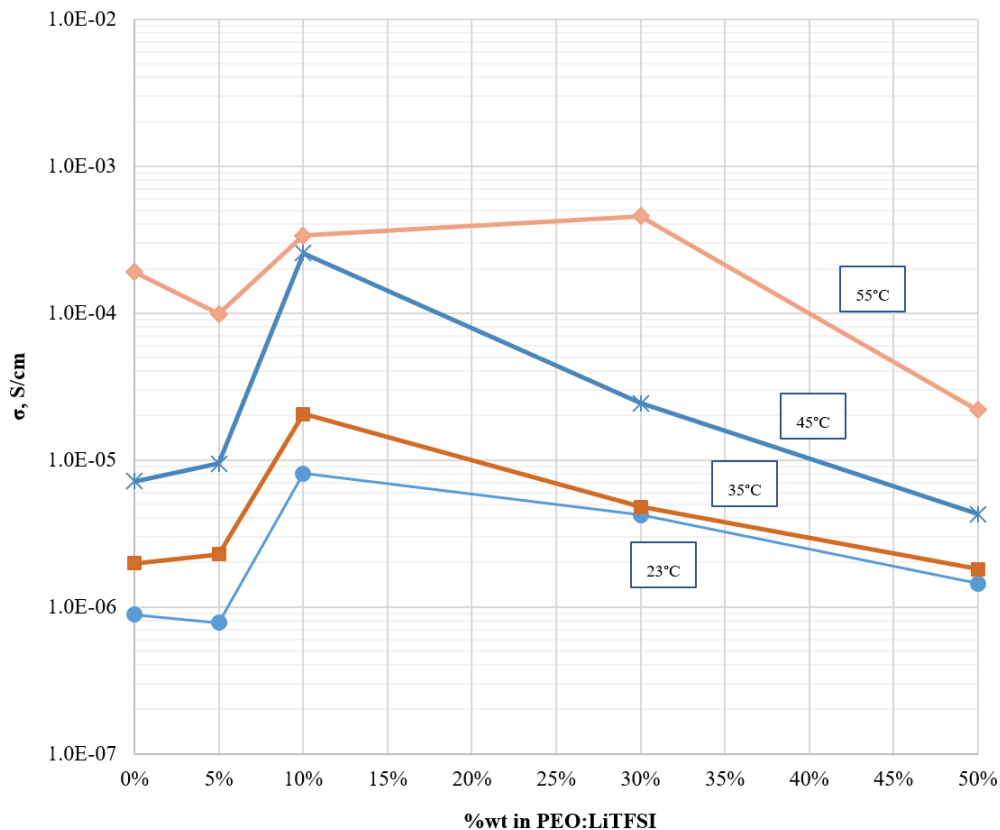


Figure 4.5 Ionic conductivity vs.  $\text{Li}_{6.25}\text{La}_3\text{Zr}_{1.25}\text{Bi}_{0.75}\text{O}_{12}$  weight load in PEO:LiTFSI. The highest ionic conductivity corresponds to 10% wt  $\text{Li}_{6.25}\text{La}_3\text{Zr}_{1.25}\text{Bi}_{0.75}\text{O}_{12}$ .

Figure 4.7 shows the ionic conductivity weight load dependence of the PEO:LiTFSI system with added  $\text{Li}_6\text{La}_3\text{ZrBiO}_{12}$  and  $\text{Li}_{6.25}\text{La}_3\text{Zr}_{1.25}\text{Bi}_{0.75}\text{O}_{12}$ . For the films containing  $\text{Li}_6\text{La}_3\text{ZrBiO}_{12}$ , an initial increase is observed, reaching an optimal load at 5% wt and a subsequent decrease, reaching a low point at 50% wt, a similar value to a 0% wt load film. It is interesting to observe the different behavior of the weight load curves. For the PCE film containing  $\text{Li}_{6.25}\text{La}_3\text{Zr}_{1.25}\text{Bi}_{0.75}\text{O}_{12}$ , the maximum ionic conductivity was reached at 10% wt and subsequently decreased as it increased to a 50% wt load.

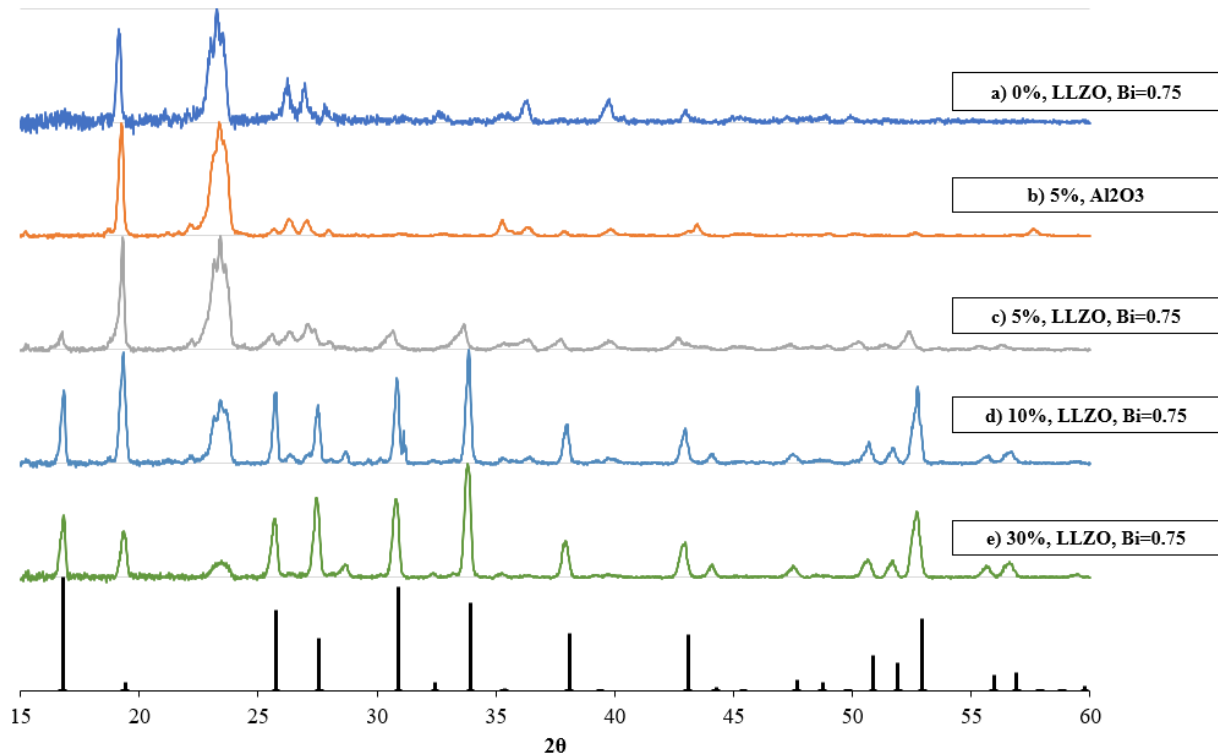


Figure 4.6 XRD scans for PEO:LiTFSI with (a) 0% wt  $\text{Li}_{6.25}\text{La}_3\text{Zr}_{1.25}\text{Bi}_{0.75}\text{O}_{12}$ , (b) 5 % wt  $\text{Al}_2\text{O}_3$ , (c) 5% wt  $\text{Li}_{6.25}\text{La}_3\text{Zr}_{1.25}\text{Bi}_{0.75}\text{O}_{12}$ , (d) 10% wt  $\text{Li}_{6.25}\text{La}_3\text{Zr}_{1.25}\text{Bi}_{0.75}\text{O}_{12}$ , (e) 30% wt  $\text{Li}_{6.25}\text{La}_3\text{Zr}_{1.25}\text{Bi}_{0.75}\text{O}_{12}$ . Bottom pattern refers to cubic LLZO (ICSD 422-259). The change in magnitude for the triple peak at  $23^\circ$  indicates a decrease in crystalline PEO, consistent with an increase in ionic conductivity.

The increment in ionic conductivity of the PEO:LiTFSI system with added  $\text{Li}_6\text{La}_3\text{ZrBiO}_{12}$  and  $\text{Li}_{6.25}\text{La}_3\text{Zr}_{1.25}\text{Bi}_{0.75}\text{O}_{12}$  and the subsequent decrement as additional filler is added, can be attributed to microstructural changes in PEO as the filler is added and on the physic-chemical properties of the LLZBO particles with different Bi content. Adding filler to the PEO:LiTFSI system is understood to hinder polymer recrystallization and increase its amorphous fraction[23]. This provides more degrees of freedom to the polymer chains to foster complexation of the lithium cation with the ether oxygen on the PEO chain that is understood to aid Li-ion diffusion[34][35] [36].

Although the change in overall polymer crystallinity indicated in Figs. 4.4 & 4.6, can be expected to impact the ionic conductivity, it does not explain the overall behavior of IC as a function of weight load. Furthermore, it is evident that a change in the Bi content of the LLZO

particles has a large effect in the bulk ionic conductivity and the weight load dependence. Therefore, other mechanism must be considered, in particular the effect of the active fillers and their physico-chemical properties on the microstructure of the polymer matrix. For example, the change in Bi-content in LLZO could potentially influence the available nucleation sites for polymer crystallization, resulting in different modifications of the polymer microstructure with particle composition.

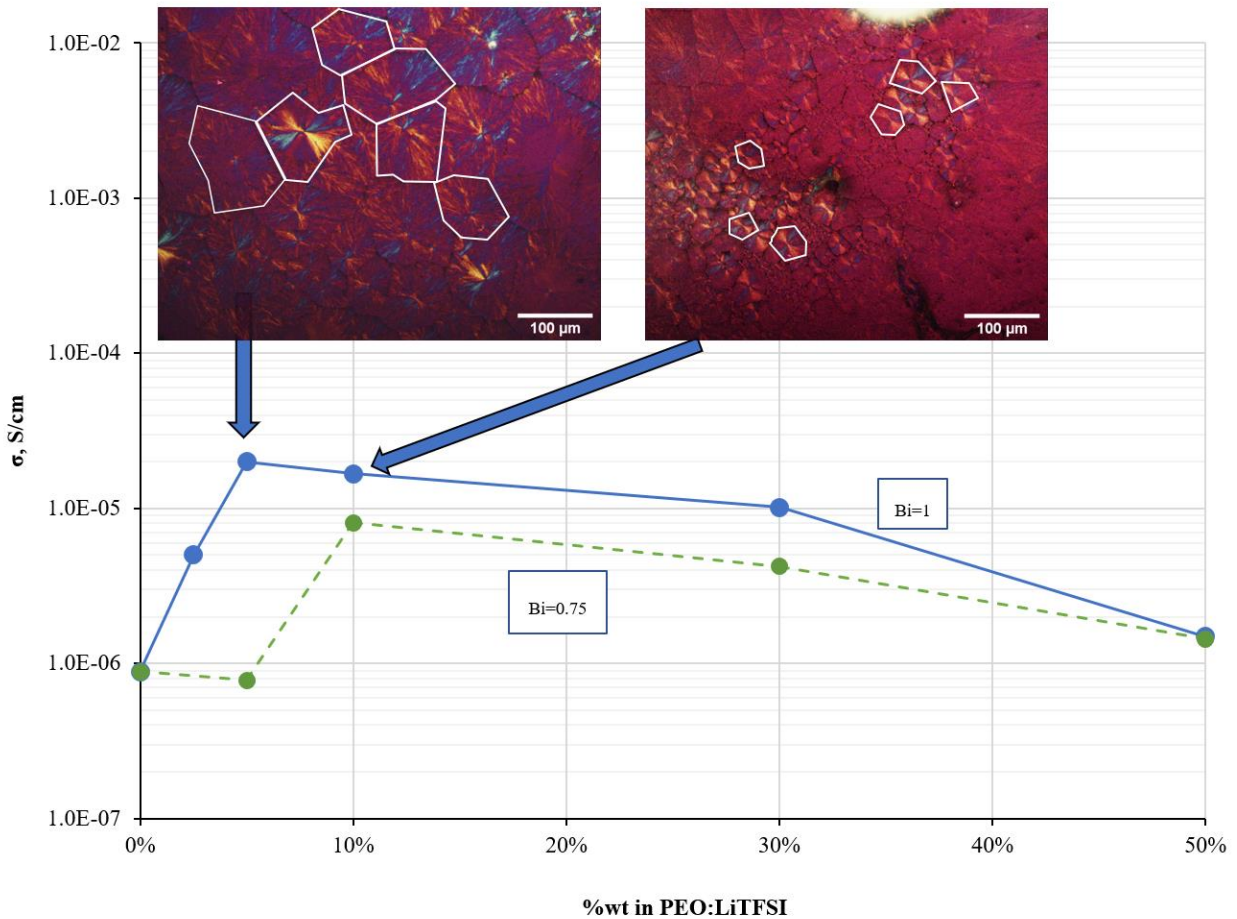


Figure 4.7 Ionic conductivity measurements of PEO:LiTFSI with added  $\text{Li}_6\text{La}_3\text{ZrBiO}_{12}$  and  $\text{Li}_{6.25}\text{La}_3\text{Zr}_{1.25}\text{Bi}_{0.75}\text{O}_{12}$  as a function of weight load at room temperature, the inset images correspond to polarized light microscopy observations. White lines added for clarity.

The role of the morphology on bulk ionic conductivity has been discussed previously[37]. There is evidence that the morphology of the PCE impacts IC and the work of Fullerton *et al.*[35] ascribes the lamellar spacing formed by spherulites in a filler-less, PEO:salt system as an important

contributor to ionic conductivity. The addition of different type of fillers modify spherulite morphology[29], however, the physical mechanism of the contributions of active filler particles such as LLZBO on ionic conduction is not fully understood.

By using Polarized light microscopy significant differences in morphology are observed. Inset in figure 7 show the difference in both number, and spherulite size in PCE films with 5% wt and 10% wt of  $\text{Li}_6\text{La}_3\text{ZrBiO}_{12}$ , and 5% wt and 10% wt  $\text{Li}_{6.25}\text{La}_3\text{Zr}_{1.25}\text{Bi}_{0.75}\text{O}_{12}$ . For a 5% wt  $\text{Li}_6\text{La}_3\text{ZrBiO}_{12}$ , large and well-defined spherulites are observed, and for the increased 10% wt load, with more particles in the polymer matrix, the number of nucleation sites increases, leading to a subsequent increase in the number of spherulites.

As the volume available for spherulite growth is decreased, the size of the spherulites also decreases, and the resulting path tortuosity for the lithium ion, could cause a decrease the bulk ionic conductivity. There is evidence from the literature that the regions between the highly-organized lamellae form a sort of “directed” transport of  $\text{Li}^+$  ions, showing a strong correlation with lamellar thickness[35]. The high ionic conductivity at low filler concentrations could come from enough sites for growth of organized channels. As the filler weight increases, the spherulites that form from nucleation sites compete in a limited volume, leading to agglomeration and less directed channels for  $\text{Li}^+$  conduction. A well-designed PCE then, necessarily needs consideration of nucleation site density and rate of polymer reorganization [38]. Through careful doping of the LLZO garnet, nucleation sites for polymer crystallization are created, resulting in an optimal PCE, with a minimum amount of LLZO used.

#### 4.4 Conclusions

In this work, the effect of adding Bi-doped LLZO to a PEO:LiTFSI system was investigated. Adding  $\text{Li}_6\text{La}_3\text{ZrBiO}_{12}$  at the 5%wt, increased the ionic conductivity of the PEO:LiTFSI system by more than an order of magnitude compared to the filler-less system. By incrementing the Bi dopant level in LLZO from  $x=1$  to  $x=0.75$ , a significant change in ionic transport was observed, and the highest ionic conductivity was obtained for a 10% wt load.

Furthermore, the ionic conductivity measured at room temperature for the 5%wt LLZBO ( $2.0 \times 10^{-5}$  S/cm), is higher than the ionic conductivity measured for the same LLZBO pellet at  $27^\circ\text{C}$

( $1.2 \times 10^{-5}$  S/cm) with a relative density of 0.84. For the case of the PEO:LiTFSI film with 10% wt of  $\text{Li}_{6.25}\text{La}_3\text{Zr}_{1.25}\text{Bi}_{0.75}\text{O}_{12}$  an ionic conductivity of  $8.1 \times 10^{-6}$  S/cm, is measured which is much lower than that of the  $\text{Li}_{6.25}\text{La}_3\text{Zr}_{1.25}\text{Bi}_{0.75}\text{O}_{12}$  pellet ( $2 \times 10^{-4}$  S/cm). The increased ionic conductivity on weight load can be correlated to increments in the amorphous fraction of the PCE films with added filler amounts. However, the different weight load dependence on Bi-content of the filler particles require other mechanisms to be involved.

Cubic LLZO plays a critical role in increasing the overall IC of the PCE system. Changing the Bi content in LLZO modifies the amount of lithium vacancies and thereby the physic-chemical properties of the particle surface. It is proposed that Li vacancies also modify the nucleation and resulting microstructure of polymer chains in the vicinity of the LLZBO added particles. This leads to PEO lamellar reorganization, forming spherulites whose morphology is influenced by the LLZBO filler particles. As the weight load is increased beyond the level for highest ionic conductivity, the number of spherulites is increased, thus increasing the tortuosity of the lithium ion transport path, resulting in an overall decrease of the ionic conductivity. We conclude that  $\text{Li}_{7-x}\text{La}_3\text{Zr}_{2-x}\text{Bi}_x\text{O}_{12}$  particle-induced amorphization is not the sole mechanism responsible for the enormous IC increments here reported. There is evidence to suggest in previous investigations that increased amorphous fractions might not result in higher IC. For example, Gadjourova *et al.*[39] report higher IC values in crystalline when compared to amorphous polymers in their study.

Furthermore, there is evidence from other investigations positing that the tortuosity of the Li ion pathway heavily influences ionic conductivity, creating a “directed” pathway for ion transport[40][35]. This suggests that controlled spherulitic growth could result in significant enhancements of ionic conductivity, even in cases where the amorphous fraction in a PCE film cannot be further increased due to mechanical stability concerns, or in cases where the limit of the EO:Li ratio has been reached.

Further studies are needed to better elucidate the role of specific dopants, or specific site substitution in the LLZO garnet. For example, doping the LLZO garnet with elements that only substitute Li, Zr, or La sites. Furthermore, by judicious manipulation of the PCE system and the doping of the LLZO garnet, competitive ionic conductivity compared to the garnet pellet can be achieved. As shown in this work, small additions of  $\text{Li}_6\text{La}_3\text{ZrBiO}_{12}$  to the polymer matrix with a

low salt concentration, provides high ionic conductivity without the need for high temperature sintering or densification.

The very small amounts of  $\text{Li}_6\text{La}_3\text{ZrBiO}_{12}$  material required drastically reduce rare-earth utilization, in addition, dispensing of the sintering cycle translate to significant materials cost reduction for the manufacturing of these promising solid state electrolytes for Li-ion battery applications. Further improvements on the IC of these PCE are anticipated employing superior polymers to PEO (ionic conductivity, thermal stability, mechanical properties, among others). In conclusion, the results here reported are most encouraging, nevertheless further studies are needed to provide a more comprehensive mechanistic understanding of ionic transport in these polymer composite electrolytes.

#### 4.5 References

- [1] B. W. Byles, N. K. R. Palapati, A. Subramanian, and E. Pomerantseva, "The role of electronic and ionic conductivities in the rate performance of tunnel structured manganese oxides in Li-ion batteries," *APL Mater.*, 2016.
- [2] P. G. Balakrishnan, R. Ramesh, and T. Prem Kumar, "Safety mechanisms in lithium-ion batteries," *Journal of Power Sources*. 2006.
- [3] L. Damen, M. Lazzari, and M. Mastragostino, "Safe lithium-ion battery with ionic liquid-based electrolyte for hybrid electric vehicles," *J. Power Sources*, 2011.
- [4] Y. A. Samad, A. Asghar, and R. Hashaikh, "Electrospun cellulose/PEO fiber mats as a solid polymer electrolytes for Li ion batteries," *Renew. Energy*, 2013.
- [5] A. . Robertson, A. . West, and A. . Ritchie, "Review of crystalline lithium-ion conductors suitable for high temperature battery applications," *Solid State Ionics*, 1997.
- [6] V. Thangadurai, H. Kaack, and W. J. F. Weppner, "Novel Fast Lithium Ion Conduction in Garnet-Type  $\text{Li}_5\text{La}_3\text{M}_2\text{O}_{12}$  (M = Nb, Ta)," *J. Am. Ceram. Soc.*, 2003.

- [7] R. Murugan, V. Thangadurai, and W. Weppner, "Fast lithium ion conduction in garnet-type  $\text{Li}_7\text{La}_3\text{Zr}_2\text{O}_{12}$ ," *Angew. Chem. Int. Ed. Engl.*, 2007.
- [8] S. D. Tillmann, P. Isken, and A. Lex-Balducci, "Gel polymer electrolyte for lithium-ion batteries comprising cyclic carbonate moieties," *J. Power Sources*, 2014.
- [9] R. C. Xu, X. H. Xia, Z. J. Yao, X. L. Wang, C. D. Gu, and J. P. Tu, "Preparation of  $\text{Li}_7\text{P}_3\text{S}_{11}$  glass-ceramic electrolyte by dissolution-evaporation method for all-solid-state lithium ion batteries," *Electrochim. Acta*, 2016.
- [10] J. C. Bachman *et al.*, "Inorganic Solid-State Electrolytes for Lithium Batteries: Mechanisms and Properties Governing Ion Conduction," *Chemical Reviews*. 2016.
- [11] J. Wolfenstine, J. Ratchford, E. Rangasamy, J. Sakamoto, and J. L. Allen, "Synthesis and high Li-ion conductivity of Ga-stabilized cubic  $\text{Li}_7\text{La}_3\text{Zr}_2\text{O}_{12}$ ," *Mater. Chem. Phys.*, 2012.
- [12] E. Rangasamy, J. Wolfenstine, and J. Sakamoto, "The role of Al and Li concentration on the formation of cubic garnet solid electrolyte of nominal composition  $\text{Li}_7\text{La}_3\text{Zr}_2\text{O}_{12}$ ," *Solid State Ionics*, 2012.
- [13] B. Commarieu, A. Paoletta, J.-C. Daigle, and K. Zaghib, "Toward high lithium conduction in solid polymer and polymer-ceramic batteries," *Curr. Opin. Electrochem.*, 2018.
- [14] E. Quartarone and P. Mustarelli, "Electrolytes for solid-state lithium rechargeable batteries: Recent advances and perspectives," *Chemical Society Reviews*. 2011.
- [15] R. C. Agrawal and G. P. Pandey, "Solid polymer electrolytes: Materials designing and all-solid-state battery applications: An overview," *J. Phys. D. Appl. Phys.*, 2008.
- [16] A. Manuel Stephan and K. S. Nahm, "Review on composite polymer electrolytes for lithium batteries," *Polymer*. 2006.

- [17] Y. H. Liao *et al.*, “Polypropylene-supported and nano-Al<sub>2</sub>O<sub>3</sub> doped poly(ethylene oxide)-poly(vinylidene fluoride-hexafluoropropylene)-based gel electrolyte for lithium ion batteries,” *J. Power Sources*, 2011.
- [18] B. Kumar, S. J. Rodrigues, and L. G. Scanlon, “Ionic Conductivity of Polymer-Ceramic Composites,” *J. Electrochem. Soc.*, 2001.
- [19] Y. J. Lim *et al.*, “Ceramic-Based Composite Solid Electrolyte for Lithium-Ion Batteries,” *Chempluschem*, vol. 80, no. 7, pp. 1100–1103, 2015.
- [20] F. Langer, I. Bardenhagen, J. Glenneberg, and R. Kun, “Microstructure and temperature dependent lithium ion transport of ceramic-polymer composite electrolyte for solid-state lithium ion batteries based on garnet-type Li<sub>7</sub>La<sub>3</sub>Zr<sub>2</sub>O<sub>12</sub>,” *Solid State Ionics*, 2016.
- [21] J. H. Choi, C. H. Lee, J. H. Yu, C. H. Doh, and S. M. Lee, “Enhancement of ionic conductivity of composite membranes for all-solid-state lithium rechargeable batteries incorporating tetragonal Li<sub>7</sub>La<sub>3</sub>Zr<sub>2</sub>O<sub>12</sub> into a polyethylene oxide matrix,” *J. Power Sources*, 2015.
- [22] Z. Li *et al.*, “Ionic Conduction in Composite Polymer Electrolytes: Case of PEO:Ga-LLZO Composites,” *ACS Appl. Mater. Interfaces*, 2019.
- [23] L. Fan, C. W. Nan, and M. Li, “Thermal, electrical and mechanical properties of (PEO)<sub>16</sub>LiClO<sub>4</sub> electrolytes with modified montmorillonites,” *Chemical Physics Letters*. 2003.
- [24] C. H. Lee *et al.*, “Low temperature synthesis of garnet type solid electrolyte by modified polymer complex process and its characterization,” *Mater. Res. Bull.*, 2016.
- [25] C. A. Geiger *et al.*, “Crystal Chemistry and Stability of ‘Li<sub>7</sub>La<sub>3</sub>Zr<sub>2</sub>O<sub>12</sub>’ Garnet: A Fast Lithium-Ion Conductor,” *Inorg. Chem.*, 2011.
- [26] N. C. Rosero-Navarro, T. Yamashita, A. Miura, M. Higuchi, and K. Tadanaga, “Preparation of Li<sub>7</sub>La<sub>3</sub>(Zr<sub>2-x</sub>Nb<sub>x</sub>)O<sub>12</sub> (x = 0-1.5) and Li<sub>3</sub>BO<sub>3</sub>/LiBO<sub>2</sub> composites at low temperatures using a sol-gel process,” *Solid State Ionics*, 2016.

- [27] W. Wiczorek, "Composite polyether based solid electrolytes. The Lewis acid-base approach," *Solid State Ionics*, 1996.
- [28] M. Marcinek *et al.*, "Effect of Filler Surface Group on Ionic Interactions in PEG–LiClO<sub>4</sub>–Al<sub>2</sub>O<sub>3</sub> Composite Polyether Electrolytes," *J. Phys. Chem. B*, 2002.
- [29] Y. W. Kim, W. Lee, and B. K. Choi, "Relation between glass transition and melting of PEO-salt complexes," *Electrochim. Acta*, 2000.
- [30] T. Yang, J. Zheng, Q. Cheng, Y. Y. Hu, and C. K. Chan, "Composite Polymer Electrolytes with Li<sub>7</sub>La<sub>3</sub>Zr<sub>2</sub>O<sub>12</sub> Garnet-Type Nanowires as Ceramic Fillers: Mechanism of Conductivity Enhancement and Role of Doping and Morphology," *ACS Appl. Mater. Interfaces*, 2017.
- [31] M. R. Oduncu, "Development of a novel polymer-garnet solid state composite electrolyte incorporating Li-La-Zr-Bi-O and polyethylene oxide," 2016.
- [32] D. K. Schwanz, A. Villa, M. Balasubramanian, B. Helfrecht, and E. E. Marinero, "Ionic conductivity enhancements and low temperature synthesis of Li<sub>7</sub>La<sub>3</sub>Zr<sub>2</sub>O<sub>12</sub> garnets by Bi aliovalent substitutions," Feb. 2019.
- [33] C. Bernuy-Lopez, W. Manalastas, J. M. Lopez Del Amo, A. Aguadero, F. Aguesse, and J. A. Kilner, "Atmosphere controlled processing of ga-substituted garnets for high li-ion conductivity ceramics," *Chem. Mater.*, 2014.
- [34] S. K. Fullerton-Shirey and J. K. Maranas, "Structure and mobility of PEO/LiClO<sub>4</sub> solid polymer electrolytes filled with Al<sub>2</sub>O<sub>3</sub> nanoparticles," *J. Phys. Chem. C*, 2010.
- [35] S. K. Fullerton-Shirey and J. K. Maranas, "Effect of LiClO<sub>4</sub> on the structure and mobility of PEO-based solid polymer electrolytes," *Macromolecules*, 2009.
- [36] K. Karthik and R. Murugan, "Lithium garnet based free-standing solid polymer composite membrane for rechargeable lithium battery," *Journal of Solid State Electrochemistry*, 2018.

- [37] M. Marzantowicz, F. Krok, J. R. Dygas, Z. Florjańczyk, and E. Zygadło-Monikowska, “The influence of phase segregation on properties of semicrystalline PEO:LiTFSI electrolytes,” *Solid State Ionics*, 2008.
- [38] M. Marzantowicz *et al.*, “Crystalline phases, morphology and conductivity of PEO:LiTFSI electrolytes in the eutectic region,” *J. Power Sources*, 2006.
- [39] Z. Gadjourova, Y. G. Andreev, D. P. Tunstall, and P. G. Bruce, “Ionic conductivity in crystalline polymer electrolytes,” *Nature*, 2001.
- [40] S. Cheng, D. M. Smith, and C. Y. Li, “How does nanoscale crystalline structure affect ion transport in solid polymer electrolytes?,” *Macromolecules*, 2014.

## **5. FURTHER ELUCIDATION OF THE PEO-BASED LLZO POLYMER COMPOSITE ELECTROLYTE: ROLE OF LI MOLAR RATIO AND POLYMER MICROSTRUCTURE**

### **5.1 Introduction**

Polymer electrolytes are potential replacements for the liquid solvent electrolytes that are used in current commercial lithium-ion energy storage devices. Polymer electrolytes are not flammable, can be prepared as solid state electrolytes, are compatible with Li metal[1], are flexible and prevent dendrite formation[2]. An important drawback of solid polymer electrolytes, is their low ionic conductivity at room temperature. By adding fillers to solid polymer electrolytes, the ionic conductivity can be raised by up to two orders of magnitude[3][4][5]. The fillers that have been used can be passive or active, where the latter conduct lithium ions and the former do not.

Additionally, fillers hinders polymer reorganization in the PCE, increasing the amount of amorphous polymer fraction. Ionic conduction occurs faster through amorphous regions, thus increasing the overall bulk ionic conductivity. Additionally, it is understood that filler particle surfaces act as nucleation centers for polymer recrystallization. Lewis acid theory explains that the nature of the particle surface can influence the bulk ionic conductivity of the PCE system[6]. It's intuitive then, to design a system with maximum amorphous fraction of the PCE system, either by increasing the lithium salt content, adding fillers. However, semicrystalline systems are reported to perform better than a fully amorphous PCE[7].

Some authors have investigated the polymer microstructure with polarized light microscopy (PLM), and characterized PEO polymer electrolytes with the addition of lithium salts[7] . Variation of the EO:Li ratio leads to changes in the number and size of polymer spherulites, as well as to different ionic conductivity values. In another paper, the lamellar thickness showed a greater correlation with ionic conductivity[8], than with the amorphous fraction. These results suggests that the mechanism of ionic transport also depends on the morphology of the PCE (spherulite formation) and not only on the average amorphous fraction. Although the authors provide important insights, the ionic conductivity in these filler-less polymer electrolytes is still very low at room temperature.

By adding a filler, the ionic conductivity of the PEO:LiTFSI system can be increased, without compromising the mechanical stability of the PCE system. Furthermore, we can contribute to elucidate the mechanism of ionic conduction by choosing a filler that alters the nucleation site density for spherulites. By doping LLZO, lithium vacancy sites are created[9], which can generate nucleation sites for polymer reorganization. If spherulite formation and size also contributes to the bulk ionic conductivity, then the addition of differently-doped LLZO can be expected to result in different values of ionic conductivity for the same weight loading.

Comparing the effect of LLZO fillers at the same weight load is important, as the ionic conductivity for PCEs reaches an optimum value for specific weight loads, and this can vary from low [10] to high weight loads[11]. In another study, tetragonal LLZO was loaded in a PAN:LiClO<sub>4</sub> polymer electrolyte and compared with a doped cubic LLZO[12]. Its ionic conductivity determined at the same 5% wt load. The differences in ionic conductivity values were not explained and as to why the best results are obtained at 5% wt load.

In this chapter, an elucidation into why optimal values for ionic conductivity are obtained at a certain weight load is attempted. The effect of different film sample geometry will also be studied. Doped cubic LLZO is synthesized, where the dopants are Bi, Ca, Ga and Nd. Table 1 shows the sample nomenclature for this chapter. The garnet powders are added to PEO:LiTFSI matrixes at the 5% wt weight load. IC are measured and compared between PCEs loaded with both Bi-LLZO and co-doped LLZO.

## 5.2 Materials and methods

In order to better understand the relationship between PCE microstructure and bulk ionic conductivity, PEO:LiTFSI films were prepared with a EO:Li=49 ratio, and LLZO powders were added as fillers. Specifically,  $\text{Li}_6\text{La}_3\text{ZrBiO}_{12}$ ,  $\text{Li}_{6.25}\text{La}_3\text{Zr}_{1.25}\text{Bi}_{0.75}\text{O}_{12}$ , and  $\text{Li}_{6.25}\text{La}_{2.8}\text{Nd}_{0.2}\text{Zr}_{1.25}\text{Bi}_{0.75}\text{O}_{12}$  were added to the PEO:LiTFSI system. For the sake of simplicity and efficiency, table 5.1 shows the garnet powders' shortened nomenclature used in this chapter.

Table 5-1 Formula and sample name for LLZO garnets synthesized and used in this work.

<b>Formula</b>	<b>Sample Formula</b>	<b>Sample name</b>
$\text{Li}_{7-x}\text{La}_3\text{Zr}_{2-x}\text{Bi}_x\text{O}_{12}$	$\text{Li}_{6.25}\text{La}_3\text{Zr}_{1.25}\text{Bi}_{0.75}\text{O}_{12}$	0.75Bi-LLZO
$\text{Li}_{7-x}\text{La}_3\text{Zr}_{2-x}\text{Bi}_x\text{O}_{12}$	$\text{Li}_6\text{La}_3\text{ZrBiO}_{12}$	Bi-LLZO
$\text{Li}_{7-x}\text{La}_{3-y}\text{Nd}_y\text{Zr}_{2-x}\text{Bi}_x\text{O}_{12}$	$\text{Li}_{6.25}\text{La}_{2.8}\text{Nd}_{0.2}\text{Zr}_{1.25}\text{Bi}_{0.75}\text{O}_{12}$	BiNd-LLZO

PCE sample films were prepared by mixing polyethylene oxide (PEO, Sigma Aldrich, molecular weight 100,000), lithium bis(trifluoromethanesulfonyl)imide (LiTFSI, Sigma Aldrich, 99.8%) and the powders of the garnets shown in table 1. Acetonitrile (ACN, Sigma Aldrich, 99.9%) was used as solvent to mix and prepare the PCE slurry. The PCE slurry was ball-milled for 12 hours at 400 rpm with a Fritsch Pulverisette 6 device, with a 2.5 to 1 acetonitrile to solids ratio. Three types of film samples were prepared: thin films (thickness range of 0.15mm to 0.3mm), thick films (thickness range of 0.9mm to 1.2mm) and fused bi-films.

To prepare the thin films, the PCE slurries was poured onto a square-shaped casting mold, with a 1mm thickness and an area of 1" x 1" area with a syringe. To prepare the thick films, the PCE slurry was poured with a syringe into a similar square-shaped casting mold (with a 2mm thickness and a 5mm by 5 mm area). All of the PCE slurries were dried for 72 hours at room temperature at atmospheric pressure, after which, the films were held in vacuum overnight to completely remove the acetonitrile solvent. To prepare the thin bi-films, sample films were dabbed with a q-tip with acetonitrile and were sandwiched together, and left to dry overnight to remove presence of acetonitrile. Optical microscopy was used to characterize the thickness of the thick films and thin bi-films.

The ionic conductivity of the of the PCE films were characterized by putting the films between two stainless steel electrodes, and employed electrochemical impedance spectroscopy (EIS) with a 50 mV AC potential in a Solartron SI 1260 impedance/gain-phase analyzer and SI 1287 setup. The frequency range was 100mHz to 300kHz. All EIS data was collected after 2 hours at each temperature point to allow thermal equilibrium of the materials and the PCE films.

### 5.3 Results and discussion

Figure 5.1 shows the ionic conductivity as a function of Bi-LLZO, 0.75Bi-LLZO and BiNd-LLZO weight load in PEO:LiTFSI. As observed from the figure, the ionic conductivity increases compared to the filler-less electrolyte. For the polymer electrolyte with Bi-LLZO, the highest ionic conductivity is reached at 5% wt ( $\sigma=2 \times 10^{-5}$  S/cm at 23°C), and starts to decrease, until 50% wt, where the added filler has only a slight effect on ionic conductivity. For the polymer electrolyte with 0.75Bi-LLZO we see again an increase in ionic conductivity, but the highest value is reached at 10% wt ( $\sigma=8.1 \times 10^{-6}$  S/cm at 23°C).

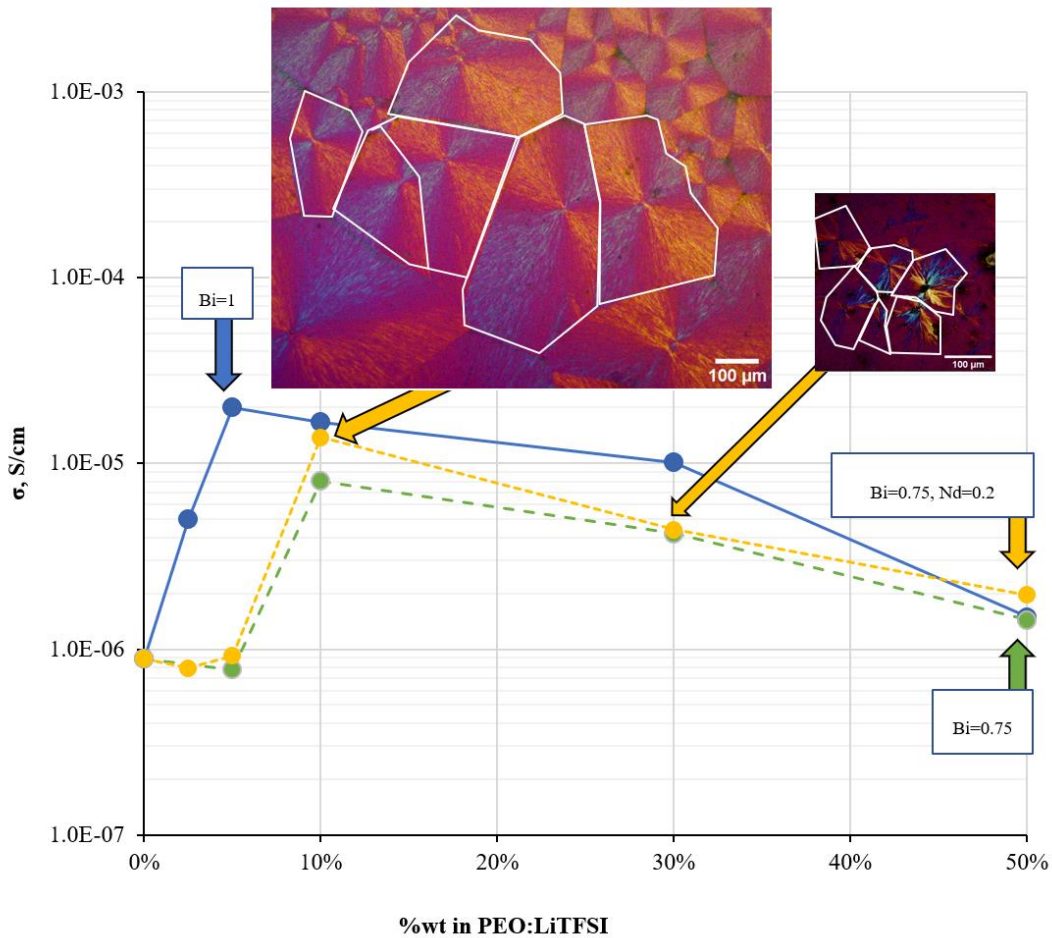


Figure 5.1 Ionic conductivity of PEO:LiTFSI films as a function of weight load for various garnet particle compositions: Bi-LLZO, 0.75Bi-LLZO, and BiNd-LLZO. Inset images: PLM images showing spherulite morphology changes as a function of weight load. White lines added for clarity.

It is unclear what the role of the LLZO dopant is determining why the optimal ionic conductivity is reached at a specific weight load[12]. From figure 5.1, it is apparent that variation in Bi and the concomitant Li molar ratio determines the optimal weight load. To validate this observation, a BiNd-LLZO-loaded PCE film was characterized and compared with a Bi-LLZO-loaded PCE film.

The ionic conductivity for both the Bi-LLZO film and the BiNd-LLZO film, increase compared to the filler-less films, and reach a maximum value at 10%wt ( $\sigma=1.38 \times 10^{-5}$  S/cm at 23°C), subsequently, it decreases as the weight load increases. Since Nd only substitutes on the La site in LLZO, without altering the Li molar ratio, this means that this particular dopant is not expected to influence the bulk conductivity of the PCE or the weight load at which the maximum value is obtained. The optimal weight load is expected to depend only on the Li molar ratio.

Changing the Li molar ratio from 6 to 6.25, the PCE microstructure is changed in a way where the optimal ionic conductivity is now achieved at 10%wt. This is supported by PLM images observed in the inset in figure 1. Note the difference in spherulite size and number. This difference means that optimal ionic conductivity does not only depend on a high amorphous fraction, but also on the generation of a morphology that provides “directed” lithium ion transport channels as alluded to in other publications[8][13].

Based on these results, the following mechanism is proposed. The Li molar ratio of the LLZO filler determines the nucleation site density for spherulite formation. This is consistent with Lewis acid-base theory, positing that particle surfaces interact with poly ether oxygens, increasing the number of free  $\text{Li}^+$  ions[14]. In the case of LLZO, Li vacancies formed from doping the garnet, can act as nucleation sites for lamellar reorganization and subsequent spherulite formation. An optimal number and size and number of spherulites results in higher ionic conductivity. This is a result of a high amorphous fraction as well as a lower tortuosity for the Li-ion path. A diagram of the proposed mechanism is given in figure 5.2. For a given film with thickness  $h$  and with same weight load of Bi-LLZO and 0.75Bi-LLZO, the change in ionic conductivity can be ascribed to the increase in tortuosity for the Li-ion path (as seen in figure 5.2 (a) to (b)).

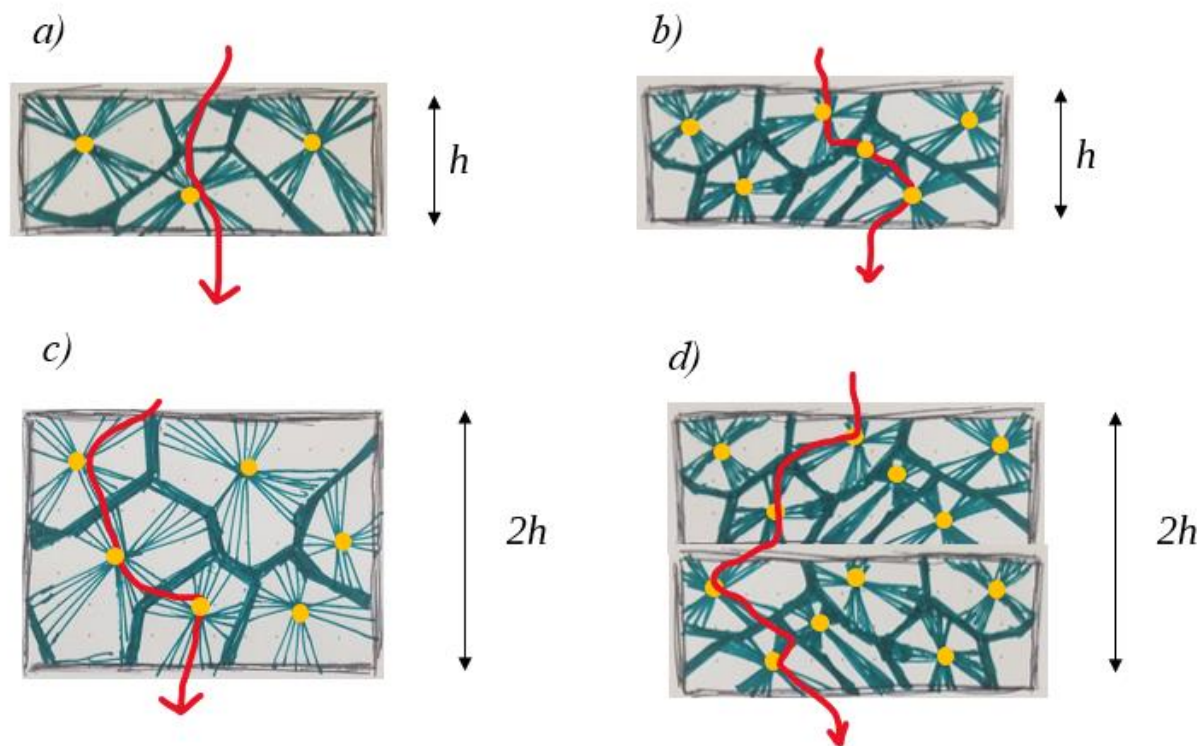


Figure 5.2 Schematic representation depicting how spherulite formation affects Li-ion conduction in a PCE. Yellow dots represent spherulite centers. Red line represents possible Li<sup>+</sup> path.

In Fig. 5.3 the ionic conductivity of thin and thick films with 10% wt 0.75Bi-LLZO and 10% wt BiNd-LLZO are shown. Ionic conductivity for the thicker films is lower compared to the thinner films. This is due to increased tortuosity resulting from larger spherulite formation in the thicker film compared to the 2D-like spherulite formation in the thinner film (as seen in figure 5.2, going from (a) to (c)).

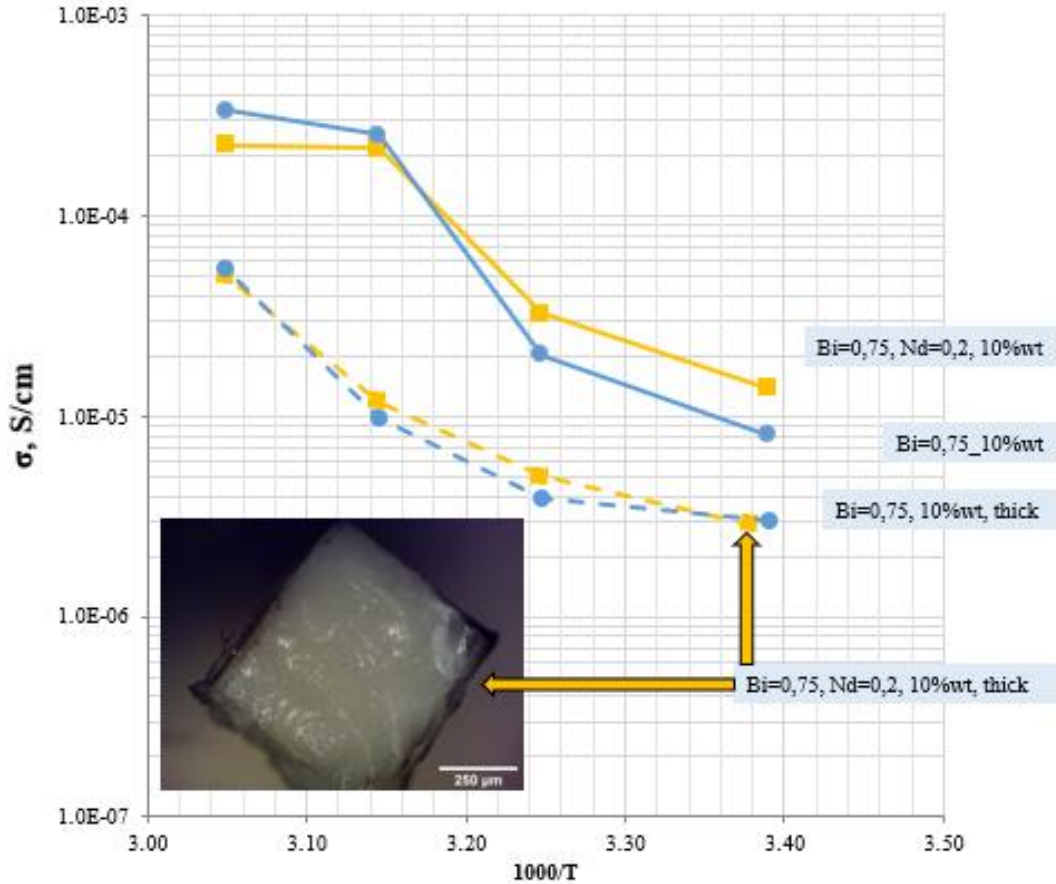


Figure 5.3 Arrhenius plots of ionic conductivity for thin and thick PCE samples loaded with 10% wt 0.75Bi-LLZO and 10% wt BiNd-LLZO. The image on the lower portion of the figure corresponds to a thick BiNd-LLZO sample.

Finally, the effect of structural morphology and order in the PCE is illustrated in Fig. 5.4. A “thick” composite of BiNd-LLZO is fabricated by fusing together two thin thinner films with the same particle weight load. An image of such fused sample is shown in the lower portion of the figure. It can be seen that the ionic conductivity for the fused bi-film for 10%wt  $\text{Li}_{6.25}\text{La}_{2.8}\text{Nd}_{0.2}\text{Zr}_{1.25}\text{Bi}_{0.75}\text{O}_{12}$  is much lower than that of the thinner identical sample and also for the equivalent thick film. The lower ionic conductivity in the thicker specimen can be explained by the higher tortuosity for ion transport that results when the two microstructurally uncorrelated thin films are fused together (as seen in figure 5.2, going from (a) to (d)).

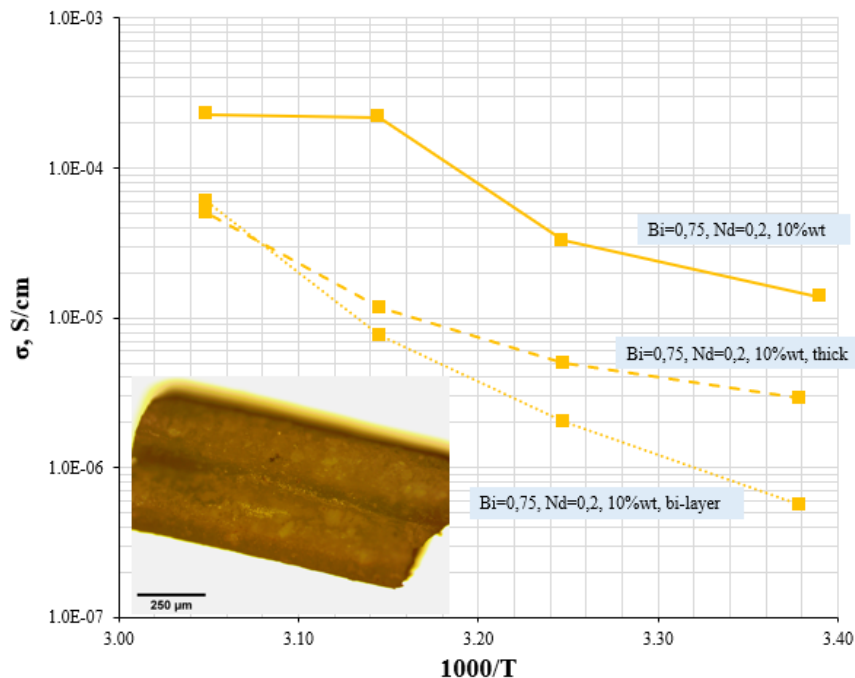


Figure 5.4 Arrhenius plots for the ionic conductivity of PCE films loaded with 10% wt BiNd-LLZO. The ionic conductivity vastly differs for thick and thin samples and an even lower value is measured for a thick sample obtained by fusing two thinner films.

## 5.4 Conclusions

In this chapter, the Li-ion transport mechanism in PCE films was investigated. By embedding a PEO:LiTFSI electrolyte with Bi-doped LLZO, the ionic conductivity was improved by an order of magnitude with a weight load of 5% wt. By adjusting the molar ratio of Bi, from Bi=1 to Bi=0.75, the ionic conductivity was also improved by an order of magnitude, but the weight load needed to achieve the highest IC value was 10% wt. A mechanism to explain these results is proposed, where the change in Bi molar ratio alters the spherulite nucleation site density in the polymer melt, as evidenced by PLM images. The change in Bi molar ratio means a change in Li molar ratio, from Li=6 to 6.25, this determines the optimum weight load at which the highest ionic conductivity is observed.

To validate the importance of the Li molar ratio, BiNd-LLZO garnets were synthesized and embedded in a PEO:LiTFSI electrolyte, where the molar ratio were Bi=0.75 and Nd=0.2. The resulting film was compared with the previous Bi-doped LLZO, where Bi=0.75. The addition of

Nd as a dopant does not alter Li molar ratio. Both PCE films behaved similarly, reaching an optimal weight load of 10%wt.

The mechanism is further elucidated by casting thicker films of the same 10%wt BiNd-LLZO electrolyte film. As Li-ion transport is influenced by PCE morphology, increasing the thickness of the film, the tortuosity for Li-ion transport is incremented, thus reducing the ionic conductivity. This is also demonstrated by a second experiment, where a 10%wt BiNd-LLZO bilayer film was characterized. The ionic conductivity decreases compared the single film, resulting from the discontinuity formed by fusing the two films, increasing the tortuosity for Li-ion pathway.

Although the role of amorphous fraction for Li-ion transport in PCEs is fairly-well understood, the reasons why different fillers need different weight loads to reach optimal ionic conductivity had not been explained thus far. The results presented in this chapter provide evidence on the role of polymer microstructure which is largely influenced by the Li vacancy ratio of the added garnet particles. These results are promising, as chemical manipulation of fillers can lead to high ionic conductivity with very low weight loads, decreasing PCE fabrication costs.

## 5.5 References

- [1] Q. Li, H. Y. Sun, Y. Takeda, N. Imanishi, J. Yang, and O. Yamamoto, "Interface properties between a lithium metal electrode and a poly(ethylene oxide) based composite polymer electrolyte," *J. Power Sources*, 2001.
- [2] C. Wang *et al.*, "Suppression of Lithium Dendrite Formation by Using LAGP-PEO (LiTFSI) Composite Solid Electrolyte and Lithium Metal Anode Modified by PEO (LiTFSI) in All-Solid-State Lithium Batteries," *ACS Appl. Mater. Interfaces*, 2017.
- [3] J. Xi *et al.*, "Composite polymer electrolyte doped with mesoporous silica SBA-15 for lithium polymer battery," *Solid State Ionics*, 2005.

- [4] L. Fan, C. W. Nan, and M. Li, "Thermal, electrical and mechanical properties of (PEO)<sub>16</sub>LiClO<sub>4</sub> electrolytes with modified montmorillonites," *Chemical Physics Letters*, 2003.
- [5] S. H. S. Cheng *et al.*, "Electrochemical performance of all-solid-state lithium batteries using inorganic lithium garnets particulate reinforced PEO/LiClO<sub>4</sub> electrolyte," *Electrochim. Acta*, 2017.
- [6] W. Wieczorek, "Composite polyether based solid electrolytes. The Lewis acid-base approach," *Solid State Ionics*, 1996.
- [7] M. Marzantowicz, F. Krok, J. R. Dygas, Z. Florjańczyk, and E. Zygadło-Monikowska, "The influence of phase segregation on properties of semicrystalline PEO:LiTFSI electrolytes," *Solid State Ionics*, 2008.
- [8] S. Cheng, D. M. Smith, and C. Y. Li, "How does nanoscale crystalline structure affect ion transport in solid polymer electrolytes?," *Macromolecules*, 2014.
- [9] K. Meier, T. Laino, and A. Curioni, "Solid-state electrolytes: Revealing the mechanisms of Li-Ion conduction in tetragonal and cubic LLZO by first-principles calculations," *J. Phys. Chem. C*, 2014.
- [10] H. Y. Sun, H. J. Sohn, O. Yamamoto, Y. Takeda, and N. Imanishi, "Enhanced lithium-ion transport in PEO-based composite polymer electrolytes with ferroelectric BaTiO<sub>3</sub>," *J. Electrochem. Soc.*, 1999.
- [11] J. H. Choi, C. H. Lee, J. H. Yu, C. H. Doh, and S. M. Lee, "Enhancement of ionic conductivity of composite membranes for all-solid-state lithium rechargeable batteries incorporating tetragonal Li<sub>7</sub>La<sub>3</sub>Zr<sub>2</sub>O<sub>12</sub> into a polyethylene oxide matrix," *J. Power Sources*, 2015.
- [12] T. Yang, J. Zheng, Q. Cheng, Y. Y. Hu, and C. K. Chan, "Composite Polymer Electrolytes with Li<sub>7</sub>La<sub>3</sub>Zr<sub>2</sub>O<sub>12</sub> Garnet-Type Nanowires as Ceramic Fillers: Mechanism of Conductivity Enhancement and Role of Doping and Morphology," *ACS Appl. Mater. Interfaces*, 2017.

- [13] S. K. Fullerton-Shirey and J. K. Maranas, "Effect of LiClO<sub>4</sub> on the structure and mobility of PEO-based solid polymer electrolytes," *Macromolecules*, 2009.
- [14] F. Croce, L. L. Persi, B. Scrosati, F. Serraino-Fiory, E. Plichta, and M. A. Hendrickson, "Role of the ceramic fillers in enhancing the transport properties of composite polymer electrolytes," *Electrochim. Acta*, 2001.

## 6. GENERAL SUMMARY AND CONCLUSIONS

### 6.1 Thesis summary

In this work a potential material set for replacing organic solvent electrolytes in Li-ion battery technology was investigated. A polymer composite electrolyte (PCE) comprising polyethylene oxide (PEO), Lithium bis(trifluoromethanesulfonyl)imide (LiTFSI) and the active filler LLZO garnet was investigated. Particular emphasis was given to understanding the role of each PCE component on the Li-ion transport and the microstructural properties of the composite. Solid polymer electrolytes are promising materials for future battery technology providing solutions to the inherent safety and performance issues of current batteries employing flammable liquid electrolytes. However, the inherent low ionic conductivity of solid state electrolytes has been a major hurdle in their implementation into battery technology. By adding passive or active fillers at a certain weight load, the ionic conductivity of the polymer-Li salt matrix can be increased by orders of magnitude. The physic-chemical mechanisms underpinning the development of high ionic conductivity in these composite solid state electrolytes is yet to be fully understood. In this work, doped LLZO particles were employed as the active fillers. The aliovalent substitution into the Zr and La sites by Bi, Ga, Ca and Nd enabled us to manipulate the Li-vacancy on the garnet Li-site and to study the effects of said aliovalent substitution on the ionic conductivity and microstructure of the PCE materials.

$\text{Li}_{7-x}\text{La}_3\text{Bi}_x\text{Zr}_{2-x}\text{O}_{12}$  garnets were fabricated using a sol-gel Pechini method. The method allowed the synthesis of the high ionic conductivity cubic phase with only minor impurity traces of phases such as  $\text{La}_2\text{Zr}_2\text{O}_7$  at record low temperatures ( $\sim 700^\circ\text{C}$ ) in significantly shorter times, when compared to solid-state reaction methods such as ball milling. Dual-doped LLZO garnets were also synthesized with the same method and their properties compared with Bi-LLZO. The co-doped garnets fabricated were: Bi and Ca (BiCa-LLZO), Bi and Ga (BiGa-LLZO) and Bi and Nd (BiNd-LLZO). This allowed the study of the effect of La-site substitution, cubic lattice parameter changes, and Li-vacancy occupancy variations on ionic conductivity. X-ray diffraction was used to verify cubic phase formation, SEM was employed to study grain morphology, the presence of dopants in the specimens was confirmed employing EDS and EIS was used to measure ionic conductivity. Ca additions appear to decrease the ionic conductivity, possibly on account of

a reduction of lattice constant, which is understood to decreasing the ionic pathway in the garnet structure. Adding Ga was expected to increment ionic conductivity, based on published results, but in this work the IC was observed to decrease when Ga was added. This is believed to be due to a depletion of molar Li, down to 5.5. Optimal ionic conductivity is believed to be at a range between 6.25 to 6.75 molar Li, as the vacancy number is optimized to allow fast single jump events for Li. Finally, the effect of adding Nd was also observed in this work to decrease the ionic conductivity, and this could be attributed to a decrement in lattice constant. Since Nd only substitutes on La sites, molar Li was not altered, and changes in ionic conductivity can be attributed to the changes in structure of the garnet unit cell. It is noted that one important limitation in this work in comparing the ionic conductivity for the various single and dual doped LiLaZrO samples fabricated is the lack of full densification and grain connectivity in the samples studied. This, as discussed in this thesis, significantly impacts the attainable value of ionic conductivity in garnet pellet samples.

To understand the effect of the Bi content in LLZO on the bulk ionic conductivity of a polymer composite electrolyte (PCE),  $\text{Li}_{7-x}\text{La}_3\text{Bi}_x\text{Zr}_{2-x}\text{O}_{12}$  samples were synthesized with  $x=0.75$  (0.75Bi-LLZO) and  $x=1$  (Bi-LLZO), and added to a  $\text{PEO}_{49}:\text{LiTFSI}$  matrix. The weight content of filler was kept at 5% wt. The materials were mixed with acetonitrile (ACN, Sigma Aldrich, 99.9%) and wet ball milled for 12 hours at 400 rpm with a Fritsch Pulverisette 6 apparatus to obtain homogenous particle size and obtain good dispersion of filler particles in the polymer matrix. XRD was used to characterize the cubic phase of each doped Bi-LLZO, as well as the crystallinity of the PCE films. SEM was used to determine how well-dispersed the particles were in the polymer matrix. EIS was used to determine ionic conductivity of the PCE films. The results show that, by varying Li content in the garnet LLZO, very different results for ionic conductivity are obtained. At room temperature and when the weight load is 5% wt, the highest value of ionic conductivity is  $2 \times 10^{-5} \text{ S/cm}$  for Bi-LLZO, and for 0.75Bi-LLZO, it is  $7.8 \times 10^{-7} \text{ S/cm}$ , two orders of magnitude lower. To better understand the role of the filler, the ionic conductivity for different Bi-doped garnets were examined as a function of weight load. The filler weight loads studied were: 2.5%, 5% wt, 10% wt, 30% wt and 50% wt. Interestingly, for the 0.75Bi-LLZO film, the ionic conductivity increased to  $8.1 \times 10^{-6} \text{ S/cm}$  when the weight load was 10% wt. The difference in optimal weight content on ionic conductivity is ascribed to changes in morphology of the polymer matrix, induced

by the change in molar Li content in the garnet particles. Utilizing PLM images, differences in spherulite number and size changes are observed for the different doped-LLZO garnets, this increments the tortuosity for Li ion conduction with concomitant changes on the PCE ionic conductivity.

In the final chapter of this thesis, a microstructure-focused approach was used to better understand the role of polymer morphology on ionic conductivity. The ionic conductivity co-doped BiNd-LLZO vs weight load was studied, and compared with its counterpart for PCE with 0.75Bi-LLZO. The results are very similar, a high value of  $1.4 \times 10^{-5} \text{S/cm}$  at 10%wt load at room temperature is achieved in both samples which subsequently decreases to lower values as the wt load is incremented. Thicker samples of the same compositions were also produced to study the effect of tortuosity on IC. With increasing thickness and under the same synthesis conditions, spherulite formation should fill out more volume compared to the thinner volume, increasing the tortuosity of the Li-ion pathway, and decreasing the ionic conductivity. The difference in the IC measured in these samples can be understood as follows:

Filler particles slow down re-crystallization kinetics of the polymer matrix through particle-polymer electrostatic interaction. In doing so, a high amorphous fraction of the polymer matrix is maintained over a longer period of time. Ionic conduction is faster through the amorphous region and so the average ionic conductivity is increased. This is supported by XRD measurement, indicating a reduction of crystallinity of PEO with added filler amounts.

Filler particles breaks apart ionic bonds of the lithium salt in the polymer matrix, thus increasing the number of free lithium ions, increasing the average ionic conductivity. LLZO has a high dielectric constant, and can disassociate more LiTFSI compared to passive particles. This is supported by the increase in peak intensity for ether oxygen in FTIR studies.

Lithium vacancies on the filler surface can act as nucleation sites for spherulite formation, and that the density of nucleation sites alter spherulite number and size. The effect on the number and size of spherulites in PCE as a function of Li-vacancies is not well-studied compared to the effect crystallinity or Tg, but there is evidence in the literature linking spherulite size (and lamellar

thickness) to ionic conductivity. This is supported by the PLM studies reported in this work on spherulitic formation.

## 6.2 Research outlook

Next-generation Li-ion batteries are increasingly a necessary step for successful integration of electric vehicles and renewable energy generation and storage. A pathway to this goal is implementation of Li-metal as an anode, but is incompatible with current commercial version of Li-ion technology, as the organic solvent electrolyte has several drawbacks already explained in this thesis. Although recent research on polymer composite electrolytes has shown that high ionic conductivity can be achieved that could compete with organic solvents at moderate temperatures (35°C), other material properties have been overlooked.

Future work that needs to be completed include a study of wettability on lithium metal, and characterization of the resistance between the PCE phase and the anode. In order to design a solid polymer electrolyte compatible with lithium metal, adding a lithium salt is essential, as the addition of free Li<sup>+</sup> ions would increase the ionic conductivity to a competitive level. This however is counter-productive, as lithium salts reactive negatively with lithium metal and increases the interface resistance. Adding a filler in an optimal amount to the polymer:salt system, while keeping the salt content low, would decrease the interface resistance, suppress lithium metal passivation, while keeping the ionic conductivity high. More research is needed into the resulting morphology of PCEs with lithium metal, as the anode surface may act as nucleation centers for crystallization, altering the necessary amounts of lithium salt and filler.

Also, a study of mechanical properties is underrepresented in the literature. Specifically, investigations into volume change after lithiation/delithiation and suitable operating temperature variation. PEO-based PCEs undergo plastic deformation on temperature change, and understanding the limits of its mechanical properties would allow a better designed next-generation Li-ion rechargeable battery.

## APPENDIX A. REFERENCES FOR FIGURE 2.6 AND 2.7.

- [1] A. K. Baral, S. Narayanan, F. Ramezanipour, and V. Thangadurai, "Evaluation of fundamental transport properties of Li-excess garnet-type  $\text{Li}_{5+2x}\text{La}_3\text{Ta}_{2-x}\text{Y}_x\text{O}_{12}$  ( $x = 0.25, 0.5$  and  $0.75$ ) electrolytes using AC impedance and dielectric spectroscopy," *Phys. Chem. Chem. Phys.*, 2014.
- [2] L. Buannic *et al.*, "Dual Substitution Strategy to Enhance  $\text{Li}^+$  Ionic Conductivity in  $\text{Li}_7\text{La}_3\text{Zr}_2\text{O}_{12}$  Solid Electrolyte," *Chem. Mater.*, 2017.
- [3] C. Deviannapoorani, L. Dhivya, S. Ramakumar, and R. Murugan, "Lithium ion transport properties of high conductive tellurium substituted  $\text{Li}_7\text{La}_3\text{Zr}_2\text{O}_{12}$  cubic lithium garnets," *J. Power Sources*, 2013.
- [4] L. Dhivya, N. Janani, B. Palanivel, and R. Murugan, " $\text{Li}^+$  transport properties of W substituted  $\text{Li}_7\text{La}_3\text{Zr}_2\text{O}_{12}$  cubic lithium garnets," *AIP Adv.*, 2013.
- [5] E. Hanc, W. Zając, and J. Molenda, "Synthesis procedure and effect of Nd, Ca and Nb doping on structure and electrical conductivity of  $\text{Li}_7\text{La}_3\text{Zr}_2\text{O}_{12}$  garnets," *Solid State Ionics*, 2014.
- [6] Y. Li *et al.*, "W-Doped  $\text{Li}_7\text{La}_3\text{Zr}_2\text{O}_{12}$  Ceramic Electrolytes for Solid State Li-ion Batteries," *Electrochim. Acta*, 2015.
- [7] Y. Li, C. A. Wang, H. Xie, J. Cheng, and J. B. Goodenough, "High lithium ion conduction in garnet-type  $\text{Li}_6\text{La}_3\text{ZrTaO}_{12}$ ," *Electrochem. commun.*, 2011.
- [8] Y. Li, J. T. Han, C. A. Wang, H. Xie, and J. B. Goodenough, "Optimizing  $\text{Li}^+$  conductivity in a garnet framework," *J. Mater. Chem.*, 2012.
- [9] Y. Li, Z. Wang, C. Li, Y. Cao, and X. Guo, "Densification and ionic-conduction improvement of lithium garnet solid electrolytes by flowing oxygen sintering," *J. Power Sources*, 2014.

- [10] Y. Meesala *et al.*, “An efficient multi-doping strategy to enhance Li-ion conductivity in the garnet-type solid electrolyte  $\text{Li}_7\text{La}_3\text{Zr}_2\text{O}_{12}$ ,” *J. Mater. Chem. A*, 2019.
- [11] D. Mori *et al.*, “Synthesis, Structure and Ionic Conductivity of Garnet Like Lithium Ion Conductor  $\text{Li}_{6.25+x}\text{Ga}_{0.25}\text{La}_{3-x}\text{Sr}_x\text{Zr}_2\text{O}_{12}$ ,” *J. Electrochem. Soc.*, 2019.
- [12] S. Ohta, T. Kobayashi, and T. Asaoka, “High lithium ionic conductivity in the garnet-type oxide  $\text{Li}_{7-x}\text{La}_3(\text{Zr}_{2-x}\text{Nb}_x)\text{O}_{12}$  ( $X = 0-2$ ),” *J. Power Sources*, 2011.
- [13] S. Ramakumar, L. Satyanarayana, S. V. Manorama, and R. Murugan, “Structure and  $\text{Li}^+$  dynamics of Sb-doped  $\text{Li}_7\text{La}_3\text{Zr}_2\text{O}_{12}$  fast lithium ion conductors,” *Phys. Chem. Chem. Phys.*, 2013.
- [14] A. Ramzy and V. Thangadurai, “Tailor-made development of fast Li ion conducting garnet-like solid electrolytes,” *ACS Appl. Mater. Interfaces*, 2010.
- [15] D. Rettenwander *et al.*, “Structural and Electrochemical Consequences of Al and Ga Cosubstitution in  $\text{Li}_7\text{La}_3\text{Zr}_2\text{O}_{12}$  Solid Electrolytes,” *Chem. Mater.*, 2016.
- [16] S. Song *et al.*, “Gd-doped  $\text{Li}_7\text{La}_3\text{Zr}_2\text{O}_{12}$  garnet-type solid electrolytes for all-solid-state Li-Ion batteries,” *Electrochim. Acta*, 2018.
- [17] Y. Wang and W. Lai, “High ionic conductivity lithium garnet oxides of  $\text{Li}_{7-x}\text{La}_3\text{Zr}_{2-x}\text{Ta}_x\text{O}_{12}$  compositions,” *Electrochem. Solid-State Lett.*, 2012.
- [18] J. Wolfenstine, J. Ratchford, E. Rangasamy, J. Sakamoto, and J. L. Allen, “Synthesis and high Li-ion conductivity of Ga-stabilized cubic  $\text{Li}_7\text{La}_3\text{Zr}_2\text{O}_{12}$ ,” *Mater. Chem. Phys.*, 2012.
- [19] J. F. Wu *et al.*, “Gallium-doped  $\text{Li}_7\text{La}_3\text{Zr}_2\text{O}_{12}$  garnet-type electrolytes with high lithium-ion conductivity,” *ACS Appl. Mater. Interfaces*, 2017.
- [20] Y. Xia *et al.*, “Preparation and enhancement of ionic conductivity in Al-added garnet-like  $\text{Li}_{6.8}\text{La}_3\text{Zr}_{1.8}\text{Bi}_{0.2}\text{O}_{12}$  lithium ionic electrolyte,” *Front. Mater. Sci.*, 2015.